TAPERED PLASTIC OPTICAL FIBER SENSORS FOR CHEMICAL DETECTION AND RELATIVE HUMIDITY MEASUREMENTS

MALATHY A/P BATUMALAY

THESIS SUBMITTED IN FULFILLMENT OF THE REQUIREMENT FOR THE DEGREE OF DOCTOR OF PHIILOSOPHY

DEPARTMENT OF ELECTRICAL ENGINEERING

FACULTY OF ENGINEERING

UNIVERSITY OF MALAYA

KUALA LUMPUR

2014

UNIVERSITI MALAYA

ORIGINAL LITERARY WORK DECLARATION

Name of Candidate: Malathy a/p Batumalay (I.C/Passport No:

Registration/Matric No: KHA110034

Name of Degree: Doctor of Philosophy

Title of Project Paper/Research Report/Dissertation/Thesis ("this Work"):

Tapered Plastic Optical Fiber Sensors for Chemical Detection and Relative Humidity Measurements

Field of Study: Photonics

I do solemnly and sincerely declare that:

(1) I am the sole author/writer of this Work;
(2) This Work is original;
(3) Any use of any work in which copyright exists was done by way of fair dealing and for permitted purposes and any excerpt or extract from, or reference to or reproduction of any copyright work has been disclosed expressly and sufficiently and the title of the Work and its authorship have been acknowledged in this Work;
(4) I do not have any actual knowledge nor do I ought reasonably to know that the making of this work constitutes an infringement of any copyright work;
(5) I hereby assign all and every rights in the copyright to this Work to the University of Malaya ("UM"), who henceforth shall be owner of the copyright in this Work and that any reproduction or use in any form or by any means whatsoever is prohibited without the written consent of UM having been first had and obtained;
(6) I am fully aware that if in the course of making this Work I have infringed any copyright whether intentionally or otherwise, I may be subject to legal action or any other action as may be determined by UM.

Candidate's Signature: **Date:**

Subscribed and solemnly declared before,

Witness's Signature: **Date:**

Name:

Designation:

Acknowledgements

Praise be to The Almighty and Gurus, this thesis would not have materialized without the help and guidance from my supervisor Prof. Sulaiman Wadi Harun and my co supervisor, Prof. Harith Ahmad. No words can describe my deepest appreciation and gratitude to Prof. Sulaiman who has not only been patient and tolerant to my quest in seeking knowledge, but also generous in sharing his expertise, immense knowledge and experience in this field of photonics.

My sincere and heartfelt gratitude goes to Husna and Fauzan for their selflessness and generous help in the lab, kind assistance and strong encouragement to complete this thesis. Not forgetting the wonderful support from those who have directly or indirectly contributed to the completion of this thesis. My appreciation also goes to the members of the Photonic Research Center. You have made the lab most enjoyable to work in despite the many challenges we have to put up with.

To my dearest father, mother, sisters, beloved husband, my lovely daughter, thank you for your love and for being there for me. Needless to say, without all the above help and support, the writing of this thesis would not been possible.

Abstract

The developments of novel tapered plastic optical fibers (POFs) devices have become the central focus of researches in recent years especially for sensing applications. In this thesis, simple sensors are proposed and demonstrated using a bare tapered polymethyl methacrylate (PMMA) fiber and tapered PMMA coated sensitive materials for various measurements. The tapered PMMA fibers were fabricated by etching method using acetone, sand paper and de-ionized water to achieve a waist diameter of 0.45 mm and tapering length of 10 mm and operate based on intensity modulation technique. Evanescent field absorption sensors were developed for various electrolyte and nonelectrolyte solutions using the PMMA tapered fiber probe. To enhance the performance of the sensing probe, tapered PMMA fibers were coated with sensitive materials such as graphene polymer, single walled carbon nanotubes polyethylene oxide (SWCNT-PEO) composite and zinc oxide nanostructures for sensing different concentration of uric acid. Subsequent performance analysis allows the identification of the experimental dependence of the surrounding refractive index sensitivity on the three different sensitive coating materials. It is observed that the transmitted light intensity improves with the sensitive material coating. The fiber itself can play an active role by acting as a sensor when the cladding is replaced with chemical sensitive material. On the other hand, RH sensors have been proposed and demonstrated using tapered PMMA in conjunction with various sensitive coating materials such as agarose gel, Hydroxyethylcellulose/ polyvinylidenefluoride (HEC/PVDF) and zinc oxide (ZnO). It is observed that the probe sensitivity improves with the sensitive coating materials. When the composite are exposed to an environment of humidity, it causes rapid surface adsorption of water molecules and changes its optical property. Furthermore, the proposed sensors also provide numerous advantages

such as simplicity of design, low cost of production, higher mechanical strength and easier to handle compared to silica fiber optic. PMMA based sensor can easily be automated and to operate at room temperature and varying pressure conditions.

Abstrak

Pembangunan novel tirus serat optik plastik (POFs) peranti telah menjadi tumpuan utama penyelidikan dalam tahun-tahun kebelakangan terutama untuk applikasi pengesan. Dalam tesis ini, sensor mudah telah dicadangkan dan ditunjukkan menggunakan gentian terdedah tirus polymethylmethacrylate (PMMA) dan PMMA tirus bersalut bahan-bahan sensitif bagi pelbagai ukuran. Gentian PMMA tirus telah direka dengan kaedah punaran menggunakan aseton, kertas pasir dan de-terion air untuk mencapai diameter pinggang sebanyak 0.45 mm dan panjang tirus 10 mm dan beroperasi berdasarkan teknik intensiti modulasi. Sensor penyerapan medan evanesen telah dibangunkan untuk pelbagai larutan elektrolit dan bukan elektrolit menggunakan alatan PMMA tirus serat. Untuk meningkatkan prestasi alatan pengesan, serat PMMA tirus telah disalut dengan bahan-bahan yang sensitif seperti polimer graphene, oksida berdinding nonotubes karbon polietilena tunggal (SWCNT - PEO) komposit dan zink oksida (ZnO) bersaiz nano untuk mengesan kepekatan asid urik. Dalam analisa yang berikut, biasan sensitiviti indeks kepada tiga bahan-bahan salutan berbeza dikenalpasti. Adalah diperhatikan bahawa keamatan cahaya meningkat dengan lapisan bahan yang sensitif. Serat sendiri boleh memainkan peranan aktif dengan bertindak sebagai sensor apabila pelapisan digantikan dengan bahan sensitif kimia. Sebaliknya, sensor RH telah dicadangkan dan ditunjukkan menggunakan PMMA tirus bersempena dengan pelbagai bahan-bahan salutan sensitif seperti gel agarose, Hydroxyethylcellulose / polyvinylidenefluoride (HEC / PVDF) dan zink oksida (ZnO). Adalah diperhatikan bahawa sensitiviti siasatan bertambah baik dengan lapisan. Apabila komposit terdedah kepada persekitaran kelembapan, ia menyebabkan penyerapan pesat molekul air dan perubahan sifat optik. Sensor-sensor yang dicadangkan memberi banyak kelebihan seperti kesederhanaan reka bentuk, kos pengeluaran yang lebih murah, kekuatan

mekanikal yang lebih tinggi dan lebih mudah untuk dikendalikan berbanding dengan gentian optik silika. Tambahan pula, sensor berasaskan PMMA tidak memerlukan bahan-bahan canggih, boleh diautomasikan dan boleh beroperasi pada suhu bilik dan keadaan tekanan yang berbeza-beza .

Table of Contents

Acknowledgement i

Abstract ii

Abstrak iv

Table of Contents vi

List of Figures ix

List of Tables xii

Acronyms/Symbols xiii

Chapter 1: Introduction

1.1 Introduction to Plastic Optical Fiber (POF) 1

1.2 Background on optical fiber sensors 2

1.3 Motivation of this study 3

1.4 Objectives of this study 4

1.5 Dissertation Overview 5

Chapter 2: Literature Review on Tapered Optical Fibers and Fiber Sensors

2.1 Introduction 9

2.2 Tapered fiber 11

2.2.1 Fiber Tapering Methods 12

2.3 Fiber Optic Techniques for Sensing 13

2.3.1 Evanescent wave sensor 14

2.3.2 Refractive index sensor 15

2.4 Tapered fiber with sensitive layer for coating 17

2.4.1 Overview on sensitive materials 18

2.4.1.1 Graphene 18

2.4.1.2 Carbon Nanotube 20

2.4.1.3 Zinc Oxide 22

2.4.1.4 Agarose Gel for use in humidity sensors 24

2.4.1.5 Hydroxyethylcellulose (HEC) 26

2.5 Plastic optical fiber (POF) 26

2.6 Methodology 27

Chapter 3: Development and Analysis of Multimode Tapered PMMA Fiber Sensors

3.1 Introduction 29

3.2 Taper Fabrication 31

3.2.1 Heat Pulling Method 31
3.2.2 Etching 33
3.3 Sensing of Sodium Chloride Refractive Index 35
3.3.1 Experimental set-up 36
3.3.2 Performances of the sensor 38
3.4 Analysis of PMMA Optical Fiber Sensitivity for use as a Chemical Concentration Sensor in Electrolyte and Non-Electrolyte Solutions. 42
3.4.1 Experiment 45
3.4.2 Performance of the sensors 46
3.5 Effect of probe arrangement on the performance of the proposed PMMA based chemical sensors. 52
3.6 Summary 59
Chapter 4: Analysis of Multimode Tapered PMMA Fiber Sensors for Uric Acid Detection
4.1 Introduction 61
4.2 Uric Acid 63
4.3 Tapered fiber coated with Sensitive Materials 64
4.3.1 Graphene 65
4.3.2 Carbon Nanotubes (CNT) 65
4.3.3 Zinc Oxide (ZnO) 66
4.4 Sensing of Uric Acid with Tapered Plastic Fiber coated with Graphene 67
4.4.1 Experiment Setup 70
4.4.2 Performance of the sensors 71
4.5 Sensing of Uric Acid with Tapered POF coated with SWCNT 77
4.6 Sensing of Uric Acid with Tapered Plastic Fiber coated with Zinc Oxide ……82
4.7 Summary 88
Chapter 5: Multimode Tapered PMMA Fiber Sensors for Relative Humidity Measurement
5.1 Introduction 90
5.2 Background on Relative Humidity (RH) and evanescent wave-based humidity sensors 91
5.3 Tapered POF for RH sensing 93
5.4 Agarose gel based RH sensor 94
5.4.1 Experimental procedure 95
5.4.2 Performance of the sensors 99

5.5 Tapered fiber with HEC/PVDF coating for RH sensor.....105
5.5.1 Experimental proceduce.....106
5.5.2 Performance of the sensors.....107
5.6 Tapered fiber with Zinc Oxide Coating for RH sensor.....112
5.6.1 Experimental procedure for ZnO based RH sensor. 113
5.6.2 Performance of the sensors.....115
5.7 Summary.....118
Chapter 6: Conclusions and Future Works
6.1 Conclusions.....121
6.2 Recommendations for future works.....125
References
Appendix

List of Figures

Figure 2.1:Schematic diagram of a tapered fiber; *n*1 is refractive index of the surrounding medium, *n*eff - effective refractive index of a core mode. 12

Figure 2.2:Structure of an intrinsic fiber-optic sensing part 16

Figure 2.3:FESEM image of the graphene.....19

Figure 2.4:FESEM image of the PEO/SWNT 21

Figure 2.5:FESEM images for zinc oxide nanoparticles (a) rods (b) tubes and (c) flowers.....24

Figure 3.1:Schematic diagram of the tapering process of the PMMA fiber. Inset compares the original and tapered fibers. 32

Figure 3.2:Microscopic image of the (a) un-tapered PMMA fiber (with diameter of 1 mm) and (b) Tapered PMMA fiber (with diameter of 0.187 mm) with heat pulling method. 33

Figure 3.3:Microscopic image of the (a) un-tapered PMMA fiber (with diameter of 1 mm) and (b) Tapered PMMA fiber (with diameter of 0.45 mm), with etching technique 34

Figure 3.4:Experimental set-up for the sodium chloride refractive index sensor using a tapered PMMA fiber. 37

Figure 3.5:Output voltage against sodium chloride concentration. 41

Figure 3.6:Output voltage against refractive index of sodium chloride concentration. ..41

Figure 3.7:Diameters of fiber against sensitivity (calcium nitrate).....46

Figure 3.8:Output voltage against calcium nitrate concentration. 48

Figure 3.9:Output voltage against sodium chloride concentrations. 49

Figure 3.10:Output voltage against glucose concentrations.....51

Figure 3.11:Output voltage against sucrose concentrations. 51

Figure 3.12:Output voltage against sodium chloride concentration at various tapered fiber arrangements.....53

Figure 3.13:Output voltage against calcium nitrate concentration at various tapered fiber arrangements. 55

Figure 3.14:The reversibility of the results obtained for two different runs (Sodium Chloride Solution).....58

Figure 3.15:The reversibility of the results obtained for two different runs (Calcium Nitrate Solution).....58

Figure 4.1:Photographic image of (a) solutions of graphene polymer composite at ratios of 2:20, 4:20 and 6:20 and microscope images of graphene polymer

composite at mixing ratios of (b) 2:20 (c) 4:20 and (d) 6:20 (scale: 200μm). 69

Figure 4.2:Microscopic images of (a) un-tapered POF (with diameter of 1 mm), (b) Tapered POF (with diameter of 0.45 mm) and (c) Tapered POF coated with graphene polymer composite with ratio of 6:20 (scale: 200μm). 69

Figure 4.3:Experimental setup for the proposed relative humidity sensor using a tapered POF without and with HEC/PVDF composite. 71

Figure 4.4:Refractive index against uric acid solution concentrations. 72

Figure 4.5:The output voltage against uric acid concentrations for the proposed tapered POF based sensor without and with graphene polymer composite of 2:20, 4:20 and 6:20. 73

Figure 4.6:The reversibility of the results obtained for two different runs (Output voltage against the concentration of Uric Acid). 76

Figure 4.7: The deposition of SWCNT-PEO composite onto the cladding surface of the tapered POF. 78

Figure 4.8:Microscope images of (a) un-tapered POF (with diameter of 1 mm), (b) Tapered POF (with diameter of 0.45 mm) and (c) Tapered POF with SWCNT-PEO composite 79

Figure 4.9:Output voltage against uric acid concentrations for the proposed tapered POF based sensor with and without SWCNT-PEO composite. 80

Figure 4.10:FESEM images of the ZnO nanostructures grown on (a) seeded tapered fiber and (b). 84

Figure 4.11:Output voltage against uric acid concentrations for the proposed tapered POF with ZnO nanostructure. 86

Figure 4.12:The reversibility of the results obtained for two different runs (Concentration of Uric Acid). 87

Figure 5.1:Photographic Image of (a) agarose gel of 0.5, 1 and 1.5% weight content (b) microscopic image of agarose gel 0.5% weight content (c) microscopic image agarose gel 1% weight content and (d) microscopic image agarose gel 1.5% weight content. 96

Figure 5.2:Microscope images of (a) un-tapered POF (with diameter of 1 mm), (b) Tapered POF (with diameter of 0.45 mm) and Fig. 2 (c), (d) and (e) Tapered POF coated with agarose gel of 0.5, 1 and 1.5% weight content respectively (scale: 1cm: 1.5mm). 97

Figure 5.3:Experimental setup for the proposed sensor to measure relative humidity using a tapered POF with agarose gel. 99

Figure 5.4:Output voltage against RH for the bare fiber and tapered fiber with agarose gel of 0.5% weight content. 102

Figure 5.5:Output voltage against RH for the bare fiber and tapered fiber with agarose gel of 1% weight content 102

Figure 5.6:Output voltage against RH for the bare fiber and tapered fiber with agarose gel of 1.5% weight content 103

Figure 5.7:The reversibility of the results obtained for two different runs (RH).....104

Figure 5.8:Image of (a) HEC/PVDF composite, (b) microscopic image of HEC/PVDF composite. 106

Figure 5.9:Microscopic images of (a) un-tapered POF (with diameter of 1 mm), (b) Tapered POF (with diameter of 0.45 mm) and (c) Tapered POF with HEC/PVDF composite.....107

Figure 5.10:Output voltage against RH for the proposed tapered POF based sensor with and without HEC/PVDF composite.....108

Figure 5.11:Performance of Humidity Sensor with and without HEC/PVDF composite 110

Figure 5.12:The reversibility of the results obtained for two different runs (RH).....111

Figure 5.13:FESEM images with ZnO nanostructures grown on seeded tapered fiber (Fig.5.13(a)) and on non-seeded tapered fiber (Fig.5.13(b)). 115

Figure 5.14:Sensing results for the proposed relative humidity sensor using a tapered POF coated with ZnO nanostructure.....117

Figure 5.15:The reversibility of the results obtained for two different runs (RH).....117

List of Tables

Table 3.1:The performance of the sodium chloride refractive index sensor.....42

Table 3.2:The performance of the tapered plastic fiber sensors with various probe arrangements (Sodium Chloride). 54

Table 3.3:The performance of the tapered plastic fiber sensors with various probe arrangements (Calcium Nitrate).....56

Table 4.1:The performance of the proposed Uric Acid Detection Sensor 77

Table 4.2:The performance of the proposed uric acid detection sensor.....82

Table 4.3:The performance of the proposed uric acid detection sensor.....88

Table 5.1:Table performance of the proposed sensor 105

Table 5.2:Performance of the proposed sensor 112

Table 5.3:The performance of the proposed RH sensor.....118

Table 6.1:Performance of chemical sensors……123

Table 6.2:Performance of the RH sensors.....124

Acronyms / Symbols

POF	Plastic Optical Fiber
GOF	Glass optical Fiber
FOS	Fiber optic sensor
EW	Evanescent wave
PMMA	Polymethyl methacrylate
HEC/PVDF	hydroxyethylcellulose / polyvinylidenefluoride
CNTs	Carbon nanotubes
WDM	Wavelength division multiplexer
TIR	Total internal reflection
RI	Refractive index
CMOS	complementary metal oxide
SWNTs	Single walled nanotubes
MWNTs	Multi walled nanotubes
PEO	Polyethylene oxide
EMI	Electromagnet interference
DNA	deoxyribonucleic acid
EWF	Evanescent wave field
NaCl	Sodium chloride
ZnO	Zinc oxide
ISEs	Ion sensitive electrodes
SDS	Sodium dodecyl sulfate
PVA	Polyvinyl alcohol
FESEM	Field emission scanning electron microscopy
RH	Relative humidity

Chapter 1

Introduction

1.1 Introduction to Plastic Optical Fiber (POF)

Plastic optical fiber (POF) is an optical fiber made out of plastic. Traditionally polymethyl methacrylate (PMMA) with acrylic in the core material, and fluorinated polymers are the cladding material. Higher-performance POF based on perfluorinated polymers have begun to appear in the market place since the late 1990s. Similar to traditional glass fiber, POF transmits light (or data) through the core of the fiber. In telecommunications, the more difficult-to-use glass optical fiber with core made of germania-doped silica is more common. Although the actual cost of glass fibers are similar to the plastic fiber, their installed cost is much higher due to the special handling and installation techniques required. The most stirring developments in polymer fibers have been the development of micro-structured polymer optical fibers, a type of photonic crystal fiber.

POFs also have applications in sensing. There are advantages of using POFs over silica fibers as it can be stretched further without breaking, simpler and less expensive components and lighter weight. Besides that, POFs have transmission windows in the visible range of 520 to 780nm. Hence, POFs have been relegated to short-distance applications typically of a few hundred meters or less compared with the hundreds of kilometers for glass. POFs have been found many applications in areas such as industrial controls, automobiles, sensors and short data links. Today, a new enthusiasm permeates the plastics side of optical fibers.

1.2 Background on optical fiber sensors

Optical fibers are currently abundantly available for various applications ranging from transmission medium, which covering a wide spectral range and sensors. The basic optical fiber structure consists of a core surrounded by cladding material of a lower refractive index and both are transparent dielectric cylindrical. The refractive index difference between core and cladding provide total internal refection which protect from contamination and reduce crosstalk between fibers. Technology has since taken optical fiber sensors to the other extreme (Ahmad, 1994). The requirement for optical fiber sensors is to have a low optical and mechanical attenuation under all anticipated operational conditions without performance degradation (Ahmad, 1994).

Fiber optic sensor (FOS) is compact and lightweight with the possibility of having distributed or quasi-distributed sensing geometries. That's means FOS can be multiplexed to measure over a continuous region or in some region (multi-channel) with large number of discrete points (Thyagarajan and Ghatak, 2007). Fiber optic sensors can be categorized into two groups: intrinsic and extrinsic. So-called intrinsic devices rely on light beam propagating through the fiber and interaction occurs actually within environmental effect of and the optical fiber itself. Extrinsic fiber optic devices were the optical fiber used to couple light. The light beam transmits and passing out of fiber to expose environment effect will be coupled back to fiber again. However, different applications of sensor require different types of transducers (optical fiber) to manipulate the incident radiation. Optical fiber sensors have been studied on accuracy, reliability, portability and cost effectiveness. It can be candidate to become a competitive alternative to the conventional sensors. To date, much of instrumentation upgrading in this particular application has been recorded. Thus, instrumentation for optical fiber sensor requires an overview.

The efforts to develop smaller but more sensitive and accurate sensors to cater to a large range of physical, chemical and biomedical measurements constitute a substantial drive for optoelectronics research today. Recently, tapered optical fibers have attracted many interest especially for sensing applications (Xu and Saeys, 2008; Rahman et al., 2011). This is due to a higher portion of evanescent field travels inside the cladding in the tapered fiber and thus the travelling wave characteristics become more sensitive to the physical ambience of its surrounding. A fiber optic taper becomes sensitive to the environment by enhancing the power fraction of evanescent wave (EW) in the cladding. The interest on tapered multimode plastic fiber has also increased considering its superior mechanical strength and ease of manufacture. Tapered optical fiber has also received much attention for sensing applications (Khijwania and Gupta, 1999; Beres, 2011; Golnabi et al., 2007; Corres, Arregui and Matias, 2006; Lim et al., 2011; Zibaii et al., 2010).

1.3 Motivation of this study

Various technologies are used in the photonics research field are based on silica fibers leaving behind POFs. However due to the advantages such as low cost, easiness in handling and immunity to electromagnetic interference, POFs become important. Recently, the interest on tapered fiber is also increasing for sensor applications. The reduction in the size of fiber within the tapered region allows the evanescent field of the propagating mode of the fiber to extend into the external environment. The deposition of a sensitive material onto the tapered fiber allows for the transmission spectrum control via the interaction of the light propagating in a fiber with the overlay material. The coating may be engineered to change the transmission spectrum in response to an external stimulus and thus sensors for a range of measurands. Today, many works have been carried out to evaluate the performance of the sensor with various sensitive coating

materials on the tapered region and many analyses on how it can enhance the performance of the sensor are also reported [Bilro et al., 2012]. The fiber plays an active role by acting as a sensor when the cladding is replaced with chemical sensitive material [Bilro et al., 2012]. In a work reported by Nagata et. al. [2007], the new deposited cladding had a refractive index slightly above the refractive index of the core and in the presence of detection medium, the refractive index decrease to values below the core. The changes in refractive indices cause an enhancement in the power output of the system.

This thesis proposes and demonstrates various new refractive index sensors based on tapered POF which featuring several advantages and potential. The working principle of the sensors is based on a simple intensity modulation technique, which uses tapered PMMA fiber coated with various sensitive coating materials as a probe. Even though they are much inferior in terms of sensitivity in comparison to the other techniques reported earlier, but they are relatively inexpensive, easy to fabricate and suitable for employment in harsh environments. Hence, these kinds of sensors might be preferred by some application requiring less cost and sensitivity. Here, the sensitivity of various sensors based on tapered fiber coated with graphene, single walled carbon nanotube, agarose gel, hydroxyethylcellulose / polyvinylidenefluoride (HEC/PVDF) composite and zinc oxide were investigated.

1.4 Objectives of this study

This work aims to explore several coating materials on tapered plastic fiber to investigate the response in detecting chemical of different concentrations and changes on relative humidity. To achieve this, few objectives have been proposed to guide the research direction, i.e.:

i. To demonstrate a tapered bare fiber as a sensor to detect different concentration of chemicals.

ii. To coat the tapered fiber with sensitive materials such as graphene polymer, single walled carbon nanotubes (CNTs) composite and zinc oxide nanostructures for application as uric acid sensor.

iii. To develop relative humidity sensor based on a tapered fiber coated with sensitive materials such as agarose gel, hydroxyethylcellulose/ polyvinylidenefluoride (HEC/PVDF) composite and zinc oxide nanostructures.

1.5 Dissertation Overview

This thesis consists of six main chapters giving a comprehensive study on tapered plastic optical fiber sensors for chemical detection and relative humidity measurements. The current chapter presents a brief introduction on fiber optics field that includes the motivation and the objectives of this research.

Chapter 2 provides a literature review on tapered plastic optical fiber (POF) where various fabrication techniques and coating methods are reviewed. Applications of POFs and various works pertaining to tapered POFs such as polymethylmethacrylate (PMMA) are also briefly described in this chapter.

Chapter 3 reports on the fabrication of tapered PMMA fibers based on two techniques; heat-and-pull method and chemical etching. The fabricated tapered fiber is then used as a sensor probe to measure the refractive index of various external liquids. It is found that chemical-etched taper provides better performance in term of repeatability. The repeatability of the etching process in terms of taper ratio and shape and its superior sensitivity has led to its further use in the following chapters as evanescent field sensors.

Chapter 4 demonstrates a tapered fiber based sensor for uric acid detection. In this work, the tapered fiber is coated with sensitive coating materials such as graphene

polymer, single walled carbon nanotube composite and zinc oxide nanostructures to enhance the sensitivity of the sensor. Subsequent performance analysis allows the identification of the experimental dependence of the surrounding refractive index sensitivity on the three different sensitive coating materials. It is found that the fiber itself can play an active role by acting as a sensor when the cladding is replaced with chemical sensitive material.

The tapered fiber is also used to develop relative humidity sensor as described in chapter 5. Various sensitive materials such as agarose gel, hydroxyethylcellulose/ polyvinylidenefluoride (HEC/PVDF) composite and zinc oxide nanostructures are successfully coated to the tapered fiber to increase the sensitivity of the proposed relative humidity sensors. The sensitive materials changes refractive indices in presence of water molecules. It is observed that the difference in refractive index between the cores and cladding influences the amount of light confinement inside the core. This proves that the proposed sensors are applicable for sensing relative humidity.

Chapter 6 gives a summary and review of the results and analysis of this study. It also includes recommendations for further research work. Attached in the appendix contain some selected published papers during this study.

The novelty of the investigations comprises:

1. Investigation of Tapering method for POFs

   It is found that chemical-etched taper provides better performance in term of repeatability. The repeatability of the etching process in terms of taper ratio and shape and its superior sensitivity has led to its further use in several set-ups as evanescent field sensors.

2. Development of Chemical Sensors

The tapered fiber with sensitive coating materials such as graphene, single walled carbon nanotube and zinc oxide are successfully demonstrated as a sensor to detect uric acid concentration

3. Development of simple Relative Humidity Sensors

   New choices of relative humidity sensors using tapered fiber with sensitive coating materials are proposed using agarose gel, hydroxyethylcellulose/ polyvinylidenefluoride (HEC/PVDF) composite and zinc oxide.

Below is a list of publications and papers presented in conferences during my research.

Papers Published

1. Batumalay, M., Harith, Z., Rafaie, H. A., Ahmad, F., Khasanah, M., Harun, S. W., ... & Ahmad, H. (2014). Tapered plastic optical fiber coated with ZnO nanostructures for the measurement of uric acid concentrations and changes in relative humidity. Sensors and Actuators A: Physical, 210, 190-196.
2. Batumalay, M., Harun, S. W., Ahmad, F., Nor, R. M., Zulkepely, N. R., & Ahmad, H. (2014). Study of a fiber optic humidity sensor based on agarose gel. Journal of Modern Optics, 61(3), 244-248.
3. Batumalay, M., Rahman, H. A., Kam, W., Ong, Y. S., Ahmad, F., Zakaria, R., ... & Ahmad, H. (2014). Evaluation of the tapered PMMA fiber sensor response due to the ionic interaction within electrolytic solutions. Journal of Modern Optics, 61(2), 154-160.
4. Harun, S., Rahman, H., Batumalay, M., Muttalib, F., & Ahmad, H. (2013). Fiber Optic Displacement Sensor Using Multimode Plastic Fiber Probe and Tooth Surface. Sensors Journal, IEEE, Vol 13, Issue 1, 294-298.

5. Harun, S., Batumalay, M., Lokman, A., Arof, H., Ahmad, H., & Ahmad, F. (2013). Tapered Plastic Optical Fiber Coated with HEC/PVDF for Measurement of Relative Humidity. Sensors Journal, IEEE, Vol 13, Issue 13, 4702-4705.
6. Lokman, A., Nodehi, S., Batumalay, M., Arof, H., Ahmad, H., & Harun, S. W. (2014). Optical fiber humidity sensor based on a tapered fiber with hydroxyethylcellulose/polyvinylidenefluoride composite. Microwave and Optical Technology Letters, 56(2), 380-382.
7. Muhammad, M. Z., Lokman, A., Batumalay, M., Arof, H., Ahmad, H., & Harun, S. W. (2013). Tapered Fiber Coated with Hydroxyethyl Cellulose/Polyvinylidene Fluoride Composite for Relative Humidity Sensor. Advances in Materials Science and Engineering, 2013.
8. Harun, S. W., Batumalay, M., Ahmad, F., Lokman, A., Jasim, A. A., & Ahmad, H. (2014). Tapered plastic optical fiber coated with single wall carbon nanotubes polyethylene oxide composite for measurement of uric acid concentration. Sensor Review, 34(1), 9-9.
9. Electrostatic Charge Interaction: A Case Study on Tapered PMMA Fiber for Calcium Nitrate Detection.
   (Emerald Sensor Review Journal)
10. Tapered Plastic Optical Fiber Coated with Graphene for Uric Acid Detection.
    (IEEE Sensors Journal)

International Conference Paper

1. Batumalay, M., & Harun, S. W. (2013, June). Relative humidity measurement using tapered plastic fiber coated with HEC/PVDF. In Technology, Informatics, Management, Engineering, and Environment (TIME-E), 2013 International Conference on (pp. 54-56). IEEE.

Chapter 2

Literature Review on Tapered Optical Fibers and Fiber Sensors

2.1 Introduction

An optical fiber is a flexible, transparent fiber made of high quality extruded glass (silica) or plastic and function as a waveguide to transmit light between the two ends of the fiber. They are currently abundantly available for various applications ranging from transmission medium, covering a wide spectral range and sensors. In earlier days, the developed optical fibers were "bare" in nature with total internal reflection at a glass-air interface. A bundle of these fibers was used in a development of fiberscope, which has an eye piece at one end and a lens at the other end [Hopkins, & Kapany, 1954]. An optical data transmission system was demonstrated by German Physicist in 1965 followed by first patent application in 1966. Kao C.K. and Hockham G.A. promoted that attenuation in optical fibers could be reduced below 20 decibels per kilometer (dB/km), making fibers a practical communication medium as the attenuation in fibers available at the time was caused by impurities that could be removed. Silica glass with high purity was proposed as a host material to reduce the light-loss properties for optical fiber. Currently, a silica fiber with a loss of less than 0.15 dB/km is commercially available. Plastic optical fiber has a slightly higher loss than silica fiber and thus it is more suitable for short distance communication and sensor applications.

The basic optical fiber structure consists of a core surrounded by cladding material of a lower refractive index and both are transparent dielectric cylindrical. The refractive index difference between core and cladding provide total internal refection which protect from contamination and reduce crosstalk between fibers. It also enables

the light to be confined in the core and causes the fiber to act as a waveguide. However, the requirement for optical fiber sensors is to have a low optical and mechanical attenuation under all anticipated operational conditions without performance degradation. Specially designed fibers are used for a variety of other applications, including fiber lasers and sensors. Technology has since taken optical fiber sensors to the other extreme [Ahmad, 1994].

Optical-fiber based technique has been developing which can be used for a variety of different sensor and applies in different purposes. The main drive of this research can complete the conventional methods with providing an effective measurement technology. Therein lies the recipe for the success of optical fiber sensors [Grattan and Sun, 2000]. Optical fiber sensors possess several advantages over conventional devices which are mainly due to the characteristics of the optical fiber itself. Fiber optic sensors can be made very small and thin, resistant to harsh (chemical) environments and immune to electromagnetic interference (EMI). They can be used in remote areas that are tackling difficult measurement situations [Thyagarajan and Ghatak, 2007]. The devices are also inherently safe because of the low optical power and the absence of electric current at the sensing point. Normally, multimode step-index fiber is most practical for use in chemical sensors based on changes in intensity and transmits more light [Thyagarajan and Ghatak, 2007]. Optical fibers, taking advantage of their unique characteristics which is susceptibility to linear and non-linear environmental effects for distributed sensing. In order to achieve optimum performance appropriate to a given measurand and measurement environment, careful matching of the system to the environment, and detailed system design are necessary.

Currently, the fiber sensor researches are focusing in many new areas such as gases and vapours sensing, medical and chemical analysis, molecular biotechnology, marine and environmental analysis industrial production monitoring, bioprocess control,

salinity and the automotive industry [Guo and Albin, 2003; Wolfbeis, 2004; Golnabi et al.,2007; Khainar, 2008; Rahman et al.,2011; Rahman et al.,2012;]. Fiber sensors can be classified into two main approaches; direct or indirect. Direct sensing is commonly used to measure intrinsic optical properties, refractive index emission or absorption [Golnabi et al.,2007; Rahman et al.,2011]. Most of the studies of optical based chemical sensors are based on the refractive index variation of the chemical under scrutiny [Khijwania and Gupta, 1999; Beres, 2011].

2.2 Tapered fiber

Over the last few years, researchers have been focusing in the fabrication of waveguides with sub wavelength dimensions, made of various materials and techniques. Fiber optic is well known for its admirable uniformity and other physical properties in term of strength and flexibility. Therefore, it can be used to realize a waveguide with sub-wavelength dimension such as a tapered fiber. To date, tapered optical fiber have already found direct potential function as wavelength division multiplexer (WDM) [Velankar & Shadaram, 2003], optical couplers [Oakley et al., 1994], filters [Hsu, et al., 2009], polarizer [Zhang, et al., 2009] and high-powered lasers [Filippov, et al., 2009].

Recently, tapered optical fibers have also attracted much interest for sensing applications due to an increasing effort to develop smaller but more sensitive and accurate sensors to cater for a large range of physical, chemical and biomedical measurements. The tapered fibers are very sensitive to the ambient environment and thus they can be used for various sensors such as refractive index, strain, temperature, humidity etc. The interest on multimode plastic optical fiber (POF) has also increased consideringly due to its superior mechanical strength and ease of manufacture for sensing applications [Golnabi et al., 2007; Corres, Arregui and Matias, 2006; Lim et al., 2011; Zibaii et al., 2010].

2.2.1 Fiber Tapering Methods

Fiber tapering is a process of reducing the fiber diameter in order to change their light coupling or light propagation properties. Previously, tapering is done by heating and pulling the fiber's ends. However, both core and cladding diameters are evenly reduced by this method. This type of tapered fiber consists of three sections; a segment where the diameter of the fiber gradually decreases (taper transition region), a taper waist where the diameter is small and uniform and a segment where the diameter of the fiber increases gradually (taper transition region). These regions are identified in figure 2.1.

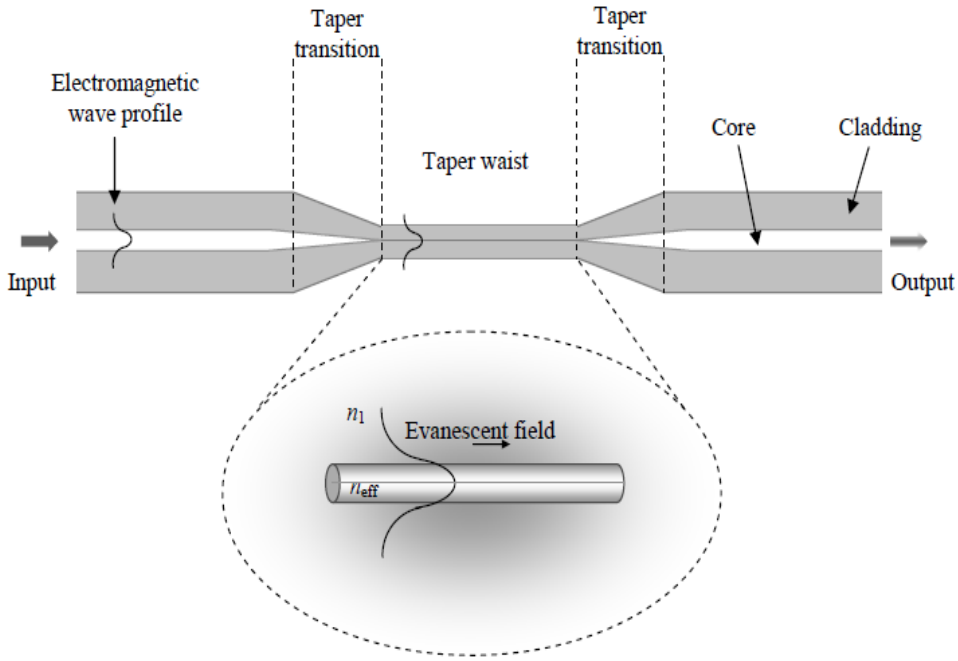

Figure 2.1: Schematic diagram of a tapered fiber; n_1 is refractive index of the surrounding medium, n_{eff} - effective refractive index of a core mode.

Local heating and subsequent pulling of an intact fiber has been well accepted as a successful method to produce silica tapered optical fibers [Sumetsky, Dulashko and Hale, 2004; Shi et al., 2006]. However, only few examples of heat-pulled plastic optical

fiber (POF) tapers have been reported [Gravina, Testa and Bernini, 2009; Xue et al., 2007; Arrue et al., 2008]. Due to the effect of heat and pull, the fiber core and cladding alter the refractive index profile. However, the fiber core of the chemical-etched taper is unaltered given that the diameter of the core is smaller than the taper. In contrast to chemical-etched fibers, the thinning of the core in the heat-pulled taper can lead to unfavorable mode distortions during the propagation of light through the tapered region. In addition to that, once the fiber core of silica fiber shrinks to a certain diameter, it becomes extremely fragile. Therefore, tapering using a chemical etching technique is investigated in our work. Chemical etching of plastic fibers is very attractive because it has the potential for batch fabrication of a larger number of identical tapered regions. Acetone, de-ionized water and sand paper were used to taper the fiber. The chemical etching technique is repeatable and does not require high operator skill. Furthermore, the etching process is gradual, which makes it simpler to monitor the waist diameter physically or optically.

2.3 Fiber Optic Techniques for Sensing

Fiber optic sensors can be divided into intrinsic and extrinsic, depending on where the transduction between light and measurand takes place, in the fiber or outside it [Udd & Spillman, 1991]. Extrinsic sensors are used in real applications where the light leaves the fiber and are obstructed before going back into fiber optic system. It can be in the form of mirror, prism or bending effect by the fiber itself. The advantage of this sensor includes a great reduction in size around the sensing area and the removal of all electrical components [Tracey, 1991]. On the other side, the fibers have problems of being affected by dirt, dust, vibration and alignment [Tracey, 1991]. The intrinsic fiber can overcome this problem by changing the light within the fiber. Among the uses of intrinsic fiber covers phase modulation, polarimetric, change in speckle pattern, colour

modulation and distributed micro bending of the fiber to achieve of the attenuation of the light [Tracey, 1991].

Various fiber-optic based sensing techniques reported with designs in extrinsic and intrinsic sensor types can also be further classified. Among those are evanescent wave and refractive index which are discussed as below.

2.3.1 Evanescent wave sensor

Light propagate along a fiber is not only confined to the core region but also extends into the surrounding cladding region. This affects the total internal reflection (TIR) effect, which varies the light attenuation inside the fiber due to the changes in the condition of critical angle criterion [Palais, 2005]. At each point of TIR, the interference between the incident and reflected signals generates a wave which extends beyond the core of the optical fiber and penetrates into the cladding region [Messica, Greenstein and Katzir, 1996]. This creates an evanescent field with amplitude that decays exponentially with distance away from the core/cladding interface and follows the form,

$$E_z = E_0 \exp^{(zd^{\mathrm{p}})} \qquad (2.1)$$

where **dp** is defined as penetration depth of amplitude, **E** is defined as evanescent field and $\mathbf{E_0}$ is defined as initial value before it decayed to 1/e at the interface of core and cladding.

The equation of penetration depth also can be derived into an equation as below:-

$$\mathrm{dp} = \frac{\lambda}{2\pi n_{core}[sin^2\theta - \left\{\frac{n_{clad}}{n_{core}}\right)2\}]\ 1/2} \qquad (2.2)$$

where **λ** is the wavelength of the propagating signal in the optical fiber, **θ** is the angle of incidence normal at the interface and, n-core and n-cladding are the refractive indices of the fiber core and cladding respectively.

Various optical fiber configurations can be used for evanescent wave sensing. A common approach is replacing portion of original fiber cladding to modified cladding material (sensitive material), we called as a tapered fiber [Yuan and El-Sherif, 2003]. The tapered fiber cause the evanescent field to extend further away from the interface, hence enhancing the interaction between light and the target analyte [Yeo, Sun and Grattan, 2008]. Beside, U-bent of optical fiber also can be characterized as evanescent sensor type. One of the popular intensity modulation techniques involves bending the fiber to induce radiation losses. Radiation losses increase and the transmitted light decreases [Udd, 1991]. Thus, with interaction within fiber and target analyte, result of optical absorption, refractive index change or scattering information can be obtained.

The evanescent radiation power is dependent on the discontinuity in the core/cladding interface, the launch angle and the fiber dimensions. The methods used to increase the interaction between the evanescent field and environmental influences are side polishing, chemical etching, heat treatment and D-optical fibers [Bilro et al., 2012]. Furthermore, the combined effect of macro-bending and refractive index sensing in highly multimode unperturbed fibers affect the performance of sensors.

2.3.2 Refractive index sensor

Refractive index change is frequently demonstrated as an approach for EW sensing. The measuring or sensing of refractive index is one of importance scientific technique since the refractive index is a fundamental material property for which its accurate measuring is crucial in many cases. Any change in the optical or structural characteristic of the chemical, provokes a change in the effective index of the optical

fiber, changing its transmission properties [Khalil, Bansal and El-Sherif, 2004]. Owing to the broad measuring range as mentioned, there is a growing interest on optical fiber refractive index sensors. There have a great attractive in these types of sensor since they offer high sensitivity, and absolute detection, broad measuring range [Jha, Villatoro and Badenes, 2008; Elosua et al., 2006). Figure 2.2 shows the refractive index based on a tapered fiber coated with modified cladding sensitive material.

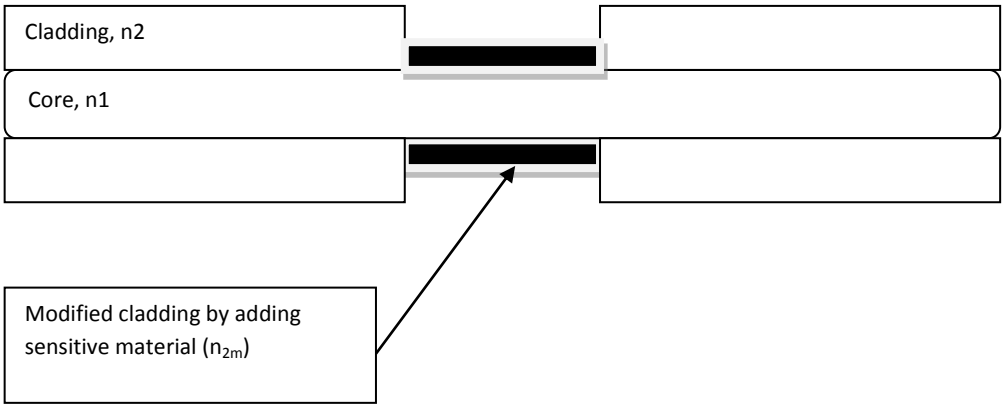

Figure 2.2:Structure of an intrinsic fiber-optic sensing part

The refractive index of the modified cladding material can be considered in two situations: a) having lower refractive index than core and b) having higher refractive index than core. Therefore, two basic types of fiber-optic intrinsic sensors can be designed according to the difference of refractive indices between the fiber core and cladding [Yuan and El-Sherif, 2003]. If the modified cladding, n2 has a lower refractive index than core n1 (n2<n1), the incident ray bends away from normal and greater than critical angle. Then the total reflection condition is met [Thyagarajan and Ghatak, 2007].

On the other hand, if modified cladding, n_2 has a higher refractive index than core n_1 ($n_2 > n_1$), the incident ray bends towards to normal and less than critical angle, part of the optical power is refracted into the cladding, and another part is reflected back

into the core (Elosua, 2006). The partial leaky-mode sensor is constructed based on the intensity modulation induced by the absorption of the refracted rays and evanescent field in the modified cladding [Yuan and El-Sherif, 2003].

Fiber-optic refractive index (RI) sensors have been widely researched in the fields of chemical sensor and biosensor in recent years. They become one of the most attractive technologies in recent years due to the advantages of the compact size, high sensitivity, multiplexing, and remote-sensing capabilities. In order to realize the optical fiber-based RI sensors, the evanescent wave is widely applied through various special fiber structures, such as tapered fibers, long period gratings, microstructure optical fibers, D-shape optical fibers, and bent optical fibers [Zhao et al., 2013]. To study the sensitivity of fiber optic evanescent field in detail, several experiment and investigations have been demonstrated with different fiber core diameter, bending radius of the probe and the refractive index of the fluid around the probe [Gupta, Dodeja, & Tomar, 1996].

2.4 Tapered fiber with sensitive layer for coating

Tapered fibers are widely used for sensing stress and pressure since 1980s [Gerdt et al. 1987; Mati et al, 2000]. Later this analysis were extended using coating functional for organic, inorganic [Shadaram et al. 1997; Arregui et al. 2000], biological samples [Golden et al. 1994; Corres et al, 2008; Gravina et al. 2009] and humidity [Bariain et al. 2000]. Tapered optical fiber has received much attention for sensing applications due to the characteristics of tapered fibers which allow a higher portion of evanescent field to reach outer environment and thus it is more sensitive to the physical changes of its surrounding. The coated tapered fiber changes optical properties in response to an external stimulus.

2.4.1 Overview on sensitive materials

To enhance the sensitivity of surrounding refractive index variation around the optical fibers, the evanescent field propagating in the fiber needs to be enhanced. Recently, a sensitive materials coating technique has been proposed and investigated to enhance the evanescent field in optical fibers for RI sensing [Zhao et al., 2013]. The behavior of sensitivity enhancement under different coating material and refractive index can be analyzed through the cladding being altered.

2.4.1.1 Graphene

Graphene is a one-atom thick sheet of carbon packed honeycomb two-dimensional lattice [Shan et al., 2009]. In graphite, atoms of carbon are bonded in two dimensions where 3 out of 4 valence electrons of each carbon atom are used in bond formation with 3 other carbon atoms. The 4^{th} electron of each carbon atom forms delocalized π–bond which spread uniformly over all carbon atoms. Graphene have two types of bonding. One of it is covalent bonding where the intermolecular are strong and pair of electrons is shared between atoms. This creates a stable balance where atoms share valence. Whereas, the other type of bonds are van der waals forces where the intermolecular are weak due to attraction and repulsion forces between molecules. Graphene sheets forms graphite by restacking due to this van der waals force [Li et al., 2008]. In addition to that, graphene is also a pure aromatic carbon system with an optical absorption beyond far infrared and electrical conductivity and charge carrier mobility surpass the most conductive polymers [Loh et al., 2010]. Figure 2.3 shows the FESEM image of the graphene.

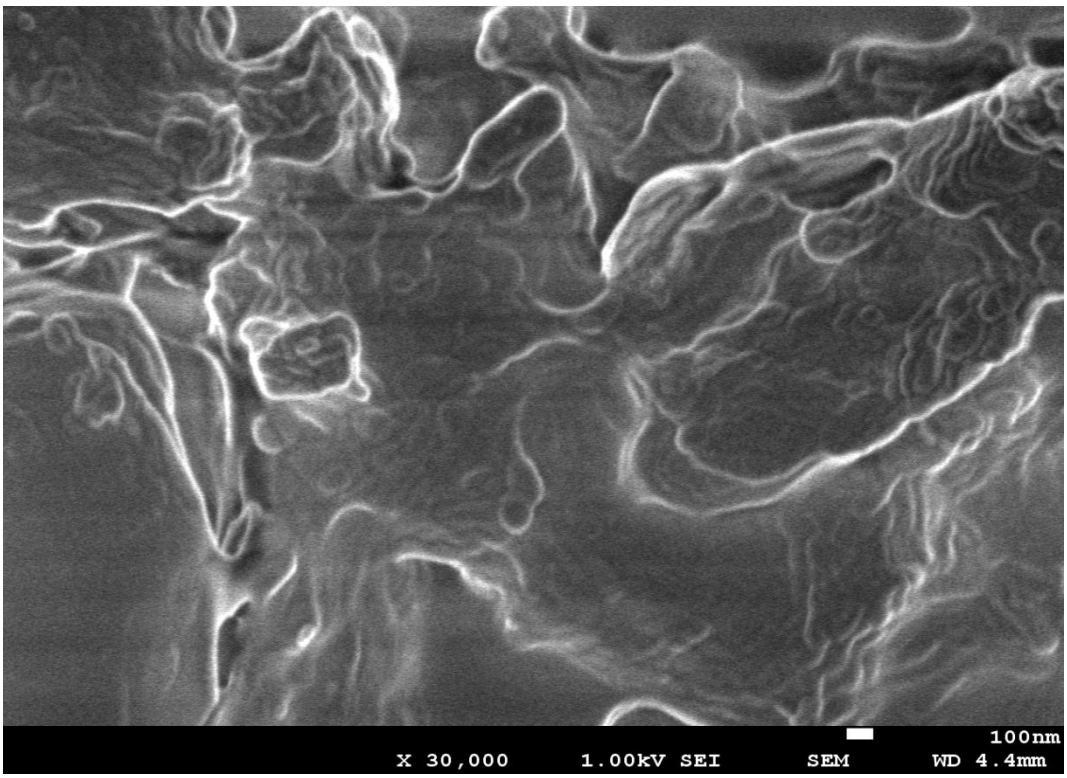

Figure 2.3:FESEM image of the graphene

Graphene was discovered by Andre Geim using simple Scotch tape method in 2004 [Loh et al., 2010] and created a revolution in condensed matter physics. In earlier days, graphene was well known for post-complementary metal oxide (CMOS) electronics due to high carrier mobility, high thermal and electrical conductivity [Loh et al., 2010]. Later graphene gave a breakthrough in chemistry due to its applications in optics, polymer composite and thin coating. Graphene has good potential applications in many fields such as nanoelectronics, nanocomposites, sensors, solar cells and liquid crystal devices [Allen at al., 2010; Li et al., 2008; Pumera, 2010]. Further research were done by Kuila and Shang for the applications in electrochemical devices due to high conductivity, fast heterogeneous electron transfer, good biocompatibility and large specific surface [Kuila et al., 2011; Shang et al., 2008].

The excellent conductivity and small band gap are favorable for conducting electrons from the biomolecular [Stankovich et al., 2006] and also high sensitivity

chemical sensors [Ao et al., 2008; Peres et al., 2006]. Furthermore, graphene can be easily obtained by chemical conversion of inexpensive graphite [Xu et al., 2008].

2.4.1.2 Carbon Nanotube

Carbon nanotubes have distinct properties due to strong demand in producing high selective, sensitive, responsive and cost effective for the next generation sensors. Carbon nanotubes sensors have excellent properties such as small size, high strength, high specific area and high electrical and thermal conductivity. Carbon nanotubes are formed by layer of graphite rolled up into a cylinder and the arrangement determine whether it is a single walled nanotubes (SWNTs) or Multi walled nanotubes (MWNTs). SWNTs have only one single layer of graphene cylinders and MWNTs have many layers [Sinha, Ma, & Yeow, 2006]. The MWNTs were developed by Iijama in 1991 [Iijama, 1991] and SWNTs were developed by Iijama, Ichihashi and Bethume in 1993 [Iijama & Ichihashi, 1993; Bethune at al., 1993] which invoke interest to many researcher.

Carbon nanotubes rolled up into a tube of diameter 1-10nm have good electro catalytic properties. It has good electrochemical sensing properties due to unique one-dimensional (1D) nature and lead to excellent conductivity. The biological function of carbon nanotubes invokes further research in biosensors and nanoprobes. The dielectric responses of the Carbon nanotubes are found to be highly anisotropic [Sinha, Ma, & Yeow, 2006]. The electronic transport in metallic SWNTs and MWNTs occurs without scattering over a long distance which is applicable for high current carrying [Sinha, Ma, & Yeow, 2006; Liang et al, 2001; Berger et al., 2003]. However the bending effect of carbon nanotubes may lead to reduction in conductivity and cause band gap opens upon twisting. Since that SWNTs have better shape of cylinder than MWNTs has lead to fewer defects and therefore it is more preferred over MWNTs for sensing [Sinha, Ma, & Yeow, 2006].

In recent years, SWNTs have been demonstrated as promising nanomaterials due to its hollow structure and applicable for chemical sensing [Kong et al., 2000; Chopra et al., 2003]. SWNTs can either be metallic or semiconducting and electrically conductor. Carbon nanotubes respond to light when there is a change in shape and cause current to be generated and the moves between electrodes [Stetter & Maclay, 2004]. The ongoing exploration on electrical, physical, chemical and mechanical properties contributes a wide range of applications such as nanoelectronics, sensors, field emission and electrodes. To date, CNTs have been utilized in biosensors in many forms such as probes [Woolley et al., 2000; Vo Dinh et al., 2000], filed- effect-transistor using a single semiconducting CNTs [Bradley et al., 2003; Star et al., 2003; Li et al., 2003], a random CNT network [Koehne et al., 2003; Koehne et al., 2004] and nanoelectrode array [Guiseppi,-Elie, Lei and Baughman, 2002; Azamian et al., 2002; Musameh et al., 2002]. Figure 2.4 shows the FESEM image of the SWNT embedded in PEO material.

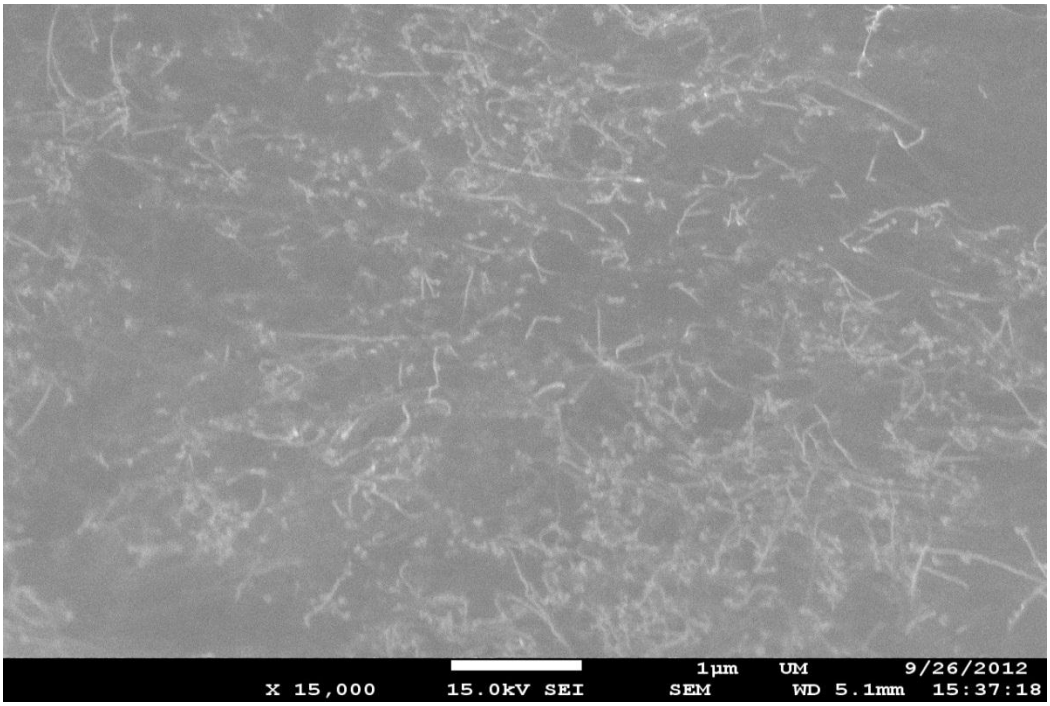

Figure 2.4:FESEM image of the PEO/SWNT

2.4.1.3 Zinc Oxide

Zinc Oxide is a vertile II-VI semiconductor used for numerous applications due to its distinctive optical, chemical and electrical properties [Zhang el at., 2005]. It becomes the focus of research in recent years especially for electronics and photonics applications. For instance, Zinc Oxide nanostructure materials could provide a suitable platform for developing high performance biosensor which is due to its unique properties such as high catalytic efficiency and strong adsorption ability. The direct wide band gap of 3.37eV, semiconductor Zinc Oxide is attractive for short light emitting devices [Yakimova et al., 2012].

The well-known Zinc Oxide with one-dimensional (1D) nanostructure such as nanowires and nanorods has also attracted much attention [Li et al., 2000; Yao, Chan & Wang, 2002; Banerjee et al., 2003]. Zinc Oxide nanorod and nanowire film have shown promising application in humidity sensors [Zhang el at., 2005]. The renewed interest in Zinc Oxide has also driven by the success in growth of single crystal, epitaxial layers and nanostructured with controlled properties [Yakimova et al., 2012]. Zinc Oxide can be prepared as thin films [Tompa et al., 2007], nanobelt [Pan and Wang, 2001], nanorods [Khranovskyy et al., 2010] and nanowires [Huang et al., 2001].

These nanostructures are applicable for designing biosensors, chemical sensors and humidity sensors. Nowadays, they become one of the most active research areas since Zinc Oxide is a very sensitive material with good selectivity as well as has outstanding specific surfaces [Yakimova et al., 2012]. Figures 2.5 (a), (b) and (c) show various structures of zinc oxide nanoparticles under FESEM.

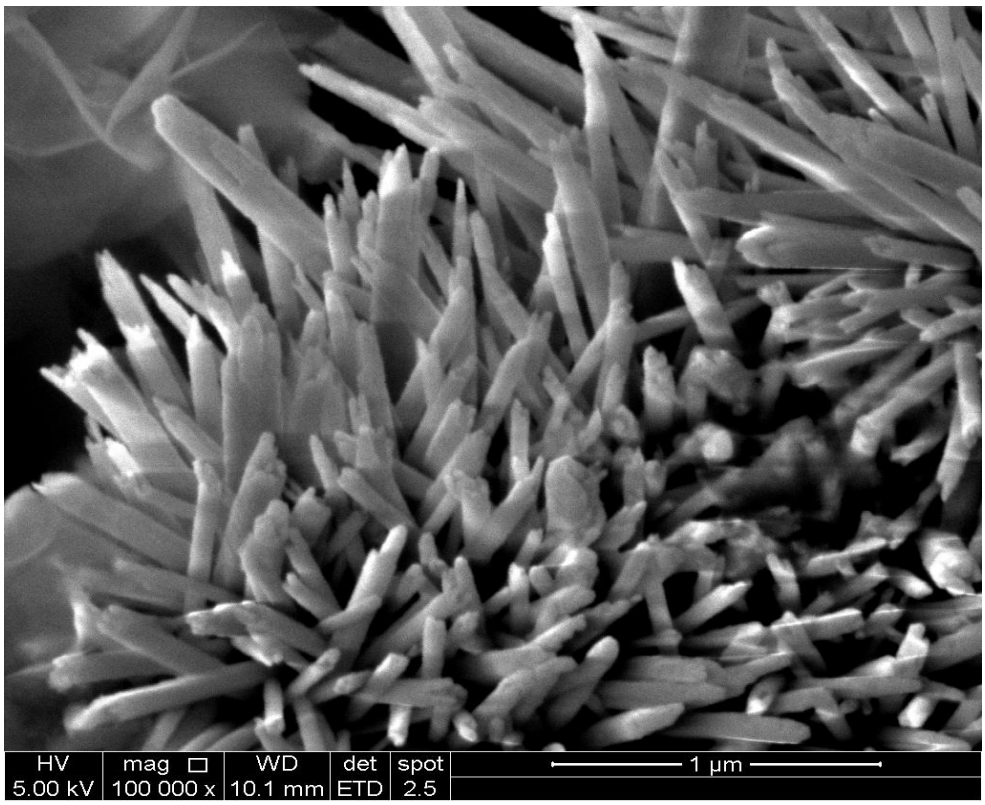
HV
5.00 kV
mag
100 000 x
WD
10.1 mm
det
ETD
spot
2.5
1 µm

(a)

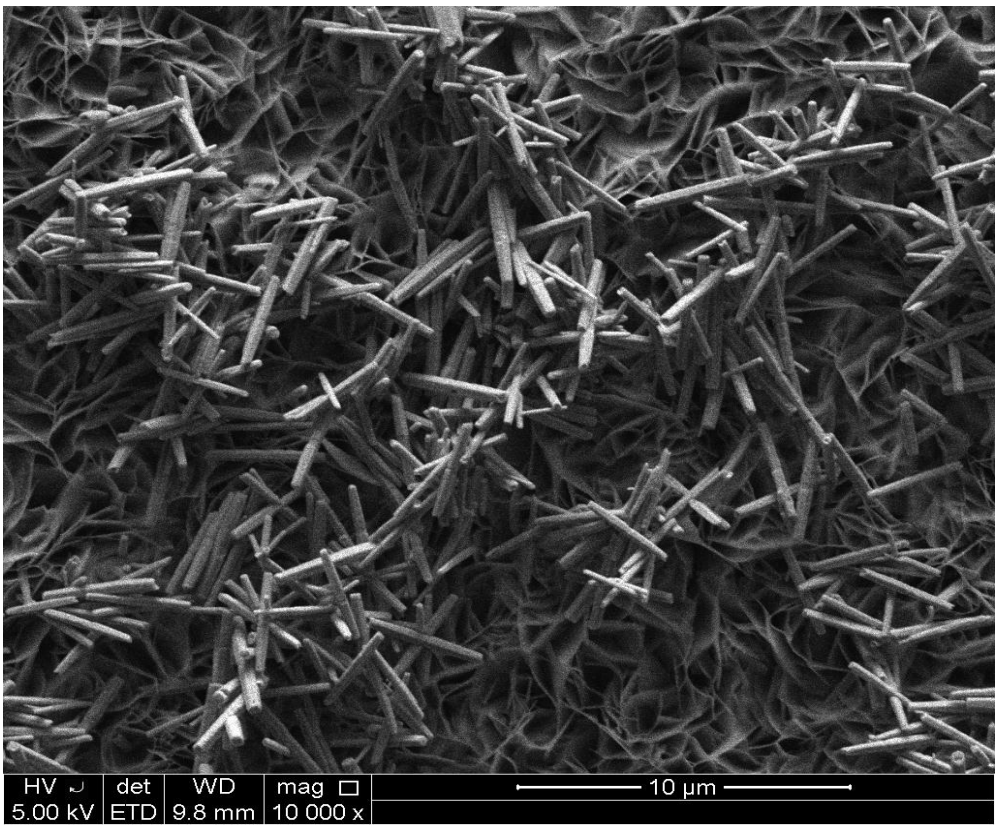
HV
5.00 kV
det
ETD
WD
9.8 mm
mag
10 000 x
10 µm

(b)

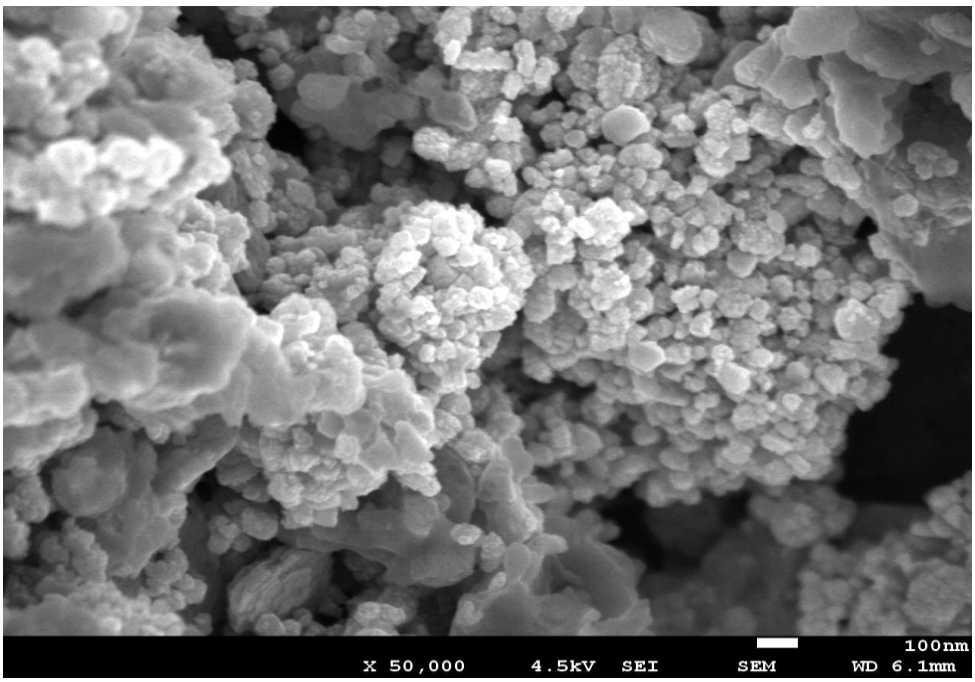

(c)

Figure 2.5:FESEM images for zinc oxide nanoparticles (a) rods (b) tubes and (c) flowers

2.4.1.4 Agarose Gel for use in humidity sensors

Currently, interest in studying about humidity sensor using POF is growing as due to advantages such as low cost, ease in handling and immunity from EMI [Muto et al.,2003]. If a mixture of swelling cellulose and hydrophilic polymer is placed as sensitive cladding layer of POF, it will cause a change in refractive index by attached water molecules. The transmission properties of tapered optical fibers have given a rise to numerous research studies for the application of sensors [Corres et al., 2006]. Stretching and waist radius reduction created in this region will cause the core/cladding interface to be redefined where the single mode fiber in the tapered region will act as multimode coupling [Corres et al., 2006]. This beating of modes in the taper very sensitive to external medium refractive index changes allowing its use in refractometry.

Agarose is considered a biopolymer, originating from a marine alga which is widely extended in the field of biochemistry for deoxyribonucleic acid (DNA) chain

separation [Kurihara et al., 1998, Bariain et al., 2000]. The gel is insoluble in water and easily deposited on the fiber and its porosity determines the quantity of water that the gel is capable of absorbing and operates as humidity sensor [Bariain et al., 2000]. The measurement environment requires sensors of extremely small size and insensitive to EMI. For these reason, optical fiber humidity sensor have an advantage over electronic sensors [Arregui et al., 2000]. This water containing gels are useful to monitor the humidity which involve the measurement of the refractive index. In the earlier work, the fabrication of sensors are based on hydrogels poly-N-vinyl methacrylate (poly-HEMA), poly-acrylamide, poly-N-vinyl pyrro-lidinone (poly-N-VP) and agarose have been used for the immobilization indicators on optical fiber. Hydrogels are materials formed by networks of crosslinked hydroplilic polymers. Among these agarose gives the best performance sensors [Arregui et al., 2003]. Later, humidity sensors based on refractive index changes of hydrogels with humidity and moisture measurement are further studied [Yeo, Sun, & Grattan, 2008]. Agarose was given special interest and been developed for the use of humidity sensor fabrication as a generic rule that the bigger the pore size, the higher the dynamic range and shorter response time. The agarose gel with a response time of around 90s with a range of application from 10-100% of Relative humidity (RH) was reported for light source 1310/1550nm [Arregui et al., 2003]. In another research, agarose gel transduction layer is intergrated with a periodic silicon nitride film to form a sensitive optical resonance structure whereas the agarose gel humidifies the resonance wavelength shifts [Lee et al., 2007].

Agarose gel is easy to apply, stable and insoluble in water [Lee et al., 2007]. In addition to that, agarose has a 3D net structure containing large pores with average pore size of ~100nm [Upcroft & Upcroft, 1993]. The agarose absorb water from ambient air and its refractive index changes with humidity [Lee et al., 2007]. In dry state, the refractive index of Agarose is larger and it operates as leaky mode for higher order

mode. In humid air it swells and its refractive index decreases and higher order mode are guided and the intensity of transmitted light increases [Mathew et al., 2007]. Barian et al. also reported in the fabrication of optical fiber humidity sensor using a hydrophilic gel (agarose) operates within the range of 30-80% of RH and a variation of up to 6.5dB of the transmitted optical output.

2.4.1.5 Hydroxyethylcellulose (HEC)

Hydroxyethylcellulose/ polyvinylidenefluoride (HEC/PVDF) composite is a class of polymeric material known for its excellent water absorption properties, as potential material for the sensing approach. A tapered POF coated by a polymer blend of HEC/PVDF composite can be used to sense the change in relative humidity. The coated tapered fiber changes optical properties in response to an external stimulus. The fiber with the composite act as an effective refractive index cladding that allow more light to be transmitted in hydrates state. The HEC/PVDF composite-coated sensor increases the sensitivity of the humidity sensor due its ability to swell in a humid atmosphere resulting in a drop in its refractive index below that of the core and thus allowing more light to be transmitted from the tapered fiber.

2.5 Plastic optical fiber (POF)

POF is a multimode fiber with a large diameter, flexible and durable characteristics, which is fabricated from different types of polymers such as PMMA. POF have several advantages over glass optical fiber (GOF) as far as sensing application is concern. POF based sensors can be realized using a simple and inexpensive techniques and equipment. New advance in technologies allows POFs to be sensitized to various measurands or have its optical and physical properties modified to enhance its sensing performance. The advantages of POFs in medical environment is

that the fiber must withstand rough handling and can easily be replaced if broken as usual as being immunity to electromagnetic interference, intrinsic safe and chemically immune. In addition to that POFs is easy to polish and cut into defined angle.

High possibility to obtained various POF sensors based on EW technique by replacing a portion of cladding with a sensitive material. The change of surrounding refractive index affects the optical properties of the fiber. The sensitivity of the sensor can be increased by further reduction of POF diameter, which increases the evanescent field penetration of guided modes. The sensitivity can be further increased by coating the tapered or etched POF with suitable sensitive materials. The POF based refractive index sensors are suitable for applications related to quality control, food industry, industrial processing, environment contamination, simple architecture, aircraft, chemical and biological analysis, biomedical applications and specimen detection. POF sensor is well known to its characteristics such as compactness, high sensitivity, in-situ measurements and immunity to external electromagnetic interference.

2.6 Methodology

This thesis focuses on developing various POF sensors for chemical, biomedical and environmental applications. A brief description of the methodology adopted in the investigation and experimentation of this work is described as follows:

Development and Analysis of Multimode Tapered PMMA Fiber Sensors

The fabrications of tapered PMMA fibers were produced by the heat and pull technique and chemical etching technique. Furthermore, this POF based sensor does not require sophisticated materials can easily be automated and can be operated at room temperature and varying pressure conditions. Then, a comparative study aimed to investigate the external liquid refractive index sensitivity in heat-pulled and chemical-

etched tapers is presented. The sensor measures the output voltage of the detector that is influenced by the interaction of the evanescent wave produced in the tapered cladding and the solution which forms its surrounding. Finally, we report on an investigation into the impact on sensitivity of electrostatic interactions between the PMMA core and the analyte solution, particularly focusing on its interaction with electrolytes and non-electrolytes.

Analysis of multimode tapered PMMA fiber sensors for uric acid detection

A new choice of refractive index sensor, featuring several advantages and potential, which is a simple intensity modulated fiber optic sensor using PMMA plastic tapered fibers with sensitive coating materials. Here, the sensitivity of tapered fibers coated with graphene, single walled carbon nanotube and zinc oxide were investigated. Variations of refractive index were achieved through the use of different concentration of uric acid solution. Subsequent performance analysis allows the identification of the experimental dependence of the surrounding refractive index sensitivity on the three different sensitive coating materials.

Analysis of multimode tapered PMMA fiber sensors for relative humidity detection

A new choice of refractive index sensor, featuring several advantages and potential, which is a simple intensity modulated fiber optic sensor using PMMA plastic tapered fibers with sensitive coating materials. Here, the sensitivity tapered fibers coated with agarose gel, hydroxyethylcellulose/ polyvinylidenefluoride (HEC/PVDF) composite and zinc oxide were investigated. Subsequent performance analysis allows the identification of the experimental dependence of the surrounding refractive index sensitivity on the three different sensitive coating materials.

Chapter 3

Development and Analysis of Multimode Tapered PMMA Fiber Sensors

3.1 Introduction

The developments of novel optical fiber devices have become the central focus of optical fiber researches in the past recent years. One in particular are the invention of tapered optical fibers that have led to various impressive applications in microscale and nanoscale photonic devices [Bariain et al., 2000; Bariain et al., 2000; Eggleton et al., 2001; Brambilla, Finazzi and Richardson, 2004; Polynkin et al., 2005; Stiebeiner, Garcia-Fernandez and Rauschenbeutel, 2010; Tian et al., 2011]. These types of waveguides have found profound applications in the fields of biochemical, biomedical, environmental and different area sensors etc. The sensitivity of the fiber is enhanced by enabling the interaction between the evanescent fields of the sensing fibers with the analyte under investigation. They are able to guide light at visible and infrared wavelengths with low loss [Shi et al., 2006; Wolchover et al., 2007].

To date, comprehensive researches have been conducted on the fabrication, characterization and use of tapered silica-core fibers. However, one practical limitation of using silica-core fibers is that when a section of cladding is removed, the exposed fiber core is very fragile and brittle which further imposes restrictions on sensor design and handling. Alternatively, POFs such as PMMA may be used as an alternative to silica-core optical fibers due to their comparatively cheaper price, and considerably more flexible structure. POF possess a strain limit of over 50%, whereas the silica-based fibers are fragile and will break under a strain of only 5%. The simplicity of use owing to the simple set-up involved and the absence of expensive termination tooling, make

POF an attractive alternative for tapered fiber sensors. Furthermore, they possess good tensile strength, higher numerical aperture, load resistance and lower bend radius limits than standard fibers [Gravina, Testa and Bernini, 2009].

The common practice for fiber tapering is by heat-pulling or chemical etching. The heat-pulling method can be achieved by using flame, electric arc or high power laser. Lasers have been reported to produce excellent tapers [Liao et al., 2010]. This method is a relatively simple process, however extra assemblies need to be made for precise control of the heating and pulling process. This is especially crucial as the PMMA used in the POF have low ductility and higher tendency for uneven melting leading to uneven profiles [Gravina, Testa and Bernini, 2009]. Tapers may also be produced with a more controllable profile by chemical etching. The cladding of POF can be chemically removed using a solution of acetone in water [Merchant, Scully and Schmitt, 1999]. The main difference between these two techniques is the index profile of the fabricated tapers. Tapers would have different optical characteristics as the cladding is removed through chemical etching but preserved in heat-pulled tapers. Light will travel through the core/air interface in the waist of the chemically-etched taper, compared to the core/cladding/air structure in the waist of the heat-pulled taper.

Likewise, refractive index sensors also gained a tremendous interest recently. They can be developed based on the EW field interaction [Villatoro, Monzon-Hernandez and Talavera, 2004; Polynkin et al., 2005; Xu, Horak and Brambilla, 2007; Wang et al., 2011] with a chemical concentration whose RI is measured. Compared to silica tapered fibers, the evanescent field absorption in surrounding solutions is not only governed by the absorption coefficient and refractive index of the solution. The sensitivity of the fiber to evanescent field absorption is also significantly affected by the surface charge interactions between the fiber and the molecule/ions in the solution [Lye at al., 2005].

In this chapter we report the fabrication and applications of tapered PMMA fibers produced by the heat and pull technique and chemical etching technique. The focus of most literatures is on the feasibility of silica tapered fiber optic sensors, leaving the PMMA tapered fiber much to be explored. The main advantages of PMMA compared to silica fibers are their ease of handling, mechanical strength, disposability and easy mass production of components and system. Then, a comparative study aimed to investigate the external liquid refractive index sensitivity in heat-pulled and chemical-etched tapers is presented. The sensor measures the output voltage of the detector that is influenced by the interaction of the evanescent wave produced in the tapered cladding and the solution which forms its surrounding. Finally, we report on an investigation into the impact on sensitivity of electrostatic interactions between the PMMA core and the analyte solution, particularly focusing on its interaction with electrolytes and non-electrolytes.

3.2 Taper Fabrication

The fabrication of tapered PMMA fiber is briefly discussed and demonstrated in this chapter. Tapering of the fiber can be done by local heating and subsequent pulling or by chemical etching. The fiber used is a step indexed multimode fiber with an overall cladding diameter of 1 mm, core diameter 980µm, a numerical aperture of 0.51 and an acceptance angle of 61°.

3.2.1 Heat Pulling Method

Local heating and subsequent pulling of an intact fiber has been well accepted as a successful method to produce silica tapered optical fibers [Sumetsky, Dulashko and Hale, 2004; Shi et al., 2006]. However, only few examples of heat-pulled POF tapers

have been reported [Gravina, Testa and Bernini, 2009; Xue et al., 2007; Arrue et al., 2008]. Figure 3.1 illustrates the fabrication set-up for the tapered fiber used in this study, which was produced using a heat-pulling method. The tapering of the fiber was done by first placing the PMMA fiber between two fiber holders which were fixed onto a translation stage on one end and a fixed stage on the other end. The built-in butane burner was fixed at the centre of the PMMA fiber before it was pulled slowly at one end to reduce the fiber waist diameter to the desired length. As a precautionary step, the flame should be clean and the burning gas flow should be well controlled. Steps should be taken to reduce any air convection flow that may cause breakage in the fiber during the drawing process. After the taper was made, the profile of the taper was measured using a microscope. Inset compares the image of the original and tapered fiber. It is observed that the fiber diameter is reduced from 1 mm to 0.187 mm by this technique. Figures 3.2(a) and (b) show the microscope image of the un-tapered and tapered PMMA fiber with a cladding diameter of 1 mm and 0.187 mm, respectively.

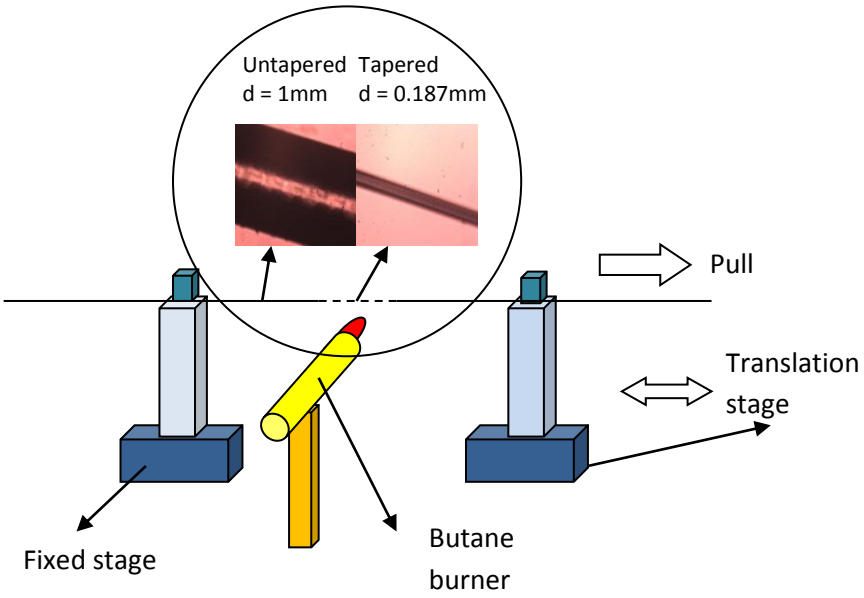

Figure 3.1:Schematic diagram of the tapering process of the PMMA fiber. Inset compares the original and tapered fibers.

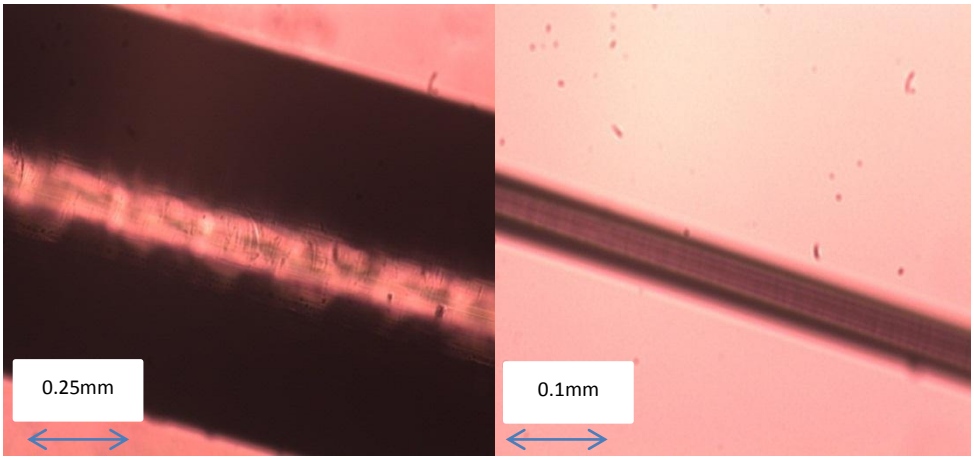

(a) (b)

Figure 3.2:Microscopic image of the (a) un-tapered PMMA fiber (with diameter of 1 mm) and (b) Tapered PMMA fiber (with diameter of 0.187 mm) with heat pulling method.

3.2.2 Etching

Chemical etching of plastic fibers is very attractive because it has the potential for batch fabrication of a larger number of identical tapered regions. Acetone, de-ionized water and sand paper were used to taper the fiber. The acetone solution was applied to the PMMA using a cotton bud. The PMMA fiber was then neutralized with de-ionized water. The milky white surface around the outer cladding of the plastic fiber was removed using sand paper for about 8-10 seconds. This process was repeated until the tapered fiber has reached the desired stripped region length of the waist diameter.

A microscopic is used to identify any areas of cladding remaining in place and hence can be removed by repeating the entire process. The core will remain in its original condition even with the exposure to the solvent provided that the exposure times are limited as described. The use of fresh solvent for each process ensures a much more consistent taper surface finish across the samples provided. Figures 3.3(a) and (b)

show the microscope image of the un-tapered and tapered PMMA fiber with a cladding diameter of 1 mm and 0.45 mm, respectively.

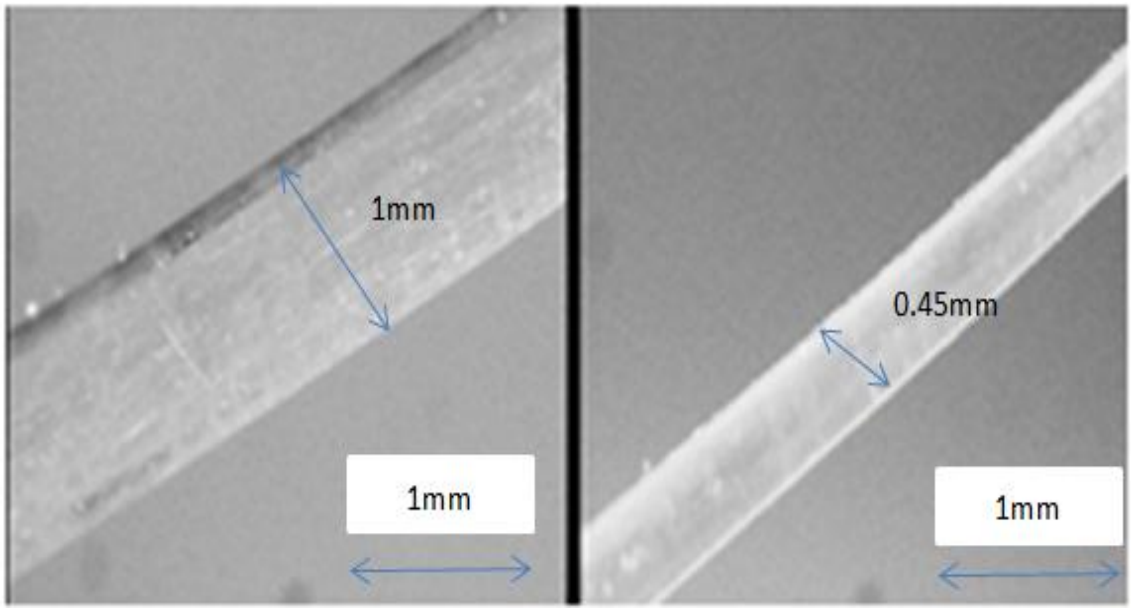

(a) (b)

Figure 3.3: Microscopic image of the (a) un-tapered PMMA fiber (with diameter of 1 mm) and (b) Tapered PMMA fiber (with diameter of 0.45 mm), with etching technique

The described process of the chemical etching technique is repeatable and does not require high operator skill. Furthermore, the etching process is gradual, which makes it simpler to monitor the waist diameter physically or optically, by measuring the transmitted power [Lovely et al., 1996]. Existing heat-pulling tapering methods for PMMA fiber have difficulty producing large numbers of identical tapered region without exact monitoring of the processes [Gravina, Testa and Bernini, 2009]. On the other hand, the heat-pulled tapers show very little surface roughness which an advantageous trait for subsequent processing, e.g. metal is coating.

3.3 Sensing of Sodium Chloride Refractive Index

The detection and measurement of small variations of refractive index within a chemical solution has recently received considerable amount of attention due to its association with the concentration of molecules. A refractive index sensor with better detection limits is capable in detecting smaller concentrations of molecules. Optical detection methods of refractive index variations enable a label-free detection of liquid molecules which does not require the liquid analyte to be marked with fluorescent dyes. Numerous fiber-based refractive index sensors have been reported based on fiber interferometers [Li et al., 2010; Park et al., 2010; Xia et al., 2010], fiber Bragg gratings [Iadicicco et al., 2004, Guo et al., 2009; Meng et al., 2010; Wong et al., 2011] and tapered fibers [Tai and Wei, 2011; Liao et al., 2011; Wang et al., 2011]. This kind of fiber sensors exhibit good performance but some optical set-ups are complicated and involve tedious fabrication processes. Furthermore, tapering of silica fibers make them more fragile and difficult to handle.

In the work presented here, a new choice of refractive index sensor, featuring several advantages and potential, which is a simple intensity modulated fiber optic displacement sensor using PMMA plastic tapered fibers. Here, the sensitivity of heat-pulled and chemical-etched tapers as a liquid refractive index sensor was investigated. Variations of refractive index were achieved through the use of different concentration of sodium chloride solution. Subsequent performance analysis allows the identification of the experimental dependence of the surrounding refractive index sensitivity on the two different tapering techniques, namely the heat pulling and chemical etching technique.

3.3.1 Experimental set-up

Two different tapers were fabricated, one from each of the heat pulling and chemical etching technique. Due to the ease in fabrication control of the chemical etching technique, it was used to produce a taper that resembled the dimensions of the heat-pulled taper. A fixed dimension ratio of 0.45 was used for both tapers based on the report by Beres et. al [2011] using tapering machine stating that PMMA fiber optic tapers with waist diameters in the range of 0.40 mm to 0.50 mm showed good sensitivity to refractive indexes variations whereas those with waist diameters above 0.55mm and below 0.30mm did not demonstrate substantial sensitivity. Furthermore, smaller waist diameters are associated with an increased tendency for fiber breakage, especially during the fabrication of the chemical-etch taper. This selected taper ratio results in a waist diameter and length of 0.45 mm and 10 mm, respectively. The experimental setup for sensing different liquid refractive index based on various concentration of sodium chloride solution is shown in Figure 3.4. The setup consists of a He-Ne light source, an external mechanical chopper, a highly sensitive photo-detector and a lock-in amplifier. The light source operates at a wavelength of 633 nm (red region) with an average output power of 5.5 mW, beam diameter of 0.80 mm and beam divergence of 1.01 mRads. The light source was set at a modulation frequency of 113 Hz before being launched into the tapered plastic fiber that was placed in a petri dish filled with the test solution. The photo-detector was placed at the other end of the fiber to convert the received optical signal into an electrical signal that was then fed into a lock-in amplifier together with the output frequency from the mechanical chopper (which acts as the reference signal for the lock-in amplifier). The reference signal from the chopper will match the input electrical signal from the photo detector. This will allow a very sensitive detection system that will remove the noises generated by the laser source, photo-detector and the electrical amplifier in the photo-detector. The light

source, the plastic fiber in the petri dish and the detector were aligned in a straight line so as to minimize bending losses that may occur in the plastic fiber, and this will increase the accuracy of the measurement. The tapered fiber which acts as a sensor probe was first immersed in de-ionized water to measure the output power of a 0 % sodium chloride concentration, followed by sodium chloride concentrations from 2 % to 12 %. The measurements were carried out for sodium chloride solutions (+80 mesh, ≥ 98% reagent grade, Sigma-Aldrich, USA) with concentrations of 1, 2, 3, 4, 5 and 6 g per 50 ml of de-ionized water. The unit of concentration is wt %. As the concentration of sodium chloride increases from 2% to 12%, the refractive index of the solution also increases from 1.336 to 1.353. The refractive index measurements were obtained using Mettler Toledo-RE4OD Refractometer. During the experiment, the error caused by temperature was taken to be negligible and the temperature was kept constant at 25^{o}C.

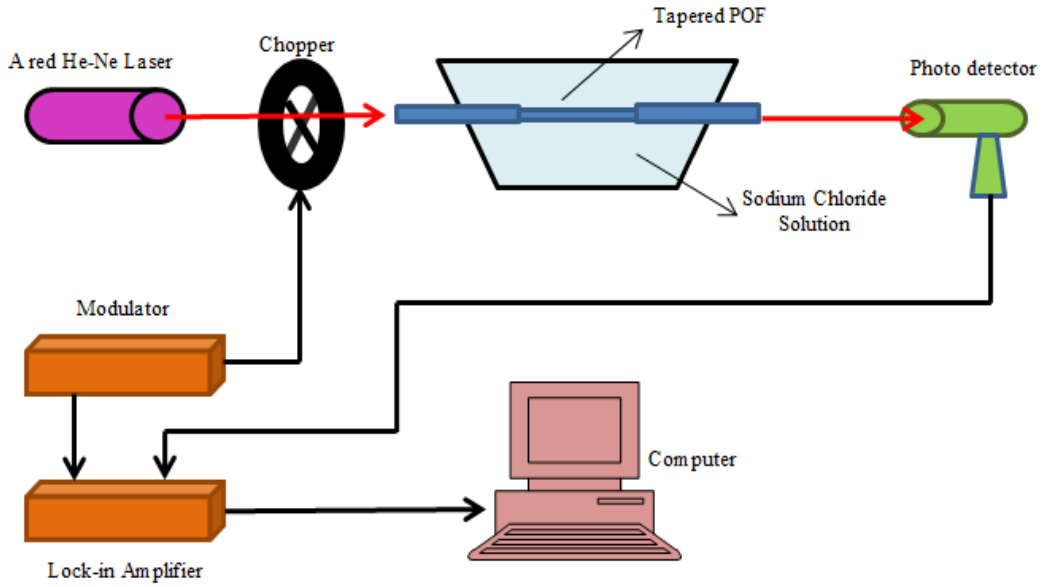

Figure 3.4: Experimental set-up for the sodium chloride refractive index sensor using a tapered PMMA fiber.

3.3.2 Performances of the sensor

The experimental results for both heat-pulled taper and chemical-etched taper are presented in Figures 3.5 and 3.6, respectively. Figure 3.5 shows the variation of the transmitted light from the tapered PMMA fiber against the concentration of sodium chloride solution. As shown in the figure, the output voltage from the photo-detector, which is proportional to the transmitted light linearly, increases as the concentration of the sodium chloride solution increases for both of the tapers. The sensitivity however is higher for the chemical-etched taper which is obtained at 0.0036 mV / % compared to the 0.0019 mV / % of the heat-pulled taper. Figure 3.6 shows the variation of output voltage with the refractive index of the sodium chloride solution. The output voltage increases from 0.056 mV to 0.075 mV for the heat-pulled taper and from 0.261 mV to 0.296 mV for the chemical-etched taper in response to the increase in the refractive index from 1.3325 to 1.353. Both of the slopes show a good linearity of more than 99%. Another important observation is that the sensitivity of the chemical-etched taper is about 1.8 times greater than that of the heat-pulled taper. By using the chemical-etched taper, the transfer function for the output voltage versus sodium chloride refractive index is obtained as follows

$$y = 2.095x - 2.5367 \tag{3-1}$$

and the following transfer function is obtained when the heat-pulled taper is used

$$y = 1.1213x - 1.442 \tag{3-2}$$

Since the diameter of the cladding in the tapered region has been reduced or completely removed as in the case of a chemical-etched taper, the refractive index of the

external medium works as passive cladding and can influence the amount of power loss as the signal passes through the tapered region. The plastic multimode fiber used in this experiment has a core and cladding refractive index of 1.492 and 1.406, respectively and the index difference between the core and cladding is relatively larger compared to those of silica multimode fiber. When immersing the tapered fiber into the sodium chloride solutions with concentration starting from 0 % to 12 %, the index difference decreases since the refractive index of sodium chloride solutions are higher than water (1.3333). The solution index also increases as the concentration increases. The refractive index profile in the heat-pulled taper is changed since both the fiber core and the cladding are affected by the heating and pulling process. However, the fiber core of the chemical-etched taper is unaltered. In contrast to chemical-etched fibers, the thinning of the core in the heat-pulled taper can lead to unfavorable mode distortions during the propagation of light through the tapered region.

This however contradicts with the transmission property of multimode fibers developed by other researchers [Guo and Albin, 2003] whereby an increase in the external medium index increases corresponds to a larger energy fraction of evanescent wave and ultimately decreases the transmission output. This is attributable to the partial charge separation in the PMMA leading to a net negative charge at the surface of the fiber where the oxygen atoms within the PMMA monomer sit. Hence, the electrostatic interaction between external ions and the PMMA core will affect the outcome of the sensor. The sodium chloride solutions (NaCl) used in this experiment is an ionic compound and a strong electrolyte. It dissolves in water completely forming Na^+ and Cl^- and the electrostatic interaction between the Na^+ ions with the surface of the fiber takes place. This results in a lower energy fraction of evanescent wave hence more Na^+ ions will be attracted to the fiber surface and consequently less power leakage. To further support this argument, several other electrolytes and non-electrolytes were used and

subsequently analyzed in the next section to observe the similarity in the trend of the sensor response.

The sensor performance is summarized in Table 3.1. For the chemical-etched taper, the sensitivity is obtained at 2.095 mV/RIU with a good linearity of more than 99 % for a refractive index range from 1.3325 to 1.33530 RIU. The limit of detection for the sensor is 718.8 x 10^{-6} and is sufficiently stable with a standard deviation of 0.58 %. For the heat-pulled taper, the sensitivity is obtained at 1.1213 mV/RIU with a good linearity of more than 99 % for a refractive index range from 1.3325 to 1.33530 RIU. The limit of detection for the sensor is 825.1 x 10^{-6} and has a higher standard deviation of 1.7 %. Throughout the experiment, a fix quantity of liquid solution was placed in the petri dish and the corresponding output voltage was measured by a lock-in amplifier which provides accurate measurements even though the signal is small compared to thousands of times larger noise sources. Furthermore, a well-regulated power supply is used for the red He-Ne laser and this minimizes the fluctuation of source intensity. These results show that the proposed sensor is applicable and useful for liquid refractive index detection especially in the industry due to the ability of the sensor to provide real time salinity detection and control of various mixtures continuously.

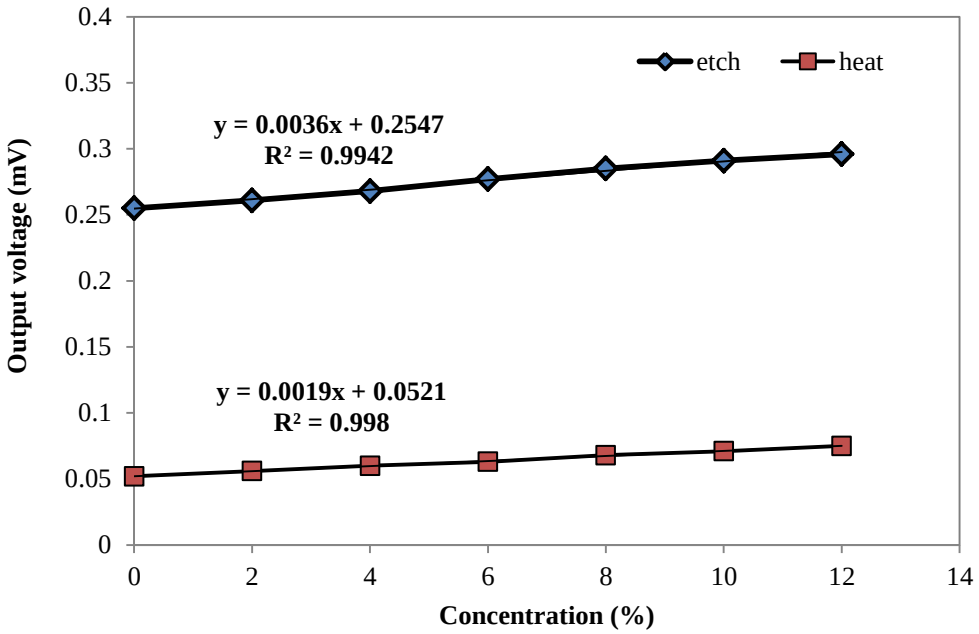

Figure 3.5:Output voltage against sodium chloride concentration.

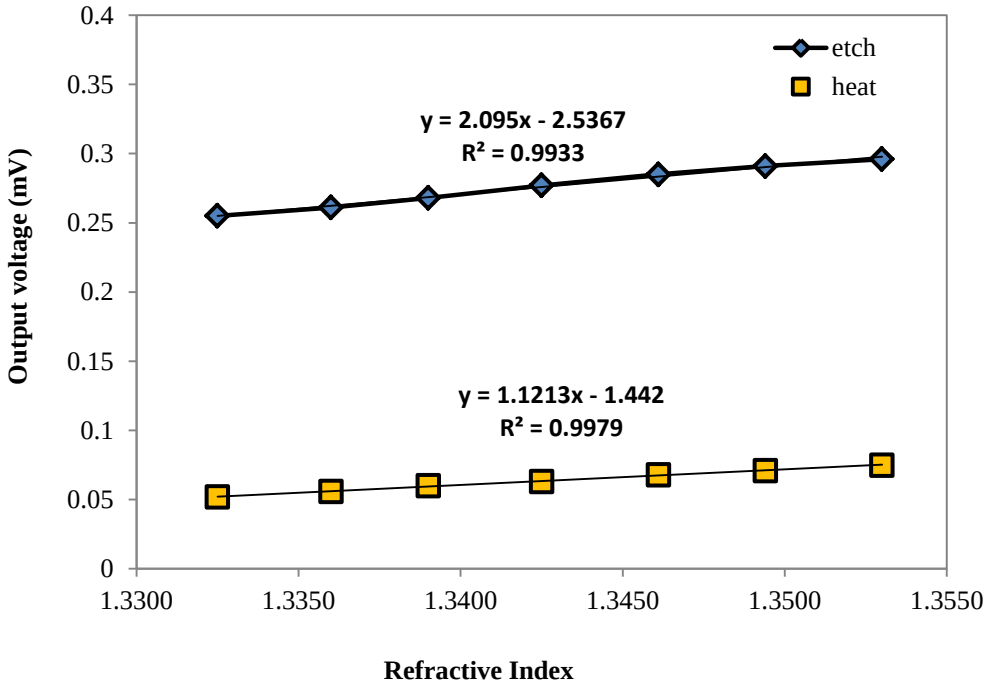

Figure 3.6:Output voltage against refractive index of sodium chloride concentration.

Table 3.1:The performance of the sodium chloride refractive index sensor

Parameter	Etch	Heat
Sensitivity	2.095 mV/RIU	1.1213 mV/RIU
Linear Range	1.3325 – 1.3530 RIU	1.3325 – 1.3530 RIU
Linearity	More than 99 %	More than 99 %
Standard Deviation	0.01 mV (0.58 %)	0.001 mV (1.7 %)
Limit of detection	718.8 x 10^{-6} RIU	825.1 x 10^{-6} RIU

3.4 Analysis of PMMA Optical Fiber Sensitivity for use as a Chemical Concentration Sensor in Electrolyte and Non-Electrolyte Solutions.

Most of the studies of optical based chemical sensors use solely the refractive index variation of the chemical under scrutiny. However, the surface charge interactions between the fiber and the ions in electrolyte solutions also play a role in the sensor response. Chemical can be classified as electrolytes and non-electrolytes depending on the dissociation of their ions in solutions [Ebbing and Gammon, 1999]. Electrolyte is defined as a substance containing free ions that make the substance electrically conductive. High proportion of solute dissociates to form free ions in strong electrolytes. Common types of electrolytes are group I and II salt solution when in the form of ionic solution and molten. Electrolytes are an important mineral in human body which affects the amount of water in body, acidify blood (pH) and muscle function [Zibaii et al., 2010]. Sodium chloride is an ionic compound and is an example of a strong electrolyte. Electrolyte is an ionic compound that can conduct electricity by

producing free ions in water. Electrical conductivity of an electrolyte is directly proportional to the concentration of the solution used because the higher the concentration of the solution, more free ions will be produced in the solution. Ionic compounds are held together by electrostatic forces (the charges of the respective ions Na^+ and Cl^- attracted to each other) and can easily break down and produce ions in water [Ebbing and Gammon, 1999]. Sodium chloride has been used by researchers for measuring salinity [Cong et al., 2002; Grossman, Yongphiphatwong and Sokol, 2005; Gentleman and Booksh, 2006; Skinner and Lambert, 2011]. Salinity sensors are becoming important recently for numerous applications such as in the detection of saltwater intrusion in drinking water and the measurement of salinity levels in seawater desalination to supplement industrial water use in large coastal cities.

Another example of a strong electrolyte is calcium nitrate ($Ca(NO_3)_2$), which is a high quality fertilizer. Calcium nitrate dissolves readily in water and goes into solution as Ca^{2+} and NO^{3-} ions. This unique combination offers many benefits to growers. Nitrate ions as supplied by calcium nitrate are immediately available for plants to use. By timing calcium nitrate application to match the crops growth rate, nitrogen efficiencies can be maximized and the risk of nitrate leaching will be minimized. Nitrates increase the plant uptake of nutrients such as magnesium, calcium and potassium while ammonium nitrate depresses their intake. The calcium ions displace sodium in the soil profile, which improves water and oxygen infiltration in soils. This is important to improve plant growth and crop quality in term of longer storage, skin presentation and disease tolerance [Ho et al., 2009; Visconti, De Paz and Rubio, 2010].

Non electrolytes are compound composed of molecules that do not conduct electricity when dissolved in molten or aqueous solutions. Non electrolytes do not ionize in aqueous solution into positive and negative ions and hence fail to work as a conductor. They are normally covalent compounds and mainly organic in nature.

Examples of non-electrolytes are glucose and sucrose. Monitoring of glucose level in food is crucial for diabetic patients to prevent the disease from becoming proliferative. It is also important to all cells from bacteria to humans as a primary source of energy, photosynthesis and fuels for cellular respiration [Wolfbeis, 2004]. Enzymatic methods have been traditionally used to measure glucose concentration and provide point sample results [Zen and Lo, 1996; Deng et al., 2008; Nagaraja et al., 2012].

Sucrose is the main transportable sugar in plants and is composed of fructose and glucose. Sucrose can be found in many crops, but sugar cane is the most popular and widely used source of sucrose. Sugar and other chemical forms of sugar can cause tooth decay, obesity, coronary heart disease, glycation, and also diabetes. The formation of high concentrations of acid may appear on the surface of a tooth, which may then lead to tooth demineralization. Sucrose is also converted to dextran that glues the bacteria to the surface of a tooth. Therefore, sucrose could initiate Streptococcus mutants to stick strongly and which then would avoid most rigorous attempts at removal. In other words, the dextran pose as the reserve food supply for the bacteria that causes tooth decay. Several studies have been made on the influence of sucrose on tooth decay [Newburn and Frostell, 2009; Cheng et al., 2009; Carucci and Casini, 2012].

In this section, a chemical concentration sensor is proposed and demonstrated using a tapered plastic multimode fiber. The aim of this work is to evaluate the output response of the proposed sensor on electrolytes and non-electrolytes. Calcium nitrate and sodium chloride solutions were used to represent electrolytes whereas glucose and sucrose solutions were used to represent non-electrolytes. The proposed sensor measures the output voltage of the detector that is influenced by the interaction of the evanescent wave produced in the tapered region and the solution which forms its surrounding. Subsequent performance analysis allows us to identify experimental

dependence of the sensor response due to the electrostatic interaction between electrolyte ions and the PMMA fiber.

3.4.1 Experiment

Chemical-etched tapers were used due to the ease in fabrication control and increased sensitivity. The fabrication method in section 3.2.2 was repeated to obtain 21 tapered fibers having stripped region lengths of 10 mm in average and waist diameters within the 0.35 mm to 0.65 mm range which were then used to experimentally identify the optimum taper ratio.

The similar set-up as in Figure 3.4 was used to observe the sensor response for two electrolyte (namely calcium nitrate and sodium chloride) and two non-electrolyte (glucose and sucrose) liquid samples of similar refractive indices. The set-up consists of a light source, an external mechanical chopper, a PMMA tapered fiber, a highly sensitive photo-detector, a lock-in amplifier and a computer. At first, the PMMA tapered fiber in the Petri dish is straightly aligned to the detector to minimize bending losses that may occur in the tapered fiber. The tapered fiber which acts as a sensor probe is first immersed in de-ionized water to measure the output power of a 0 % liquid concentration (pure de-ionized water), followed by sodium chloride concentrations from 2 % to 12 %. All the other liquid solutions follow this process order. The measurements were carried out for calcium nitrate solutions (Calcium Ntrate Tetrahydrate grade AR, m. Wt 236, 15g/mol, Friendemann Schmidt Chemical, Australia), sodium chloride solutions (+80 mesh, ≥ 98% reagent grade, Sigma-Aldrich, USA), glucose solutions ((D (+) - Glucose (C6H12O6 g/mol), John Collin Corporation, United Kingdom)) and sucrose solutions ((D (+) - Saccharose ($C_{12}H_{22}O_{11}$, g/mol), ≥ 99.5% reagent grade, Sigma-Aldrich, USA)) with concentrations of 1, 2, 3, 4, 5 and 6 g per 50 ml of de-ionized water. The refractive index measurements of the liquid solutions were obtained

using Mettler Toledo-RE4OD Refractometer. The effect of the tapered fiber arrangements on the performance of the sensor was also investigated. The straight tapered fiber was bent to form a u-shape and knot where the same process was repeated for measuring sodium chloride and calcium nitrate solution concentrations.

3.4.2 Performance of the sensors

At first, the experiment was carried out to study the variation of the sensor sensitivity against the different diameter of PMMA plastic fiber ranging from 0.35mm to 0.65mm. The result is shown in Figure 3.7, in which the optimum sensitivity of the sensor is obtained when the taper diameter is around 0.45 mm. This agrees with the findings reported by Beres et al. [2011] and henceforth was used throughout the remaining experiments.

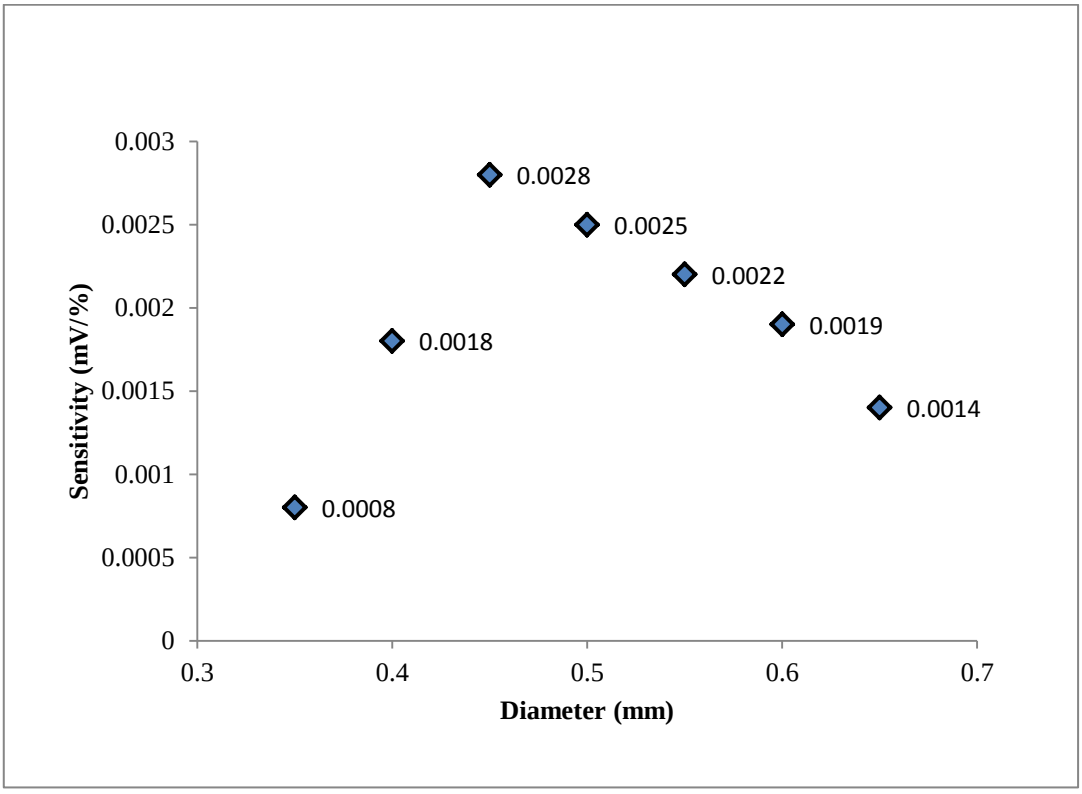

Figure 3.7:Diameters of fiber against sensitivity (calcium nitrate)

The experiment was then carried out to study the variation of the transmitted power against the different calcium nitrate concentration as presented in Figure 3.8. The figure shows that the slope of the plot is positive and the experimental data points are fitted very well (more than 99% linearity), by a linear function as follows

$$y = 0.0028x + 0.6531 \quad (3\text{-}3)$$

The transfer function demonstrates that the sensitivity of the measured output voltage to calcium nitrate concentration increases as the concentration is increased. This is because calcium nitrate is a strong electrolyte hence permitting electrostatic interaction between the positive ions and the tapered surface. As a result, the power leakage from the tapered region to the surrounding is reduced. The refractive indices of the calcium nitrate solution concentrations were obtained at 1.3334 – 1.3452 for the 2% - 12% calcium nitrate concentrations implying that the output voltage is proportional to the refractive indices of a liquid solution which contradicts with the transmission property of multimode fibers developed by Guo & Albin [2003].

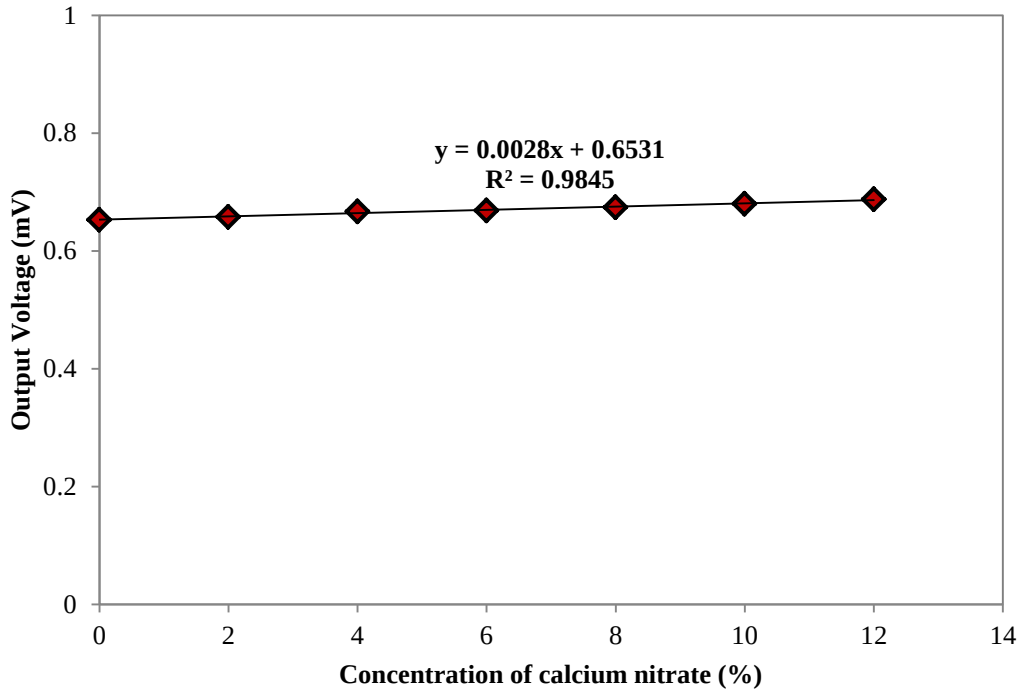

Figure 3.8:Output voltage against calcium nitrate concentration.

Figure 3.9 shows the output voltage from the tapered PMMA fiber against sodium chloride concentrations. Similarly, it is found that an increase in sodium chloride concentration can be detected by an increase in the output power because the sodium chloride solution is also a strong electrolyte where the amount of Na^+ ions being attracted to the surface of the fibre also increases as the concentration increases. The output voltage increases linearly with the concentration with sensitivity of 0.0023mV/wt.% and a good linearity of more than 99%.

The following transfer function is obtained

$$y = 0.0023x + 0.1191 \quad (3\text{-}4)$$

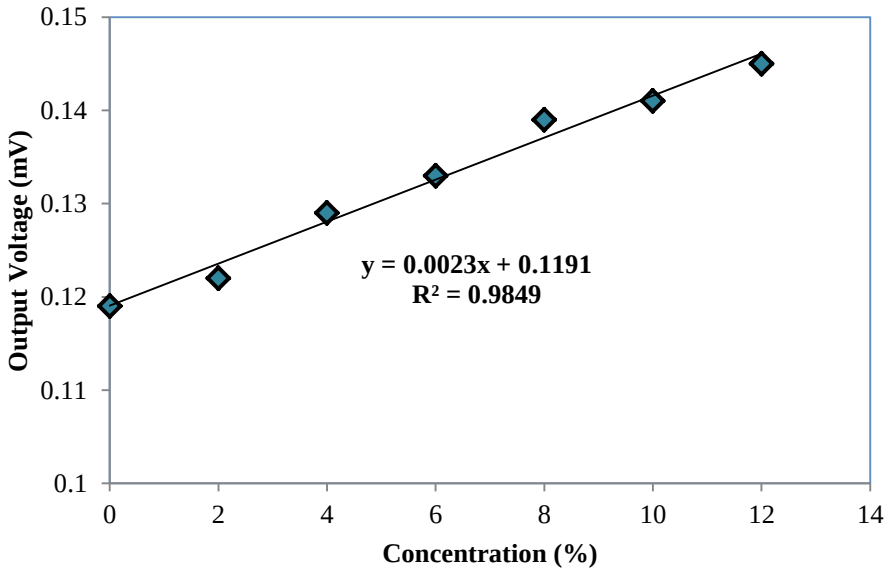

Figure 3.9:Output voltage against sodium chloride concentrations.

The refractive index of the sodium chloride solution concentrations varies from 1.336 to 1.353 as its concentrations increases from 2% to 12%. The result is within the similar range of the 2% -12% calcium nitrate solution concentrations.

Figure 3.10 shows the output voltage against glucose concentrations. It is shown that the output voltage is inversely proportional to the increment of glucose concentration which is opposite to the trend obtained from the calcium nitrate and sodium chloride solutions. This is attributed to the non-electrolyte nature of the chemical. Therefore, no electrostatic interaction occurs [Ebbing and Gammon, 1999] since the glucose does not change into ions even though it dissolves in water. As the concentration of glucose increases, the refractive index increases and as a result the output voltage decreases since the energy fraction of evanescent wave gets larger. The refractive indices of the glucose solution concentrations were obtained within 1.336 to 1.353 for the range of glucose concentrations within 2% to 12%. The plot of Fig. 3.10 shows the sensitivity of the glucose sensor is obtained at 0.0013mV/wt.% with a

linearity of more than 92% and limit of detection of 0.94%. The following transfer function is derived

$$y = -0.0013x + 0.052 \quad (3\text{-}5)$$

A similar sensor response is also observed for sucrose concentration sensor as depicted in Figure 3.11. A linearly inverse relationship is obtained as sucrose is also a non-electrolyte. The refractive indices of the sucrose solution concentrations were within 1.335 to 1.352 for the increasing sucrose concentrations of 2% to 12% (which also falls within the range of the other solutions examined earlier). The sensitivity is obtained at 0.0391mV/wt.% with a linearity of more than 98% and limit of detection of 1.25%. The following transfer function is obtained

$$y = -0.0391x + 1.5661 \quad (3\text{-}6)$$

The data presented in Figures 3.8 – 3.11 give rise to observable trends in sensor response relative to ionic properties of a chemical solution. The fact that the slope of the sensor response can have either sign for calcium nitrate, sodium chloride, glucose and sucrose solutions of similar refractive indices supports the contention that the sensor does not sense the refractive indices alone but rather is sensitive to the ionic nature of the solute.

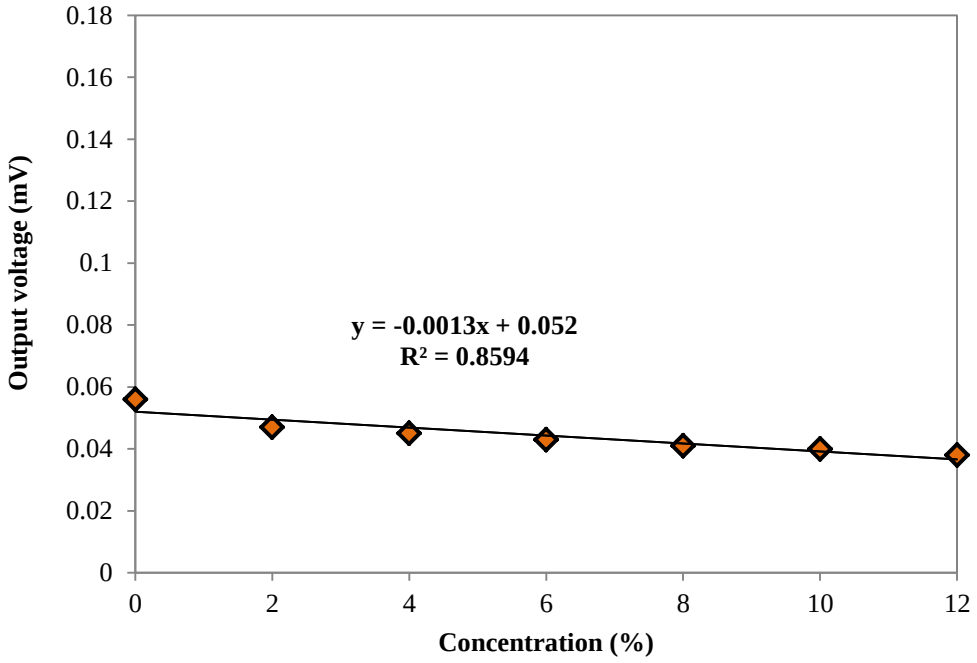

Figure 3.10:Output voltage against glucose concentrations.

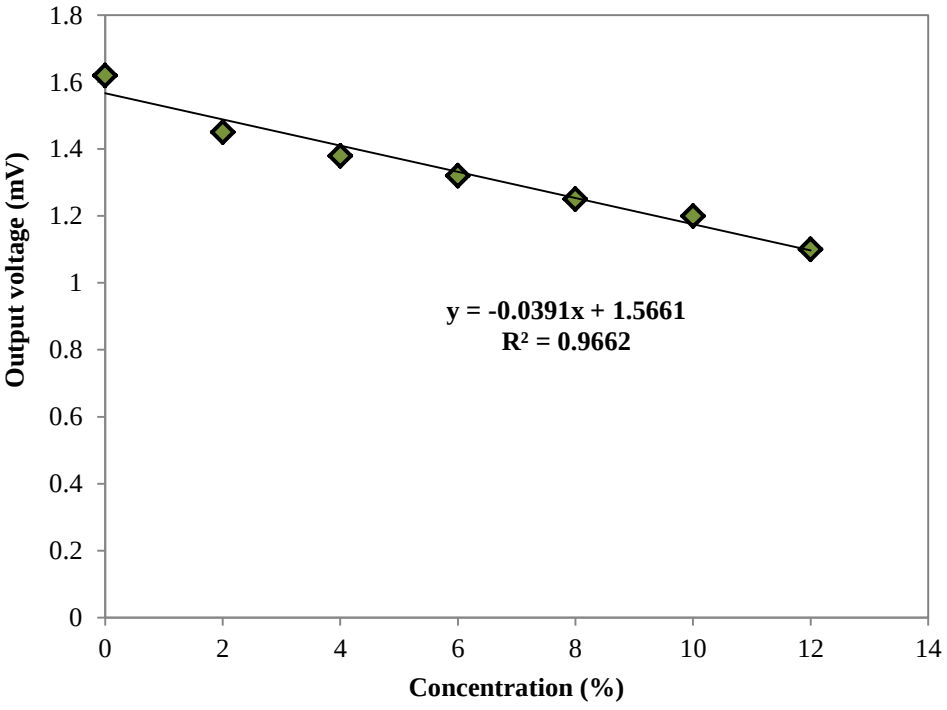

Figure 3.11:Output voltage against sucrose concentrations.

3.5 Effect of probe arrangement on the performance of the proposed PMMA based chemical sensors.

The effect of the probe arrangement on the performance of chemical sensor is investigated in this section. The similar experimental setup as in Figure 3.4 was used to observe the sensor response for two electrolyte (namely calcium nitrate and sodium chloride) liquid samples of similar refractive indices. In the experiment, the tapered fiber diameter is fixed at 0.45 mm. The set-up consists of a light source, an external mechanical chopper, a PMMA tapered fiber, a highly sensitive photo-detector, a lock-in amplifier and a computer. At first, the PMMA tapered fiber in the Petri dish was straightly aligned to the detector to minimize bending losses that may occur in the tapered fiber. The tapered fiber which acts as a sensor probe was immersed in both solutions at various concentrations ranging from 0 wt.% to 12 wt.%. The experiment is then repeated for other cases where the straight tapered fiber is bent to form a U-shape and a knot shape for comparison purposes. During the experiment, the errors caused by temperature are taken to be negligible and the temperature is kept constant at 25°C.

Figure 3.12 shows the output voltage from the tapered PMMA fiber against sodium chloride concentrations for 3 different arrangements of probes. As shown in the figure, the output voltage increases as the concentration of sodium chloride increases for all probes. The highest sensitivity of 0.0022mV/% is obtained for the straight tapered fiber with a linearity of more than 99% and limit of detection of 0.96%. The limit of detection is calculated by dividing standard deviation with the sensitivity to shows that the system is more efficient. It is noted that the straight, u-shape and knot shape of PMMA tapered fiber sensor experience an increase in voltage due the number of ions in the solution which turns it to be more conductive [Ebbing and Gammon,1999; Guo and Albin 2003; Rahman et al., 2011]. The bending effect of fiber induces loss in both the u-shape and knot shape tapered fiber. The highest loss is obtainable with the knot tapered

fiber as more bending loss occurs for this type of configuration [Kude and Khairnar, 2008; Khijwania and Gupta, 1999; Beres et al., 2011].

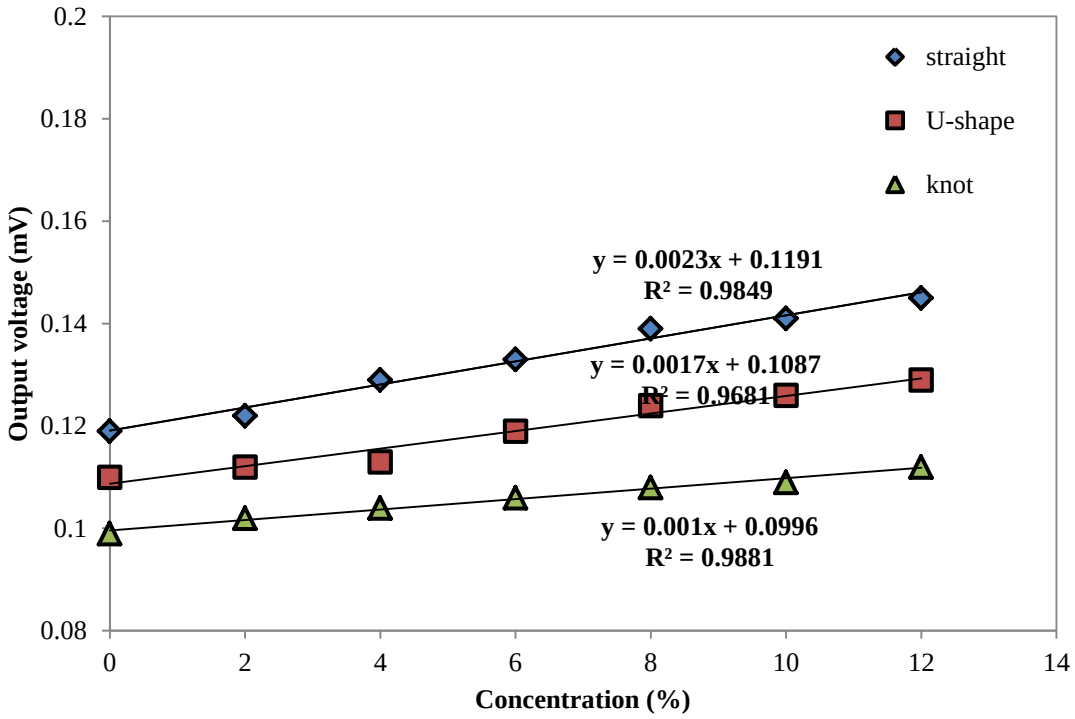

Figure 3.12: Output voltage against sodium chloride concentration at various tapered fiber arrangements.

The performance of sodium chloride concentration sensor is summarized in Table 3.2 for straight, u-shape and knot-shape tapered fiber. For the u-shape tapered fiber, the sensitivity is obtained at 0.0017mV/% and the slope gives a linearity of more than 98% for a 1.00% limit of detection. The result can be represented by the following transfer function;

$$y=0.0017x+0.1087 \quad (3\text{-}7)$$

For the knot shape tapered fiber, the sensitivity is obtained at 0.001mV/% with a linearity of more than 99% for a 1.29% limit of detection and thus it has the following transfer function

$$y=0.0001x+0.0996 \quad (3\text{-}8)$$

Overall, the sensor is observed to be sufficiently stable with a standard deviation of 1.86% for straight tapered fiber, 1.42% for U-shape tapered fiber and 1.05% for knot-shape tapered fiber.

Table 3.2:The performance of the tapered plastic fiber sensors with various probe arrangements (Sodium Chloride).

Parameter	**Straight**	**Bend**	**Knot**
Sensitivity (mV/%)	0.0023	0.0017	0.001
Linear Range (%)	0 – 12	0 – 12	0 – 12
Linearity (%)	> 99	> 98	> 99
Standard Deviation (mV)	0.0022 (1.86 %)	0.0017 (1.42 %)	0.0013 (1.05 %)
Limit of detection (%)	0.96	1.00	1.29

Figure 3.13 shows the variation of the transmitted light from the tapered plastic fiber against the concentration of calcium nitrate solution for three different tapered fiber arrangements; straight, u-shape and knot. As shown in the figure, the output voltage from the photo-detector, which is proportional the transmitted light linearly

increases as the concentration of the calcium nitrate solution increases for all arrangements. It gives a linear increase in output voltage against concentration. The sensitivity is obtained at 0.028mV/% and the slope gives a good linearity of more than 98% for a 1.05% limit of detection for the straight fiber. For the u-shape fiber, the sensitivity is obtained at 0.0013mV/% and the slope gives a linearity of more than 96% for a 1.30% limit of detection. While for the knot shape fiber, the sensitivity is obtained at 0.0016mV/% with a linearity of more than 76% for a 1.07% limit of detection. Therefore, the transfer functions for u-shape and knot shape sensors are derived as

$$y=0.0013x+0.2608 \tag{3-9}$$

and

$$y=0.0016x+0.1975 \tag{3-10}$$

respectively.

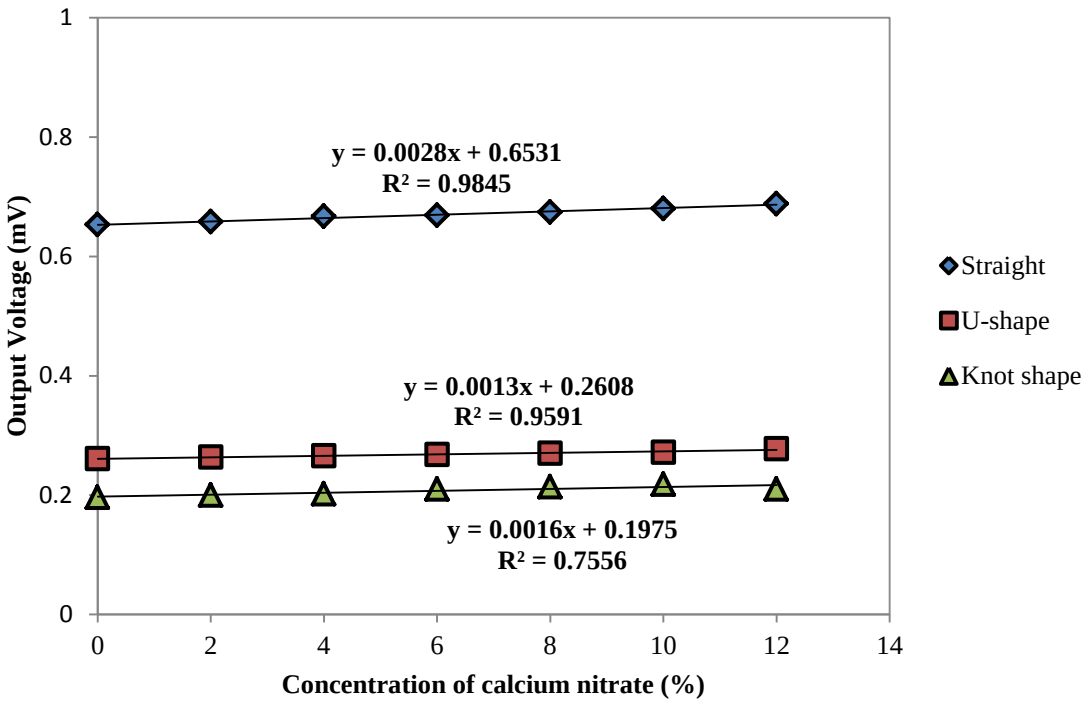

Figure 3.13:Output voltage against calcium nitrate concentration at various tapered fiber arrangements.

The sensor performance at the optimum tapered fiber diameter of 0.45 mm is summarized in Table 3.3 for straight, u-shape and knot arrangements respectively. Overall, the sensor is observed to be sufficiently stable with a standard deviation of 0.5% for straight fiber, 0.68% for U-shape fiber and 0.78% for knot arrangements. These results show that the proposed sensor is applicable and useful for chemical detection especially in the detection of calcium and nitrate ions level. The results also show that the dissociation ability of the ions within the test solution plays an important role on the output performance. The ability of the sensor to provide a good sensitivity without the need of highly sensitive control electronics and its simple setup are attractive traits for chemical sensing applications.

Table 3.3:The performance of the tapered plastic fiber sensors with various probe arrangements (Calcium Nitrate)

PROBE/PARAMETER	**STRAIGHT**	**U-SHAPE**	**KNOT**
Sensitivity	0.0028mV/%	0.0013mV/%	0.0016mV/%
Linear Range	0-12%	0-12%	0-12%
Linearity	More than 98%	More than 96%	More than 76%
Standard Deviation	0.003mV[0.5%]	0.0017[0.68%]	0.0017[0.78%]
Limit of Detection	1.07%	1.30%	1.07%

The physical configuration of the optical fiber and surface charge interaction between fiber and solutions significantly affects the sensitivity of the fiber to evanescent

field (Lye et al., 2005). Reduction of the fiber size increases the evanescent field penetration of guided modes (Barlett et al., 2000). Fiber made from PMMA will have a net negative charge at the surface of the fibre (Lye et al., 2005). This fiber surface interacts with the calcium nitrate solution by attracting the positive ions due to electrostatic charge interaction. This interaction forms a thin layer which enlarges the pathway for signal to pass through. The sensitivity of the fiber is influenced by the interaction length, bending effect and electrostatic interaction between different concentration of solution and the PMMA (Lye et al., 2005).

Reversibility of the results is another important factor in the operation of any sensor system, so in the next study, this parameter was tested for the reported system. The results of the output measurement as a function of concentration were recorded for two different runs and the results were compared for both sodium chloride and calcium nitrate solution and demonstrated in figures 3.14 and 3.15, respectively. As can be noticed from figure 3.14, the maximum difference between the two runs is about ±0.02mV, which is acceptable for a full-scale output of 0.145mV while from figure 3.15, the maximum difference between the two runs is about ±0.01mV, which is acceptable for a full-scale output of 0.688mV.

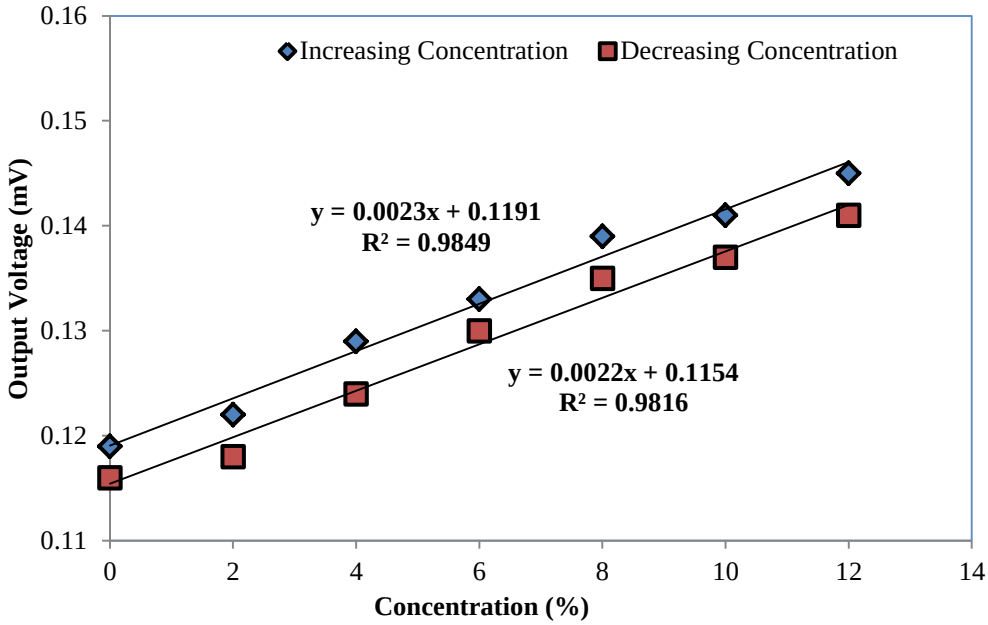

Figure 3.14:The reversibility of the results obtained for two different runs (Sodium Chloride Solution)

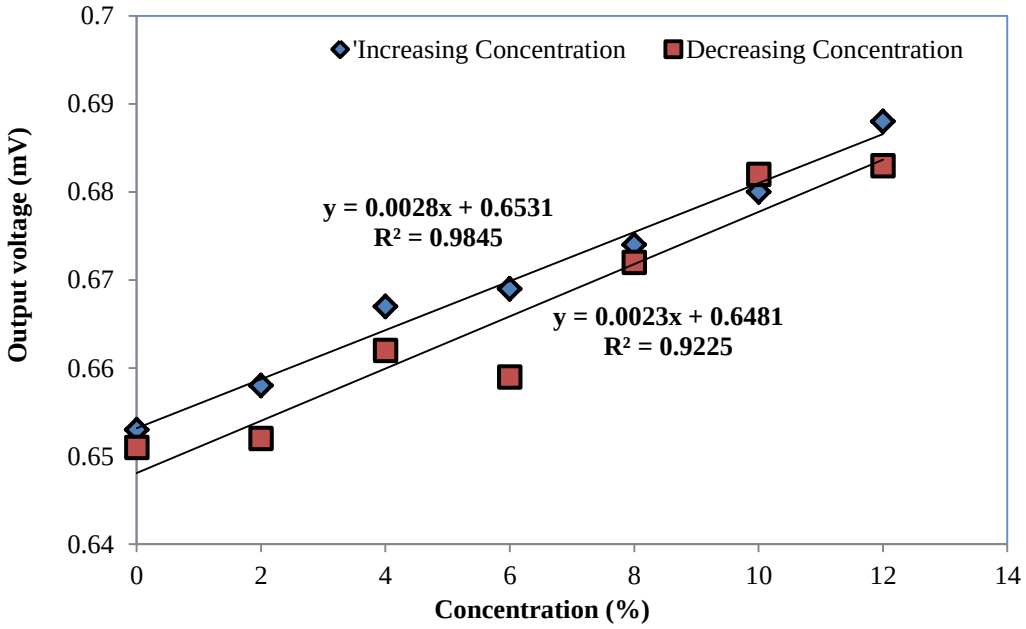

Figure 3.15:The reversibility of the results obtained for two different runs (Calcium Nitrate Solution)

3.6 Summary

The fabrications of tapered PMMA fibers were firstly demonstrated based on the heat-and-pull technique and chemical etching technique. The sensors were demonstrated to measure the refractive index of the external liquid using a probe, which is obtained on the two techniques. It is found that chemical-etched taper provides better performance compared to heat pulling method. The repeatability of the etching process in terms of taper diameter and its superior sensitivity has led to its further use in several set-ups as evanescent field sensors. Various evanescent field absorption sensors are developed for various electrolyte and nonelectrolyte solutions using the PMMA tapered fiber probe. The results show that the dissociation ability of the ions within the test solution plays an important role on the output performance. The sensitivity of the fibers to a liquid analyte is influenced by the polarity of the electrolyte owing to electrostatic interactions between the ions within the electrolyte and the negative surface charge residing on the surface of the fiber core.

The reduction of the fiber size increases the evanescent field penetration of guided modes [Barlett et al., 2000]. Fiber made from PMMA have a net negative charge at the surface of the fiber [Lye at al., 2005]. The fiber interact with electrolyte to attract the positive ions due to electrostatic charge and form a thin layer which enlarge the pathway for signal to pass through. The sensitivity of fiber is influenced by the taper diameter, bending effect and electrostatic interaction between different concentration of solution and the PMMA. The highest sensitivity was obtained for the straight tapered fiber.

Therefore, the proposed sensor provides numerous advantages such as simplicity of design, low cost of production, higher mechanical strength and easier to handle compared to silica fiber optic. The effect of chemical etching, size of fiber for better sensitivity, bending effect and refractive index of the solvent on the sensitivity of the

sensor were reported successfully. Results shows that tapered fiber enable to increase the conductance of fiber and applicable as a chemical sensors.

Chapter 4

Analysis of Multimode Tapered PMMA Fiber Sensors for Uric Acid Detection

4.1 Introduction

Optical fibers are currently abundantly available for various applications ranging from transmission medium, which covering a wide spectral range and sensors. The fiber sensor researches are focusing in many new areas such as gases and vapors sensing, medical and chemical analysis, molecular biotechnology, marine and environmental analysis industrial production monitoring, bioprocess control, salinity and the automotive industry [Guo and Albin, 2003; Wolfbeis, 2004; Golnabi et al., 2007; Kude and Khairnar, 2008; Rahman et al., 2011. As discussed in earlier chapters, tapered optical fibers attract many interests especially for sensing applications. This is due to a higher portion of evanescent field travels inside the cladding in the tapered fiber and thus the travelling wave characteristics become more sensitive to the physical ambience of its surrounding [Rahman et al., 2011]. The interest on tapered multimode fiber is also increased since it is mechanically stronger and also easier to manufacture compared to that of single mode one. Therefore, it was demonstrated previously as a chemical sensor with a simple setup [Guo and Albin, 2003].

Optical fiber consists of a cylindrical core and surrounded with cladding. The core is generally doped to make its refractive index slightly higher than the refractive index of cladding. This resulted in light propagating with total internal reflection (TIR) consisting two components: the guided field in the core and the exponentially decaying evanescent field in the cladding. In a uniform-diameter fiber, the evanescent wave field decays to almost zero within the cladding. Therefore the lights do not interact with the

surroundings. If the cladding of the fiber is reduced or removed, the evanescent field can interact with the surroundings [Leung, Shankar, and Mutharasan, 2007].

If the cladding of the fiber is removed, the optical output of the fiber is then a measure of the changes in magnitude of the evanescent field. Tapering will not only exposes the evanescent field to the surrounding but also increases the evanescent field magnitude and penetration depth [Leung, Shankar, and Mutharasan, 2007]. Taper sensitivity depends on the mode coupling, which can be modified when depositing new layers of material or sensitive material onto the fiber. At the same time, fiber optic RI sensors have been widely researched in the field of chemical sensor and biosensor [Zhao et al., 2013]. Refractive index sensing stands as one of the most important techniques in the development of highly sensitive sensors which is immune to external electromagnetic interference [Guzman-Sepulveda et al., 2013].

Plastic Optical fiber (POF) offers some advantages such as ease of handling, flexibility, low cost test equipment, visible wavelength operating range and high numerical aperture. Even though POF fiber causes higher loss when compared to Glass optical Fiber (GOF) in tranmission, the effect can be beneficial in design of the fiber sensors. POFs operate successfully at wavelengths 650 to 1300nm with the light sources developed for 650nm [Golnabi and Azimi, 2007; Bilro et al., 2012].

Apart of that, researchers evaluate the performance of the proposed sensor with various sensitive coating materials on tapered fiber and analyze how it can enhance the performance of the sensor. Sometimes the fiber itself can play an active role by acting as a sensor when the cladding is replaced with chemical sensitive material [Bilro et al., 2012]. In a work reported by Nagata et. al. [2007], the new deposited cladding had a refractive index slightly above the refractive index of the core and in the presence of detection medium, the refractive index decrease to values below the core. The changes in refractive indices cause an enhancement in the power output of the system.

In the work presented here, a new choice of refractive index sensor which featuring several advantages and potential, is demonstrated. It is based on a simple intensity modulated fiber optic sensor using tapered PMMA plastic fibers with sensitive coating materials as a probe. Here, the sensitivity tapered fibers coated with graphene, single walled carbon nanotube and zinc oxide were investigated.

Variations of refractive index were achieved through the use of different concentration of uric acid solution. Subsequent performance analysis allows the identification of the experimental dependence of the surrounding refractive index sensitivity on the three different sensitive coating materials.

4.2 Uric Acid

Uric acid is a metabolite of purines, nucleic acids and nucleoproteins which is found in biological fluids, mainly blood, urine or serum and is excreted by the human body. High level of serum uric acid is also considered as a risk factor for myocardial infarction and stroke (Ivekovic et al., 2012). In order to avoid diseases like gout, renal failure, hyperuricaemia, Lesh-nyhan, physiological disorder and Wilson's disorder, the monitoring of uric acid is essential (Minas et al., 2004). Therefore, the need for uric acid biosensors is tremendously increasing (Hoshi, Saiki and Anzai, 2003; Zhao et al., 2009; Ali et al., 2012; Liao et al., 2006).

Several uric acid detection techniques such as Amperometric principles, Potentiometer, zinc oxide (ZnO) nanowires, nanotubes and nonporous material have attracted great interest to researchers. Amperometric biosensor used for the detection of oxygen consumption, chemiluminescense and fluoride ions where in practice, this detection method requires the electrode to be held at approximately 0.7V where biological electro active molecules react with the surface of the electrode. On the other hand, potentiometer based on ZnO nanoflakes and immobilized uricase can reduce the

interferences but a limitation of ion sensitive electrodes (ISEs) which can only detect charged molecules (Ali et al., 2012). ZnO have unique advantages in combination with immobilized enzymes and can enhance the direct electron transfer between the enzyme's active sites and the electrons (Ali et al., 2012). ZnO nanowires grown on the surface of gold coated flexible plastic substrate results as good uric acid biosensor. However, the cost for the fabrication of ZnO nanowires grown on the surface of gold coated is high and researchers are looking forward to reduce it.

Therefore, ongoing researches are focusing on coating methods considering easy fabrication and cost effectiveness.

4.3 Tapered fiber coated with Sensitive Materials

Tapered plastic optical fibers have been used as transducers in order to get coated by these sensitive Nano films for their use in sensing applications. The linear type of tapered plastic fiber are a simple device and very sensitive to changes of the surrounding refractive index. As a fiber is tapered, the core/cladding is redefined in such a way that the single mode fiber in the central region of the taper acts as a multimode fiber and the light becomes guided through the cladding of the fiber, which plays the role of the new core and the new cladding is the external medium [Corres, Arregui and Matías, 2007]. The shape that the fiber acquires after the tapering process, which depends on the method employed in its fabrication, has a high impact on the light transmission properties [Corres, Arregui and Matías, 2007]. This chapter focuses on developing a low cost uric acid sensor using a tapered POF coated with sensitive material. Three different materials; graphene, carbon nanotubes and ZnO were explored for use as the sensitive material.

4.3.1 Graphene

Graphene is a unique nanostructure material with high surface area, excellent electrical conductivity and electron mobility (Geim and Novoselov, 2007; Novosolev et al., 2004, Stankovich et al., 2006; Kang et al., 2009). As a high conductivity carbon material, graphene has attracted increasing attention for applications in optoelectronic devices, super-capacitors, sensors and nanocomposite applications (Wang, Zhi and Mullen, 2008; Vivekchand et al., 2008; Ao, Yang and Liang, 2008; Leenaerts, Partoens and Peeters, 2008; Schedin et al., 2007, Ang et al., 2008; Lian et al., 2010, Li et al., 2010; Shen et. al., 2010). The excellent conductivity due to small gap is favourable for conducting bio-molecules electrons (Stankovich et al., 2006; Kang et al., 2009). Furthermore graphene based biosensors are sensitive with low electronic noise from thermal effect (Kang et al., 2009; Wang, Zhi and Mullen, 2008; Vivekchand et al., 2008; Ao, Yang and Liang, 2008). In addition to that, graphene is easily obtained by chemical conversion of the inexpensive graphite when compared to the production of CNT (Kang et al., 2009; Xu and Saeys, 2008).

4.3.2 Carbon Nanotubes (CNT)

The discovery of carbon nanotubes (CNTs) (Ijima, 1991) has generated great interest among researchers to develop high performance devices. The ongoing exploration on electrical, physical, chemical and mechanical properties contributes a wide range of applications such as nanoelectronics, sensors, field emission and electrodes. The electrical properties of CNTs are extremely sensitive to charge transfer and chemical doping effects by various molecules. Either electron-withdrawing molecules or electron-donating molecules will interact with the p-type semiconducting CNTs. This will change the density of the main charge carriers in the ‘bulk’ of the

nanotube and changes the conductance of CNTs. This is where CNTs is applicable as electrical chemical sensors (Zhang et al., 2008).

Recently, the potential of carbon nanotubes (CNTs) as sensing elements and tools for biomolecular analysis as well as sensors for gases and small molecules have been demonstrated (Li and Ng, 2003). CNTs integrated with biological functionalities are expected to have great potential in biomedical applications due to their unique one-dimensional quantum wires with high surface-to-volume ratio. Their electronics properties are very sensitive to molecular absorption and it is expected that the CNTs sensing elements will be affected if coupled with biomolecules which is high ions carrier (Star et al., 2003; Li et al., 2003). To date, CNTs have been utilized in biosensors in many forms such as probes (Woolley et al., 2000; Vo=Dinh et al., 2000), filed-effect-transistor using a single semiconducting CNTs (Bradley et al., 2003; Star et al., 2003; Li et al., 2003), a random CNT network (Koehne et al., 2003; Koehne et al., 2004) and nanoelectrode array (Guiseppi,-Elie, Lei and Baughman, 2002; Azamian et al., 2002; Musameh et al., 2002).

4.3.3 Zinc Oxide (ZnO)

ZnO nanoparticles are extremely important materials in a broad range of high-technology applications. It is widely explored for the uses of field-effect transistor, light-emitting diode, ultraviolet laser, biological detector and solar cells [Liu et al., 2012]. Various fabrication techniques for growing ZnO nanorods includes vapor transport, physical vapor deposition and chemical vapor deposition which require a relatively high temperature during the synthesis procedure [Liu et al.,2012]. Since ZnO is a high refractive-index material to fiber, the structure allows fiber-guided light couple into ZnO nanorod waveguides [Voss et al., 2007]. The well-arrayed nanorods are very favorable for sensing applications as it has large surface to volume ratio [Liu et

al.,2012] and optical coupling between the fiber and nanorods are potentially promising for various novel optical sensing applications.

A wide variety of nanostructures such as zinc oxide (ZnO) nanowires, nanotubes and nonporous material have also attracted great interest to researchers due to its unique advantages in combination with immobilized enzymes and can enhance the direct electron transfer between the enzyme's active sites and the electrons [Ali et al., 2012]. Nanostructures have the advantage of a high surface area, and electronic processes are strongly influenced by surface processes. ZnO nanostructures have been widely used for sensing applications because of their high sensitivity to the chemical environment [Schmidt.M. & MacManus.D., 2007]. For instance, ZnO nanowires grown on the surface of gold coated flexible plastic substrate results as good uric acid biosensor [Usman Ali et al., 2011]. Furthermore, ZnO nanowires have demonstrated high sensitivity even at room temperature [Schmidt.M. & MacManus.D., 2007].

4.4 Sensing of Uric Acid with Tapered Plastic Fiber coated with Graphene

In preparing a graphene polymer composite, the first step is to produce graphene flakes using the electrochemical exfoliation process. A constant voltage difference of 20V is applied to two electrodes (graphite rods) placed 1 cm apart in an electrolysis cell filled with electrolyte (1% sodium dodecyl sulfate (SDS) in deionized water). During the electrochemical exfoliation process, hydroxyl and oxygen radicals were released due to electrolysis of the water at the electrode. Then oxygen radicals start to corrode the graphite anode. This was followed by the intercalation of anionic surfactant and finally graphene sheets were formed in the solution. In our work, black sediments (graphene) start to peel off from the anode after several minutes. The exfoliation process was extended for another 2 h to obtain a stable graphene suspension in the SDS solution. The stable graphene suspension is centrifuged at 3000 rpm for 30 min to remove large

agglomerates. Afterward, the supernatant portion of the suspension was decanted. The concentration of the centrifuged graphene was estimated from the weight of the suspension used. To fabricate the composite, 1 g of polyethylene oxide (PEO) (Mw = 1 000 000 gmol-1) was dissolved in 120 ml of deionized water. The graphene solution obtained from the electrochemical exfoliation was then mixed with PEO solution at various ratios; 2:20, 4:20 and 6:20 of graphene : PEO in ml respectively. Figure 4.1 (a) shows the photographic image of the prepared graphene polymer composite while figures 4.1 (b), (c) and (d) show the microscopic images (x100) of graphene polymer composite deposited on glass slides (scale: 200μm) for mixing ratios of 2:20, 4:20 and 6:20 respectively.

The tapered POF was then prepared based on chemical etching technique using acetone, de-ionized water and sand paper as discussed in Chapter 3. This process uses tapered fiber with the waist diameter of 0.45 mm and a total length of the tapered section is 10 mm. The tapered POF fiber is cleansed again using de-ionized water. Figures 4.2 (a) and (b) show the microscopic images of the original un-tapered, tapered POF, which have a cladding diameter of 1 mm and 0.45 mm respectively. Figure 4.2 (c) shows the tapered fiber coated with graphene polymer composite with ratio of 6:20. The image shows the presence of a layer of graphene polymer composite on the waist of the tapered fibre.

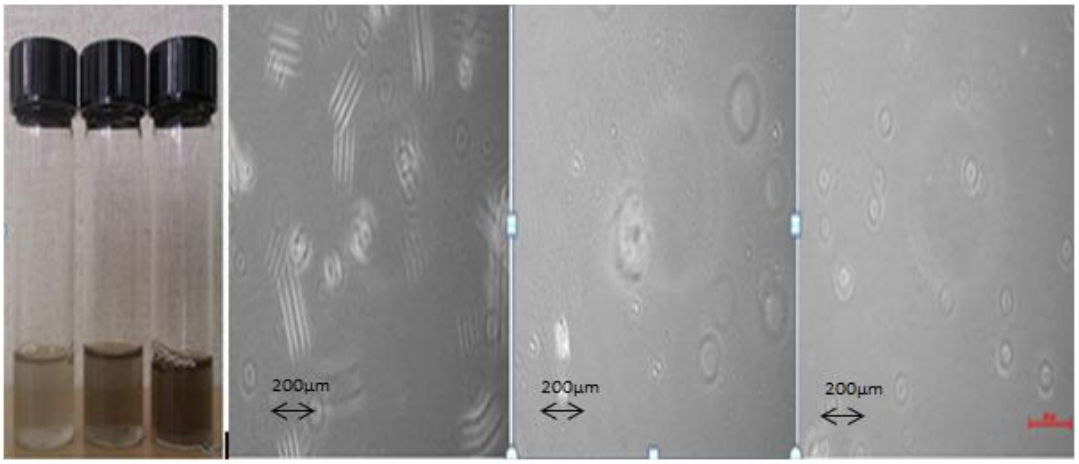

(a) (b) (c) (d)

Figure 4.1:Photographic image of (a) solutions of graphene polymer composite at ratios of 2:20, 4:20 and 6:20 and microscope images of graphene polymer composite at mixing ratios of (b) 2:20 (c) 4:20 and (d) 6:20 (scale: 200µm).

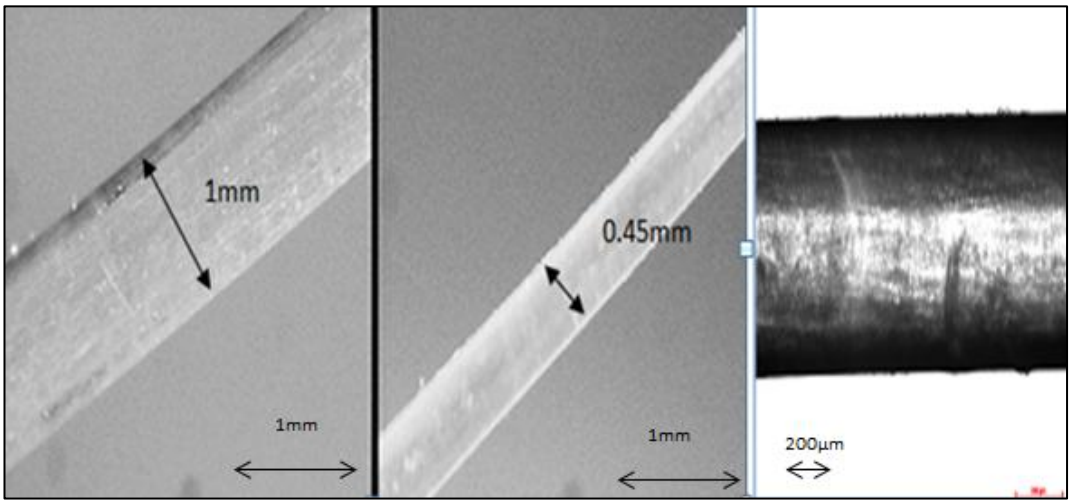

(a) (b) (c)

Figure 4.2:Microscopic images of (a) un-tapered POF (with diameter of 1 mm), (b) Tapered POF (with diameter of 0.45 mm) and (c) Tapered POF coated with graphene polymer composite with ratio of 6:20 (scale: 200µm).

4.4.1 Experiment Setup

Figure 4.3 shows the experimental setup for the proposed sensor to detect different uric acid concentration using the tapered POF coated with the composite of different graphene / PVA ratios; 2:20, 4:20, 6:20 as a sensing medium. The setup consists of a light source, an external mechanical chopper, the sensor probe, a highly sensitive photo-detector, a lock-in amplifier and a computer. The input and output ports of the tapered POF were connected to the laser source and photo-detector, respectively. The light source used in this experiment is a He-Ne laser operating at a wavelength of 633 nm with an average output power of 5.5 mW. It was chopped at a frequency of 113 Hz by a mechanical chopper to avoid the harmonics from the line frequency which is about 50 to 60 Hz. The 113Hz frequency was chosen as an odd number to prevent multiplication of 50 and 60 Hz besides it is an acceptable value of output and stability. The light source was launched into the tapered POF placed in a Petri dish filled with the uric acid solution. The output light were sent into the silicon photo-detector (818 SL, Newport) and the electrical signal was fed into the lock-in amplifier (SR-510, Stanford Research System) together with the reference signal of the mechanical chopper. The output result from the lock-in amplifier was connected to a computer through an RS232 port interface and the signal was processed using Delphi software. The reference signal from the chopper was matched with the input electrical signal from the photo-diode. This allows a very sensitive detection system that will remove the noise generated by the laser source, photo-detector and the electrical amplifier in the photo-detector. In the experiment, the performance of the proposed sensor was investigated for various uric acid concentrations. During the experiment, the errors caused by temperature were considered negligible and the temperature was kept constant at 25°C.

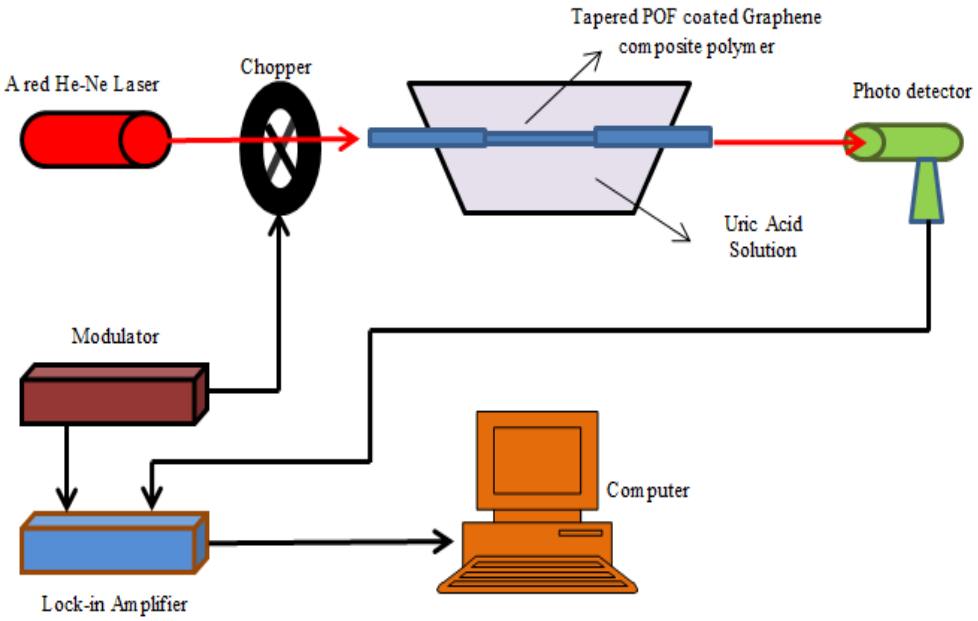

Figure 4.3: Experimental setup for the proposed relative humidity sensor using a tapered POF without and with HEC/PVDF composite.

4.4.2 Performance of the sensors

Figure 4.4 shows the refractive index of the uric acid solution (as measured by using METTLER Toledo RE40D refractometer) against the uric acid concentration. As the concentration of uric acid increases from 0 ppm to 500 ppm, the refractive index of the solution also increases from 1.3330 to 1.3336. The refractive index of graphene polymer composite used in this experiment was also measured using the same refractometer and the measured value was obtained at 1.3342, which is slightly higher than refractive index of water (1.3330). The digital refractometer can measure the refractive index and other related parameters with high precision within a short time.

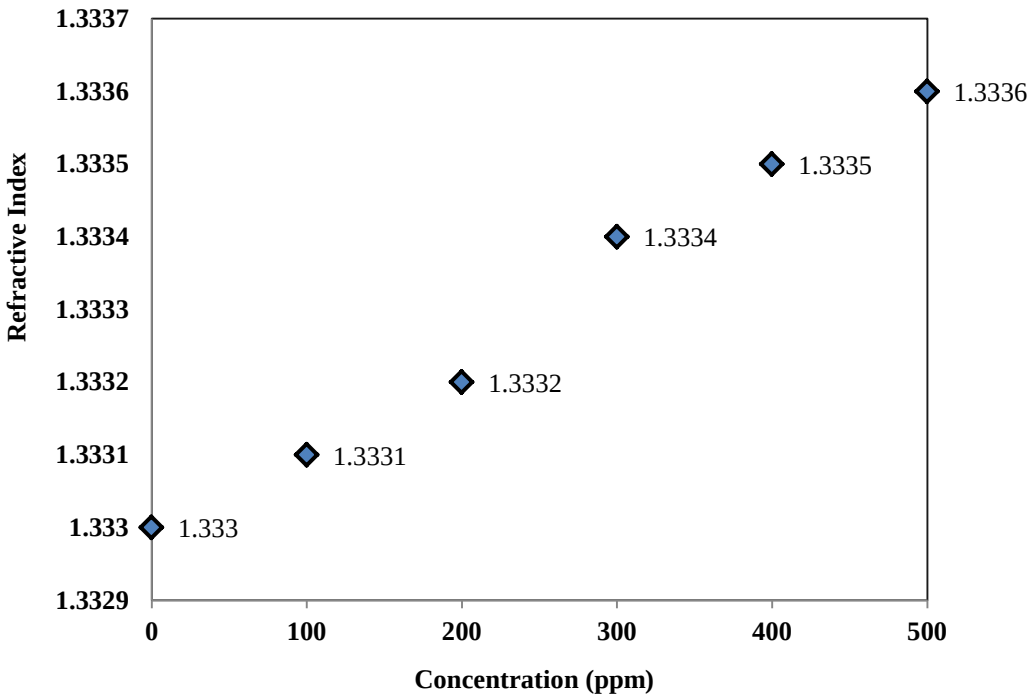

Figure 4.4: Refractive index against uric acid solution concentrations.

Figure 4.5 shows the variation of the transmitted light from the tapered POF with concentrations of uric acid solution for the probe with various graphene polymer coating ratios of 2:20, 4:20 and 6:20. The result obtained by the probe without coating is also given for comparison purpose. It is observed that the transmitted light intensity improves with the graphene coating. This is attributed to the difference in refractive index between the core and cladding (graphene with RI = 1.3342) becomes smaller and thus improves the light confinement inside the core. As shown in the figure, the output voltage from the photo-detector, which corresponds to the transmitted light intensity, linearly increases with the concentration of the uric acid solution.

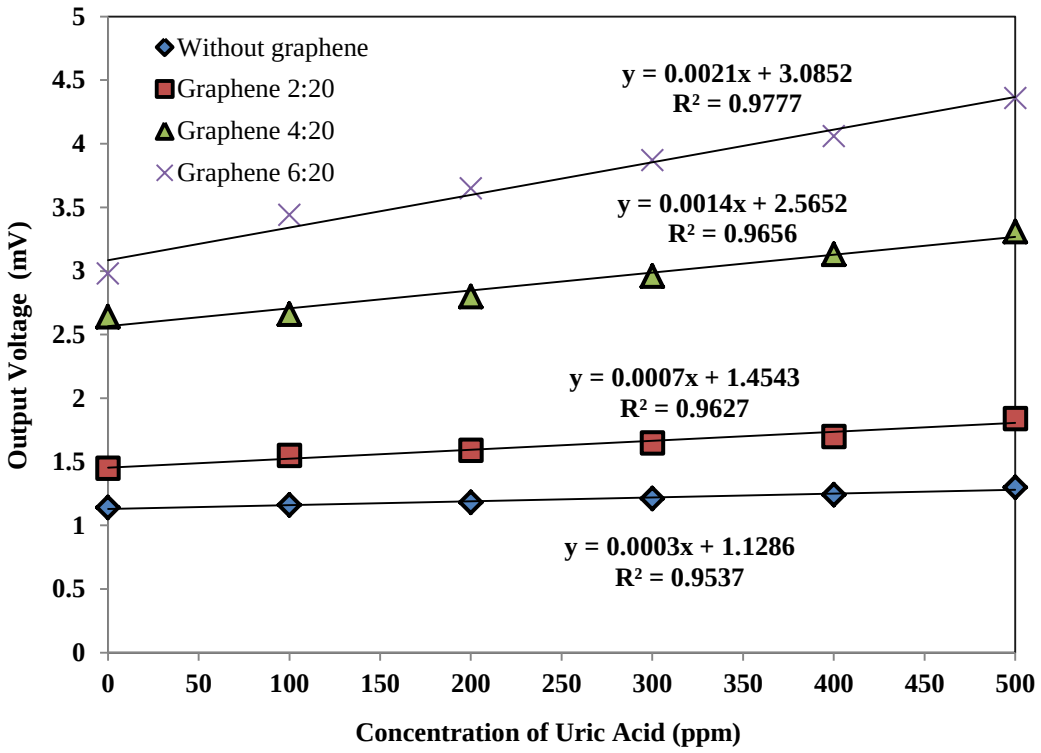

Figure 4.5: The output voltage against uric acid concentrations for the proposed tapered POF based sensor without and with graphene polymer composite of 2:20, 4:20 and 6:20.

The transfer function for the output voltage versus concentration of uric acid with different refractive index is obtained as follows for graphene polymer coating ratios of 2:20, 4:20 and 6:20 respectively.

$$y = 0.0007x + 1.4543 \quad (4\text{-}1)$$

$$y = 0.0014x + 2.5652 \quad (4\text{-}2)$$

$$y = 0.0021x + 3.0852 \quad (4\text{-}3)$$

and the following transfer function is obtained for the fiber without the graphene coating;

$$y = 0.0003x + 1.1286 \quad (4.4)$$

The fiber without the graphene coating has lowest sensitivity of 0.0003mV/ ppm with a slope linearity of more than 97.65%. On the other side, the transmitted light intensity is observed to be highest with graphene polymer coating of 6:20 since the graphene concentration is the highest. Compared to the sensor configured without the coating, the proposed sensor produces a better sensitivity of 0.0021mV/ppm with a better slope linearity of more than 98.88%. The response time of the sensor is taken for 100 seconds with and the sample size for standard deviation is 100. The average standard of deviation is divided with sensitivity to calculate the limit of detection. The limit of detection for fiber without graphene polymer is 96.67 ppm whereas for fiber with graphene polymer coating of 6:20 is 7.61ppm. The limit of detection is lower compared to the uncoated fiber, which indicates that the system is more efficient. It is found that as the concentration of graphene increases, the sensitivity and linearity of the sensor also increases. The electrical properties of graphene are extremely sensitive to charge transfer and chemical doping effects by various molecules. Either electron-withdrawing molecules or electron-donating molecules will interact with graphene. This will change the density of the main charge carriers in the graphene and changes its conductance [Barlett et al., 2000; Dong et al., 2012; Lian et al., 2012].

Since the cladding area of the tapered POF has been reduced, the surrounding medium works as passive cladding and its refractive index can influence the amount of power loss as the signal propagates through the tapered region. The reduction of the fiber size increases the evanescent field penetration of guided modes [Liu et al., 2008; Beres et al., 2010]. When immersing the tapered fiber into the uric acid solutions with various concentrations ranging from 0 ppm to 500 ppm, the effective refractive index of the surrounding medium increases since the refractive index of uric acid is larger than water (1.333). Since the refractive index of the composite increases as the concentration increases, the core and cladding index difference for the proposed sensor drops with the

increment of the concentration of the acid [Rahman et al., 2011]. Therefore, we observe less leakage from the light that propagates inside the tapered region to the surrounding, which results in the output voltage increasing. Thus, when the concentration of uric acid solution increases, the output voltage also increases for both cases of the POF with and without graphene coating. However, the experimental results also indicate that the sensitivity of the tapered POF is enhanced when coated as the transmitted light intensity is higher. The reason is because the polymer composite has a much higher refractive index compared to water solution. When coated with graphene polymer composite, the effective cladding refractive index of the POF increases and thus more light is allowed to be transmitted. In addition, the proposed sensor provides numerous advantages such as simplicity of design, low cost of production, higher mechanical strength and easier to handle compared to silica fiber optic [Barlett et al., 2000]. In addition to that, as mentioned in chapter 3, the electrical properties of graphene are extremely sensitive to charge transfer and chemical doping effects by various molecules. Either electron-withdrawing molecules or electron-donating molecules will interact and change the density of the main charge carriers and changes the conductance of graphene. This is where graphene is applicable as electrical chemical sensors.

Reversibility of the results is another important factor in the operation of any sensor system, so in the next study, this parameter is tested for the reported system. The results of the output measurement as a function of concentration are recorded for two different runs and the results are compared. As can be noticed from Figure 4.6, the maximum difference between the two runs is about ±0.13 mV, which is acceptable for a full-scale output of 4.36mV.

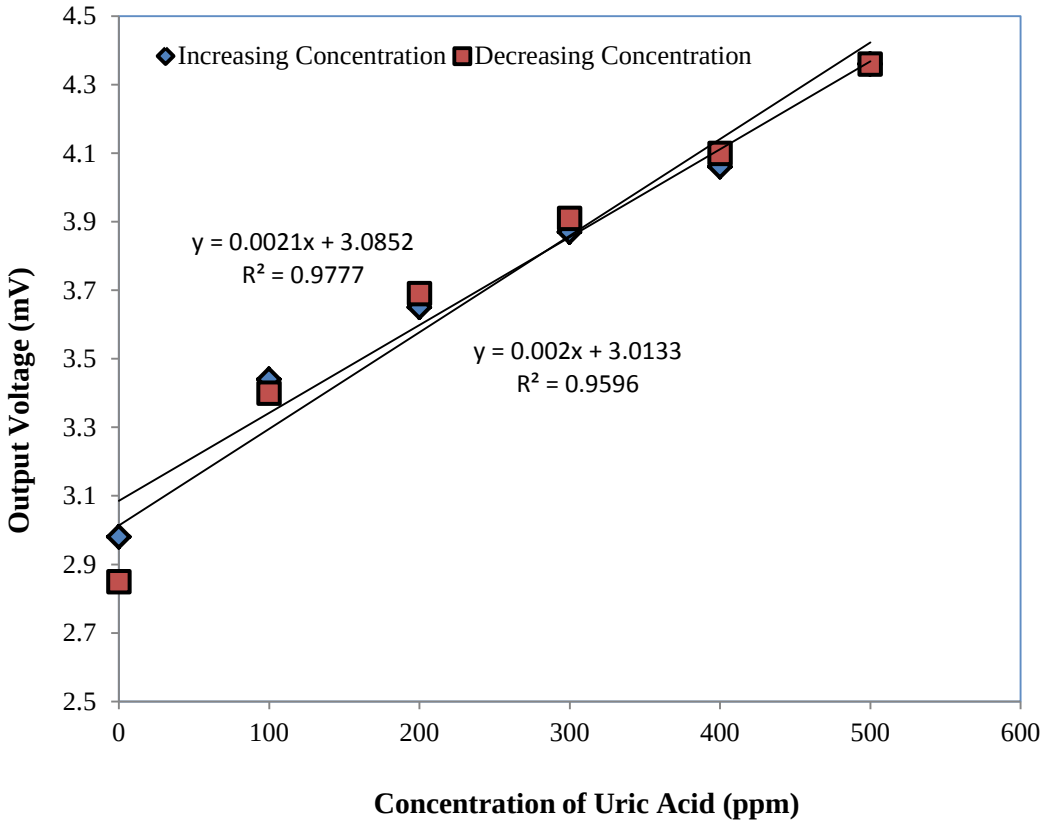

Figure 4.6: The reversibility of the results obtained for two different runs (Output voltage against the concentration of Uric Acid).

The performance characteristic of the proposed sensor is summarized in Table 4.1. Overall, the sensor was observed to be sufficiently stable with standard deviations of 0.029 mV and 0.0.016 mV for POF probe without and with graphene polymer composite coating as recorded for duration of 100 second. Throughout the experiment, a fix quantity of liquid solution was placed in the petri dish and the corresponding output voltage was measured by a lock-in amplifier which provided accurate measurements even though the signal was relatively very small compared to noise. Furthermore, a well-regulated power supply is used for the red He-Ne laser and this minimizes the fluctuation of source intensity. These results show that the proposed sensor is applicable

and useful for the detection of uric acid. The sensor also has the ability to provide real time measurement.

Table 4.1:The performance of the proposed Uric Acid Detection Sensor

Performances	**Bare Fiber**	**Coated Fiber (Graphene 6:20)**
Sensitivity	0.0003mV/ppm	0.0021mV/ppm
Linearity	97.65%	98.88%
Standard deviation	0.029mV	0.016mV
Limit Of Detection	96.67ppm	7.61ppm

.

4.5 Sensing of Uric Acid with Tapered POF coated with SWCNT

A homogeneous solution was prepared by mixing SWCNTs (99% pure, diameter of 1-2nm and length of 3-30 μm) with SDS solvent (average molecular weight of 288.38 g/mol) and then ultrasonicating it for 30 minutes at 50 W. The solution was centrifuged at 1000 rpm to remove large particles of undispersed SWCNTs to obtain dispersed suspension that is stable for weeks. PEO solution was then prepared by disolving 1 g of PEO with an average molecular weight of 1 x 10^6 g/mol in 120 ml of deionized water. An SWCNT-PEO composite was fabricated by using a solution casting method, whereby the SWCNT solution with concentration of 18 wt. % was mixed with the PEO solution. The function of the PEO is to bind the SWCNT for easier handling because it hard to obtain a pristine SWCNT.

The tapered POF was then prepared based on chemical etching technique using acetone, de-ionized water and sand paper as discussed in Chapter 3. The tapered fiber has a stripped region waist diameter of 0.45mm and both ends of the POF were held and straightened onto translation stages to deposit the SWCNTs onto the tapered fiber. In the process, the prepared PEO/SWCNT polymer composite solution was slowly dropped onto the tapered region of the fiber using syringe as shown in Figure 4.7. The refractive index of PEO/SWCNT polymer composite used in this experiment was also measured using the same refractometer and the measured value was obtained at 1.3337, which is slightly higher than refractive index of water (1.3330).

Figures 4.8 (a) and (b) show the microscope images of the original un-tapered and tapered POF, which have a cladding diameter of 1 mm and 0.45 mm respectively. Figure 4.8 (c) shows the tapered fiber with SWCNT-PEO composite.

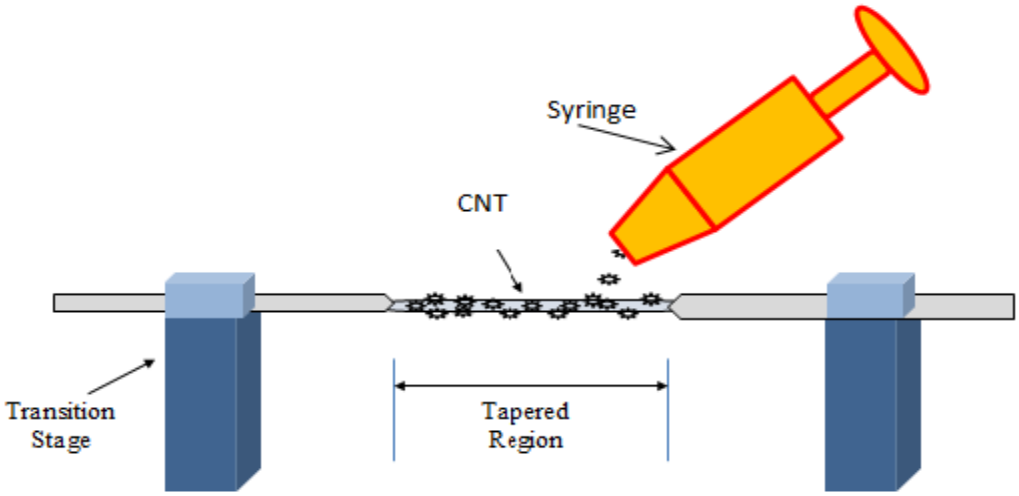

Figure 4.7: The deposition of SWCNT-PEO composite onto the cladding surface of the tapered POF.

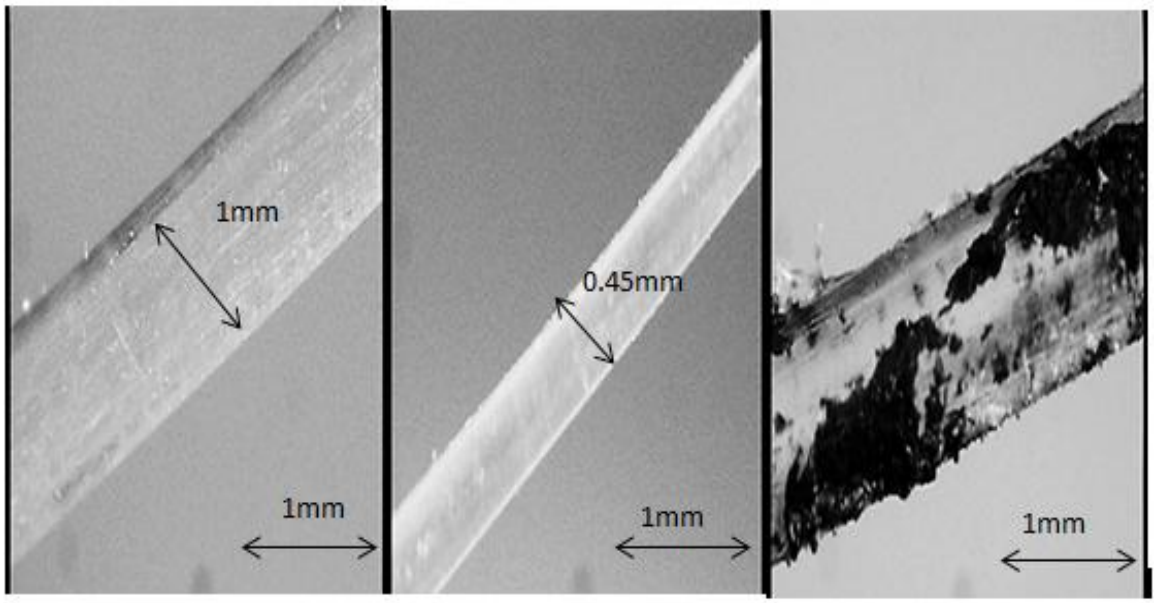

(a) (b) (c)

Figure 4.8:Microscope images of (a) un-tapered POF (with diameter of 1 mm), (b) Tapered POF (with diameter of 0.45 mm) and (c) Tapered POF with SWCNT-PEO composite

The sensor experiment was carried out using a similar setup of Figure 4.3. In the experiment, the transmitted output voltage is measured for different uric acid concentrations using the fabricated tapered POF coated with SWCNT-PEO composite as a probe. Figure 4.9 shows the variation of the transmitted light from the tapered POF against the concentration of uric acid solution with and without SWCNT-PEO composite deposited onto the tapered region. The transmitted light intensity is observed to be higher with SWCNT-PEO composite coating since the coating has a much higher refractive index compared to water solution. With the composite, the effective cladding refractive index increases and thus more light is allowed to be transmitted from the tapered POF. As shown in the figure, the output voltage from the photo-detector, which corresponds to the transmitted light intensity linearly increases as the concentration of the uric acid solution increases. Without the composite, the sensitivity of the sensor is

obtained at 0.0003 mV/ % with a slope linearity of more than 97.6% and limit of detection of 9.67 ppm.

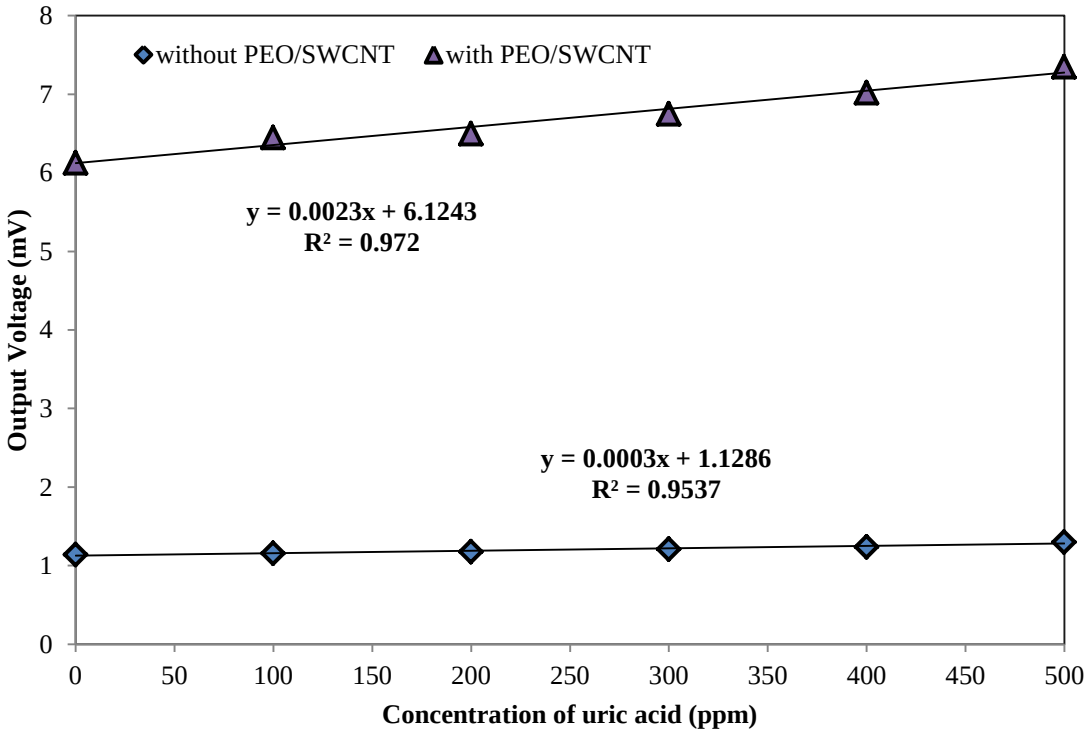

Figure 4.9: Output voltage against uric acid concentrations for the proposed tapered POF based sensor with and without SWCNT-PEO composite.

The transfer function for the output voltage versus concentration of uric acid with different refractive index is obtained as follows:

$$y=0.0023x+6.1243 \quad (4\text{-}5)$$

without the SWCNT coating, the following transfer function was

$$y=0.0003x+1.1286 \quad (4.6)$$

This result shows that the sensor with SWCNT-PEO composite coating performs better than that of without the coating. It produces a sensitivity of 0.0023 mV/% with a slope linearity of more than 98.6 % and a limit of detection of 6.95 ppm.

Since the diameter of the cladding of the tapered POF has been reduced, the refractive index of the surrounding medium works as passive cladding and influenced the amount of power loss as the signal propagates through the tapered region. When immersing the tapered fiber into the uric acid solutions with various concentrations ranging from 0 ppm to 500 ppm, the index of the surrounding medium increases since the refractive index of uric acid is larger than water. Since, the refractive index of the composite increases as the concentration increases as depicted in Figure 4.4, the core and cladding index difference for the proposed sensor reduces with the increment of concentration. Therefore, less light that propagating inside the tapered region leaks to the surrounding, which resulted in the output voltage increment [Bradley et al., 2003]. In addition to that, CNTs are extremely sensitive to charge transfer and chemical doping effects by various molecules. Either electron-withdrawing molecules or electron-donating molecules will interact with the p-type semiconducting CNTs. This will change the density of the main charge carriers in the ‘bulk’ of the nanotube and changes the conductance of CNTs. This is where CNTs is applicable as electrical chemical sensors.

The performance characteristic of the proposed sensor is summarized in Table 4.2. Overall, the sensor is observed to be sufficiently stable with standard deviations of 2.9% and 1.6% for POF probe without and with SWCNT-PEO composite as being recorded for the time duration of 100 second. The lower standard of deviation and limit of detection of the POF probe with SWCNT-PEO composite indicates that the sensor stable and efficient. Throughout the experiment, the lock-in amplifier provides accurate measurements even though the signal is relatively very small compared to noise.

Furthermore, a well-regulated power supply is used for the red He-Ne laser and this minimizes the fluctuation of source intensity. These results show that the proposed sensor is applicable and useful for the detection of bimolecular concentration such as uric acid. The sensor also has the ability to provide real time measurement.

Table 4.2:The performance of the proposed uric acid detection sensor.

Performances	**Without SWCNT-PEO**	**With SWCNT-PEO**
Sensitivity	0.0003 mV/ppm	0.0023 mV/ppm
Linearity	97.6 %	98.6 %
Standard deviation	0.029mV	0.016mV
Limit of detection	96.67 ppm	6.95 ppm

4.6 Sensing of Uric Acid with Tapered Plastic Fiber coated with Zinc Oxide (ZnO)

This section describes another approach for uric acid concentration measurement using ZnO nanostructure as a sensing medium. The tapered PMMA POF prepared based on chemical etching technique with a stripped region waist diameter of 0.45 mm were cleansed again using de-ionized water before the coating process. These samples were then coated with seeding and non-seeding ZnO nanostructures.

The preparation for ZnO nanostructures on the fiber consists of two primary steps: First, the seed layer to grow the ZnO nanostructures on the fiber was developed using a simple manual dip coating technique. The seeded solution was prepared using zinc acetate dehydrate ($Zn(CH_3COO)_2 \cdot 2H_2O$) as a precursor dissolved in isopropanol with molarity of 0.025 M. The solution was stirred at 60° C for 2 hours in ambient to

yield a clear and homogenous solution. Then, the solution was cooled down to room temperature for the coating process. The fiber was manually dipped into the seeding solution and was dried at 50° C to evaporate the solvent and to remove the organic residuals. This coating and drying method was repeated for 5 times to increase the thickness of the fibers.

Following this, another solution was prepared to grow ZnO nanostructures on the bare tapered fiber and ZnO seeded tapered fiber. This was done by dissolving 0.01M zinc nitrate hexahydrate ($Zn(NO3)_2.6H_2O$ and 0.01M hexamethylenetetramine (HMTA) in 100ml deionized water. The deposition process of ZnO nanorods on the fibers was performed using sol-gel immersion method by suspending the bare and seeded-ZnO fibers in the growth solution at 60°C for 15 hours.

Figures 4.10 (a) and (b) shows the field emission scanning electron microscopy (FESEM) images of the ZnO nanostructures grown on the seeded and non-seeded tapered fibers, respectively. It is observed than ZnO deposited on seeded tapered fiber showed well defined nanorods structures (Figure 4.10 (a)) when compared to the non-seeded sample (Figure 4.10 (b)). Evidently seeding the tapered fiber with ZnO nanoparticles as seeds has enhanced the growth of nanorods. In the non-seeded sample, the morphology of the ZnO layer was unstructured suggesting the growth of layers comprising of nanoparticles.

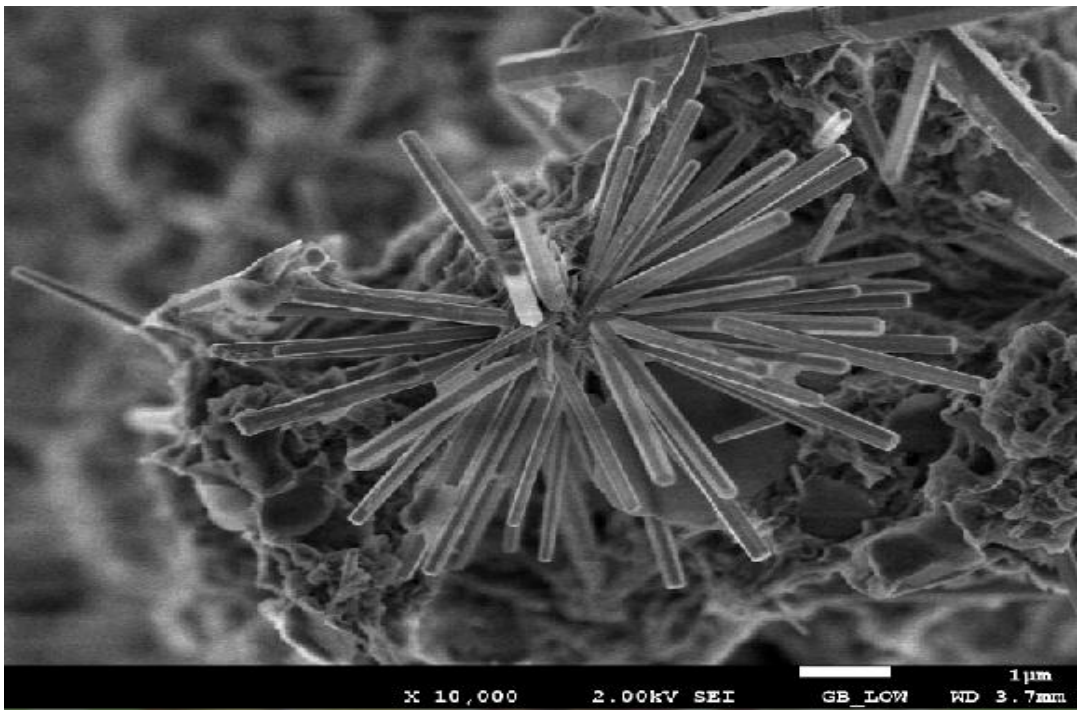

(a)

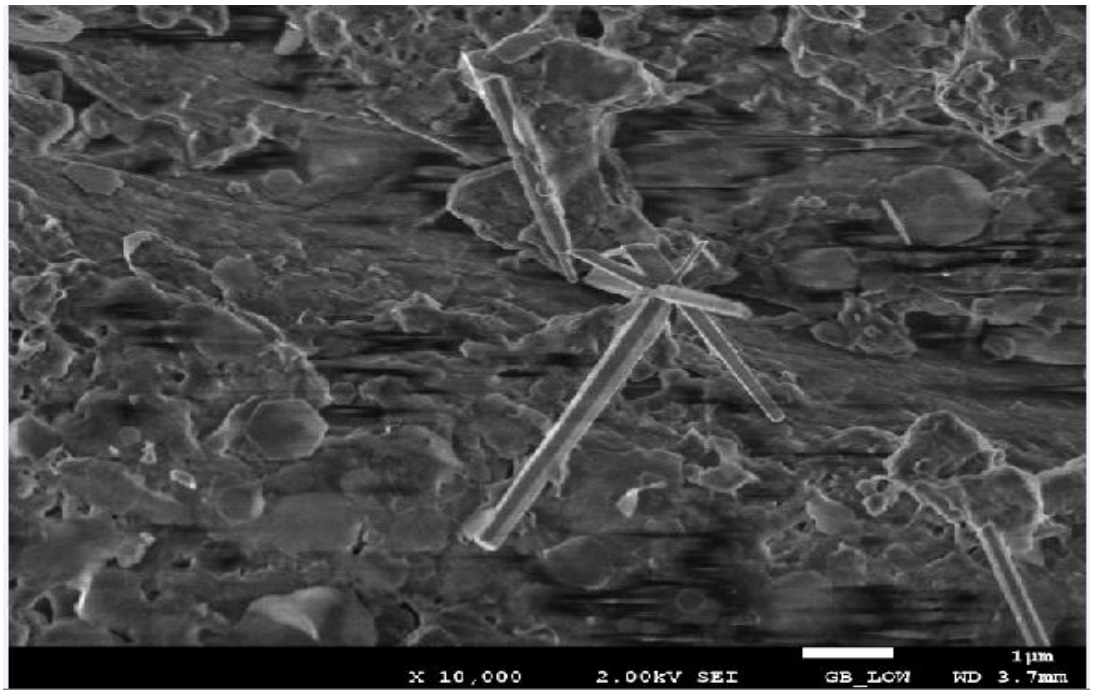

(b)

Figure 4.10:FESEM images of the ZnO nanostructures grown on (a) seeded tapered fiber and (b).

The experimental arrangement for the proposed biosensor to measure uric acid concentration using the fabricated tapered POF with ZnO nanostructures is similar with

Figure 4.3. Figure 4.11 shows the variation of the transmitted light from the tapered POF coated with ZnO nanostructures against the concentration of uric acid solution. As shown in the figure, the output voltage from the photo-detector, which corresponds to the transmitted light intensity linearly, increases as the concentration of uric acid solution increases. The sensitivity of tapered POF with seeded ZnO is 0.0025mV/ppm with a slope linearity of more than 98.28% and limit of detection of 5.6ppm. The transfer functions for the output voltage versus concentration of uric acid variation are:

$$y = 0.0025x + 1.1352 \quad (4\text{-}7)$$

and

$$y = 0.0009x + 0.7667 \quad (4.8)$$

with the use of probe with seeded and non-seeded tapered fiber respectively.

It is found that the sensitivity of the tapered POF with non-seeded ZnO is 0.0009 mV/ ppm with a slope linearity of 98.19 % and limit of detection of 18.9 ppm. In general, various chemicals can be classified as electrolytes and non-electrolytes depending on the dissociation of their ions in solutions [Ebbing & Gammon, 1999]. In case of uric acid, it is considered as an electrolyte since it contains of free ions that make the substance electrically conductive. The tapered POF coated with ZnO nanostructures interact with uric acid due to strong electrostatic interaction and response with the increasing concentration [Usman Ali et al., 2011]. However the seeded ZnO nanostructure could significantly enhance the transmission of the sensor that is immersed in solutions of higher concentration. These results show that the proposed

sensor is applicable and useful for the detection of biomolecular concentration such as uric acid.

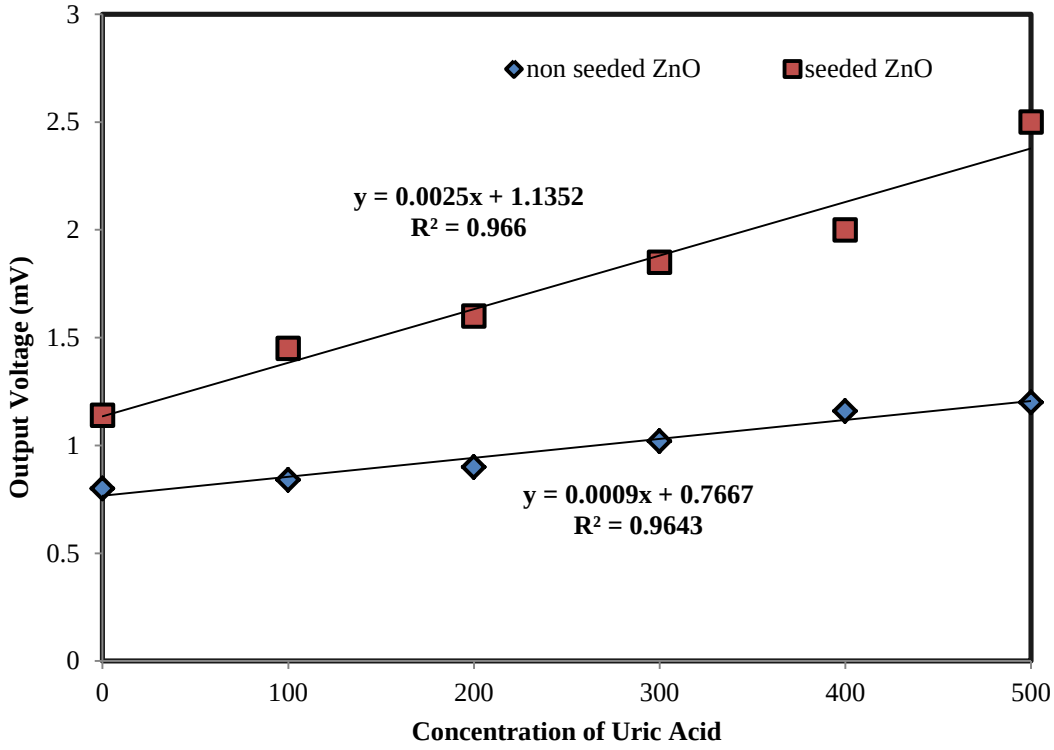

Figure 4.11:Output voltage against uric acid concentrations for the proposed tapered POF with ZnO nanostructure.

Reversibility of the results is another important factor in the operation of any sensor system, so in the next study, this parameter is tested for the reported system. The results of the output measurement as a function of concentration are recorded for two different runs and the results are compared. As can be noticed from Figure 4.12, the maximum difference between the two runs is about ±0.05mV, which is acceptable for a full-scale output of 7.15mV.

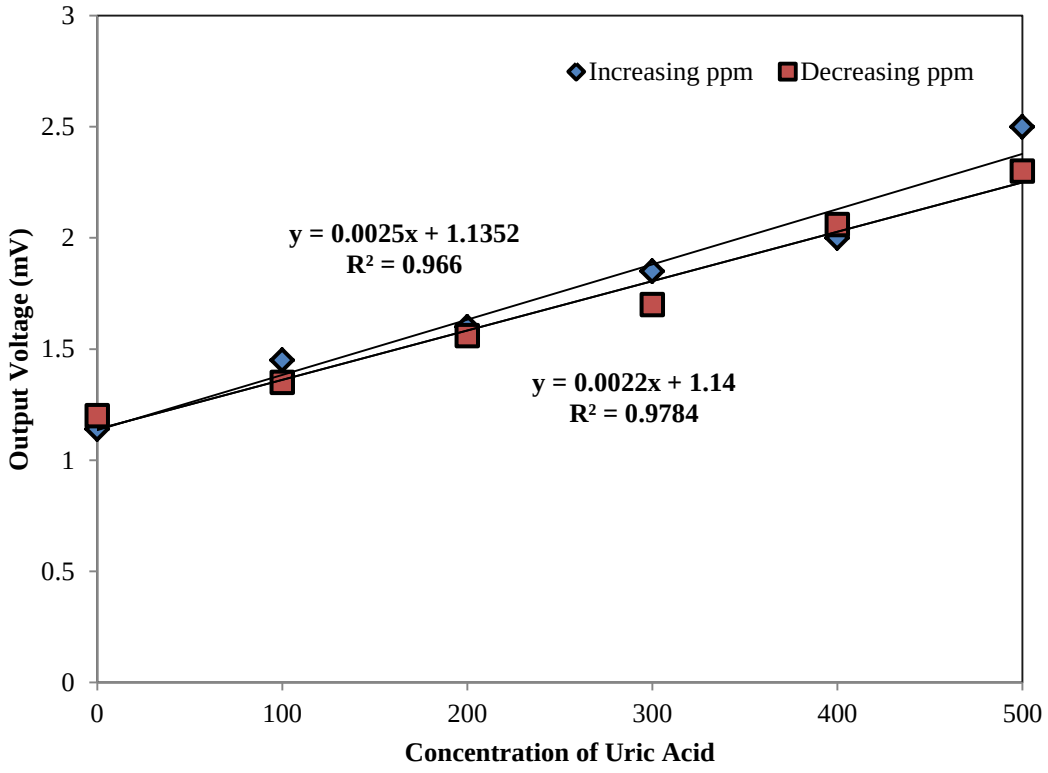

Figure 4.12:The reversibility of the results obtained for two different runs (Concentration of Uric Acid).

The performance characteristic of the proposed sensor is summarized in Table 4.3. Overall, the sensor is observed to be sufficiently stable with standard deviations of 0.017mV and 0.014mV for tapered POF coated with ZnO nanostructures tested on uric acid with different concentration as being recorded for the time duration of 100 second for non seeded and seeded respectively. This result show that the proposed sensor coated with ZnO nanostructures grown on seeded fiber is suitable and showed better performance in measuring uric acid because the lower value for stability shows that the system is more stable. The limit of detection is lower compared to indicate that the system is more efficient.

Table 4.3:The performance of the proposed uric acid detection sensor.

Performances	ZnO Coating	ZnO Grown
Sensitivity	0.0009 mV/ppm	0.0025 mV/ppm
Linearity	98.19 %	98.28 %
Standard deviation	0.017mV	0.014mV
Limit of detection	18.9 ppm	5.6 ppm

4.7 Summary

The tapered fiber with sensitive coating materials such as graphene, single walled carbon nanotube and zinc oxide were successfully demonstrated as a sensor to detect uric acid concentration. The sensor is based on an intensity modulation technique, which employs tapered PMMA fiber coated with sensitive coating materials. Variations of refractive index were achieved through the use of different concentration of uric acid solution. Subsequent performance analysis allows the identification of the experimental dependence of the surrounding refractive index sensitivity on the three different sensitive coating materials. It is observed that the transmitted light intensity improves with the sensitive material coating. The fiber itself can play an active role by acting as a sensor when the cladding is replaced with chemical sensitive material. Since the cladding area of the tapered POF has been removed, the sensitive material works as passive cladding and its refractive index can influence the amount of power loss as the signal propagates through the tapered region. This is attributed to the difference in refractive index between the core and cladding that influences the amount of light confinement inside the core.

The lower standard of deviation and limit of detection of the POF probe with sensitive materials indicates that the sensors stable and efficient. Throughout the experiment, the lock-in amplifier provides accurate measurements even though the signal is relatively very small compared to noise. Furthermore, a well-regulated power supply is used for the red He-Ne laser and this minimizes the fluctuation of source intensity. These results show that the proposed sensor is applicable and useful for the detection of biomolecular concentration such as uric acid. This shows that the sensitive coating materials have successfully enhanced the performance of the fiber sensor.

Chapter 5

Multimode Tapered PMMA Fiber Sensors for Relative Humidity Measurement

5.1 Introduction

Plastic optical fibers (POFs) have received wide attention in constructing various optical sensor devices due to many advantages as discussed in chapter 3 and 4. To widen the range of applications, the development of functional POF in humidity sensing is investigated. In a similar way to temperature, strain or pressure for example, humidity (or moisture content) constitutes one of the most commonly required physical quantities [Yeo, Sun, & Grattan, 2008; Gopel et al., 2008]. The term *humidity* refers to the presence of water in gaseous form but it is often used to refer to expressions which are related to water vapour characteristics and in the field of measurement, there are various terms associated with such water vapour measurements [Yeo, Sun, & Grattan, 2008].

The monitoring of humidity is important in numerous fields especially in chemical, biomedical and big structures such as bridges or planes [Cgen et al., 2002; Luo et al., 2002; Copper et al., 2004; Yeo et al., 2006; Corres, Matias, & Arregui, 2008]. Therefore relative humidity measurement has been extensively studied to develop great sensors. These sensors are normally based on optical fibre technology, which uses optical fiber probe to guide a light signal which is modulated with ambient humidity and then collected back by a detector [Corres, Matias, & Arregui, 2008]. The fiber optic sensors are commonly divided into instrinsic and extrinsic. However, in practice, most of humidity sensors are extrinsic type because the fibre is immuned to humidity with the exception of special fibers fabricated using sensitive coating materials. Likewise, tapered POF have received a tremendous interest in recent years

for various sensor applications. For instance, we have proposed and demonstrated uric acid sensors by using a tapered POF coated with various sensitive materials to enhance the performance of the sensor as discussed in the previous chapter. In this chapter, various relative humidity (RH) sensors are proposed and demonstrated using tapered POF in conjunction with various sensitive coating materials. The performances of the RH sensors are compared from various sensitive coatings such as agarose gel, hydroxyethylcellulose/polyvinylidenefluoride (HEC/PVDF) composite and Zinc-Oxide nanostructure. The next section gives a general background on RH and evanescent wave based humidity sensors.

5.2 Background on Relative Humidity (RH) and evanescent wave-based humidity sensors

Humidity is an important physical quantity being investigated for today's era of environmental protection, meteorology, defense, aerospace, warehousing, industrial and agricultural production sector. Relative humidity (RH) is a term used to describe the amount of water vapor in a mixture of air and water vapor. It is defined as the ratio of the partial pressure of water vapor in the air–water mixture to the saturated vapor pressure of water at the prescribed temperature. RH, simply represents the ratio of the amount of water vapour present in the atmosphere to the maximum amount the atmosphere can hold [Yeo, Sun, & Grattan, 2008] and is often expressed as a percentage using the following equation,

$$\text{Relative Humidity (RH)} = \frac{P_w}{P_{ws}} X\ 100\% \qquad (5\text{-}1)$$

where P_w is the partial pressure of the water vapour and P_{ws} is the saturation water vapour pressure. It can be measured through the properties of some bulk material such as the change in either physical dimensions or refractive index [Corres, Matias, & Arregui, 2008].

As discussed in previous chapters, the fiber sensor researches are focusing in many new areas such as humidity, gases and vapours sensing, medical and chemical analysis, molecular biotechnology, marine and environmental analysis industrial production monitoring, bioprocess control, and the automotive industry. The discovery of refractive index change as an approach used in the Evanescent Wave sensing method (Muto et al., 2003) has generated great interest among researchers to develop high performance devices such as humidity sensors. Humidity sensors are based on reversible absorption of water (H_2O) from the ambient atmosphere into a porous thin-film interferometer that sits on the tapered fiber and changes the refractive index of the thin films and subsequently transforms the lossy fiber into a light guide. Various RH sensors have been explored using a glass silica fiber. For instance Arregui et. al. (2003) uses a tapered silica fiber coated with hydrogels while Bariain et al. (2000) uses the tapred fiber coated with agarose gel for humidity sensing based on refractive index change. Using on the same approach, humidity sensors was also proposed based on a tapered silica fibers coated with nanostructured films using the ionic self-assembled monolayer (ISAM) deposition technique (Corres et al., 2006; Corres et al., 2007). Many works have also been reported on using a side-polished silica optical fiber coated with a humidity sensitive layer for humidity sensing. Such a sensor was fabricated by means of polishing the flat surface parallel to the fiber axis in order to remove the cladding. The side polishing was realized by first fixing the optical fiber in a rigid holder, forming a rectangular block with fiber extending out from the two end faces of the block orthogonal to the fiber axis. The advantage of this scheme is that the sensing element

can be fabricated using inexpensive components and a variety of coating materials can be deposited onto the flat surface of the fiber block. However, the fabrication procedure is very time consuming, dependent upon the design of the fiber block and has limited exposed interaction length. Later, (Gaston et al., 2003; Gaston, Perez and Sevilla, 2004) proposed a humidity sensor based on a single mode, side-polished fiber with a PVA overlay which was tested with 1310nm and 1550nm laser sources and showed different sensing characteristics.

5.3 Tapered POF for RH sensing

As mentioned earlier, tapered optical fibers have gained much popularity in various sensing applications due to its high sensitivity. Compared to silica based fiber, POFs show several advantages such as ease of handling, mechanical strength, disposability and easy mass production of components and system. In this work, tapered POF is coated by a sensitive layer that can sense the change in relative humidity. The coated material will act as a functional cladding layer and its optical properties change in response to an external stimulus. The measurement will be based on intensity modulation technique where the output voltage of the transmitted light through the tapered POF is investigated for changes in RH. As a functional cladding layer, the swelling polymer causes swelling effect as the material is exposed to water molecules and changes its refractive index. The light intensity that passing through the sensor probe (tapered POF) changes remarkably depending on the RH of the surrounding. The proposed probes are based on PMMA fiber and thus give good robustness to the sensors.

Here, the performances of various RH sensors based on tapered POF coated with agarose gel, HEC/PVDF composite and zinc oxide were investigated. Variations of refractive index are achieved when swelling polymers such as agarose gel and

HEC/PVDF composite by exposing it to water molecules. On the other hand, Liu et al. (2012) reported that the effective refractive index of ZnO composite varies with RH change. When the composite are exposed to an environment of humidity, it causes rapid surface adsorption of water molecules. The optical properties of ZnO composite surfaces are modulated by the surface adsorption of water molecules. The increase of water molecules being absorped on ZnO composite results in an increase of RH [Liu et al., 2012]. The increasing water molecules cause an increase in both effective refractive index of surrounding medium and absorption coefficient of the ZnO composite surfaces and leads to larger leakage of light in the tapered fiber. The dependence of the surrounding refractive index sensitivity on the three different sensitive coating materials is investigated in this study.

5.4 Agarose gel based RH sensor

Agarose is a polysaccharide consisting of a linear polymer (repeating units) of D-galactose and 3,6-anhydro L-galactose. Agarose is known to be structurally strong enough to be molded into micro scale structures [Jain, Yang & Erickson, 2012]. Commercially, agarose are extracted from seaweed and purified for use in electrophoresis. The movement of molecules through an agarose gel is dependent on the size, charge of molecules and the pore sizes present in the agarose gel. It is reported that the refractive index of agarose changes with humidity and its concentration [Bariain et. al. 2000, Jain, Yang & Erickson, 2012].

As mentioned earlier, the measurement of humidity is essential in chemical and food processing, air conditioning, electronic processing, ion-selective membranes, and immobilization matrixes for the entrapment of sensing indicators. Thus, the development of a low-cost humidity sensor with fast response has assumed great importance. An experimental study on the use of hydrogels in the fabrication of optical

fiber humidity sensors was conducted by Arregui et al. [2003] using silica fiber. This has triggered our curiosity to see what happens if a POF taper replaces the silica fiber taper in a new set of experiments. In this section, a new POF-based humidity sensor is proposed and demonstrated using agarose gel deposited on the tapered POF. The optical properties of the coated tapered POF change in response to a change in the external humidity level. The measurement is based on the intensity modulation technique where the output voltage of the transmitted light is investigated for changes in RH.

5.4.1 Experimental procedure

In this experiment, agarose powder obtained from Sigma Aldrich (no. A6013) was dissolved in water, in proportions of 0.5, 1 and 1.5% in weight. The mixture was heated to 50°C. A small portion of the mixture was deposited on the tapered area of the fiber. Then, the fiber was left to dry for a day. Figure 5.1 (a) shows the photographic image of the prepared agarose gel while Figures 1(b), (c) and (d) show the microscopic images (X50) of agarose gel deposited on glass slides (scale: 200μm) for 0.5, 1 and 1.5% weight composition respectively.

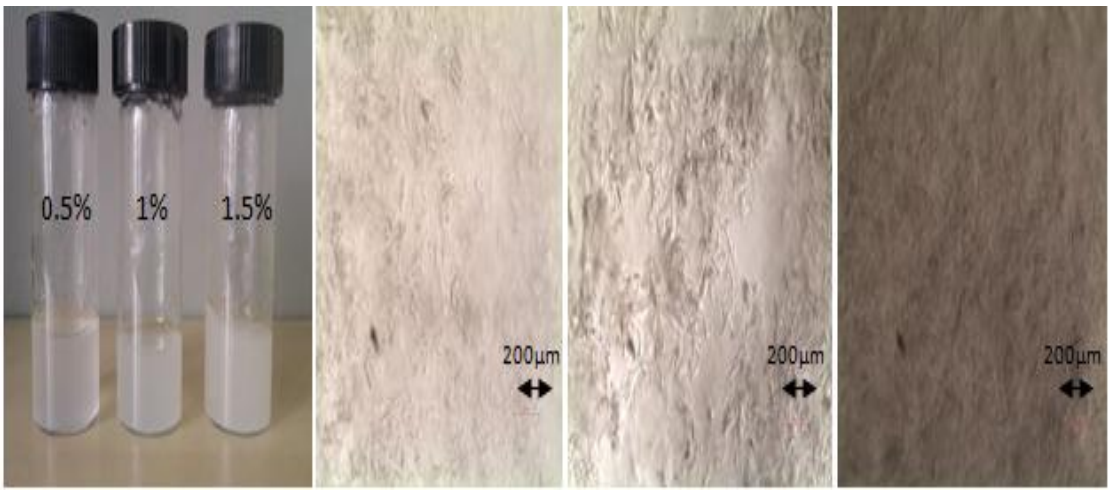

(a) (b) (c) (d)

Figure 5.1:Photographic Image of (a) agarose gel of 0.5, 1 and 1.5% weight content (b) microscopic image of agarose gel 0.5% weight content (c) microscopic image agarose gel 1% weight content and (d) microscopic image agarose gel 1.5% weight content.

The tapered POF was then prepared based on chemical etching technique using acetone, de-ionized water and sand paper. The POF used had an overall cladding diameter of 1 mm, a numerical aperture of 0.51 and an acceptance angle of 61°. The refractive index of the core and cladding were 1.492 and 1.402 respectively. The tapered fiber with stripped region waist diameter of 0.45mm was placed with both ends of the fiber held and straightened onto translation stages for the deposition of agarose gel. In the process, the prepared agarose gel solution was slowly dropped onto the tapered region of the fiber using syringe and left to dry for 1 day. Figures 5.2 (a) and (b) shows the microscope images of the original un-tapered and tapered POF, which have a cladding diameter of 1 mm and 0.45 mm respectively. Figures 5.2(c), (d) and (e) show the tapered fiber with agarose gel of 0.5, 1 and 1.5% weight content respectively.

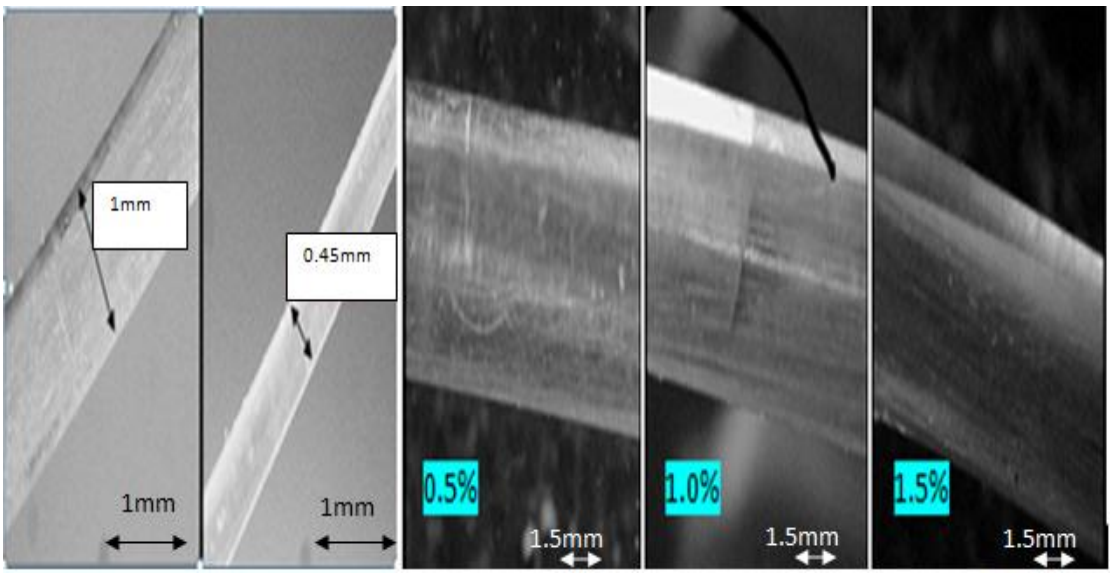

(a) (b) (c) (d) (e)

Figure 5.2:Microscope images of (a) un-tapered POF (with diameter of 1 mm), (b) Tapered POF (with diameter of 0.45 mm) and Fig. 2 (c), (d) and (e) Tapered POF coated with agarose gel of 0.5, 1 and 1.5% weight content respectively (scale: 1cm: 1.5mm).

Figure 5.3 shows the experimental setup for the proposed sensor to detect change in RH using the tapered POF with and without agarose gel. The setup consists of a light source, an external mechanical chopper, the proposed sensor, 1365 data logging humidity-temperature meter, a highly sensitive photo-detector, a lock-in amplifier and a computer. The input and output ports of the tapered POF were connected to the laser source and photo-detector, respectively. The light source used in this experiment was a He-Ne laser operating at a wavelength of 633 nm with an average output power of 5.5 mW. It is chopped at a frequency of 113 Hz by a mechanical chopper to avoid the harmonics from the line frequency which is about 50 to 60 Hz. The 113Hz frequency was chosen as an odd number to prevent multiplication of 50 and 60 Hz besides it is an acceptable value of output and stability. The He-Ne light source was launched into the

tapered POF placed in a sealed chamber with a dish filled with saturated salt solution. The sealed chamber was constructed with a hole and the tapered POF was introduced through it into the sealed receptacle and suspended in the air above different saturated salt solutions in order to measure different values of RH [Corres et al., 2006]. The output light sent into the silicon photo-detector (818 SL, Newport) and the resulting electrical signal fed into the lock-in amplifier (SR-510, Stanford Research System) together with the reference signal of the mechanical chopper. The output from the lock-in amplifier relayed to a computer through an RS232 port interface to be processed using Delphi software. The reference signal from the chopper was matched with the input electrical signal from the photo-diode. This creates a very sensitive detection system that is able to remove the noise generated by the laser source, photo-detector and the electrical amplifier in the photo-detector. In the experiment, the performance of the proposed sensor was investigated for a series of changes in RH ranging from 50 to 80% using 1365 data logging humidity-temperature meter.

Throughout the experiment, the corresponding output voltage was measured by a lock-in amplifier which provides accurate measurements even though the signal is relatively very small compared to noise. Furthermore, a well-regulated power supply is used for the red He-Ne laser to minimize the fluctuation of source intensity.

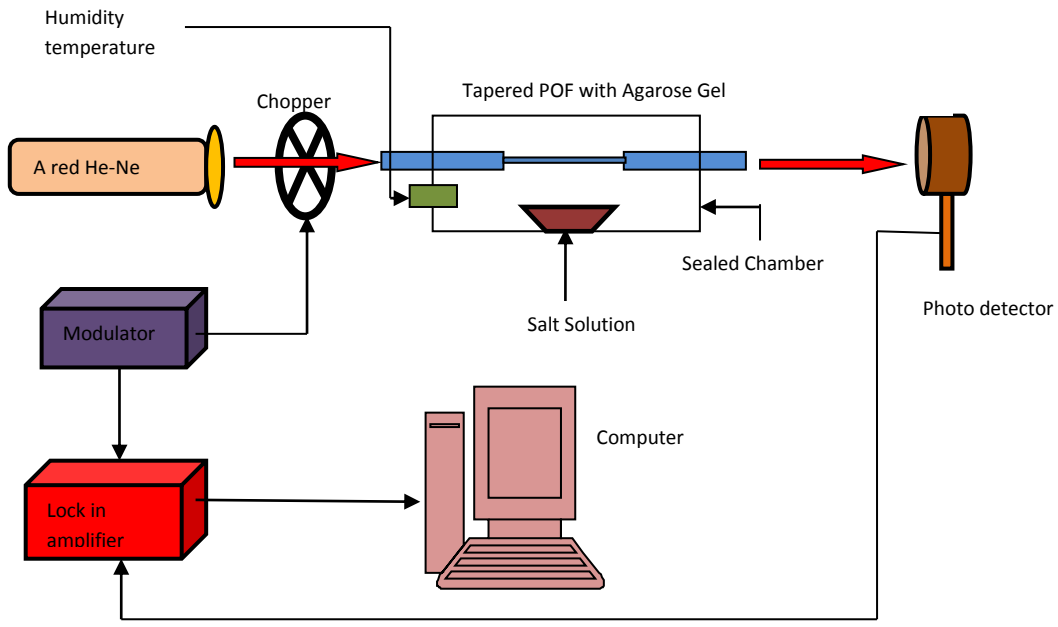

Figure 5.3:Experimental setup for the proposed sensor to measure relative humidity using a tapered POF with agarose gel.

5.4.2 Performance of the sensors

The refractive index of agarose gel used in this experiment was measured using the digital refractometer, which can measure the refractive index and other related parameters with high precision within a short time. The measured refractive index values for the agarose gel were obtained at 1.3339, 1.3299 and 1.3297 for 0.5, 1 and 1.5 % of weight contents, respectively. Figure 5.4 shows the variation of the transmitted light from the tapered POF against the RH for fiber without and with agarose gel of 0.5% weight content deposited onto the tapered region. It is observed that the intensity of the transmitted light through the agarose coated tapered fiber decreases as relative humidity increases from 50 to 80%. Without the agarose coating, the sensitivity of the sensor is obtained at 0.0033 mV/% with a slope linearity of more than 96.54% and limit of detection of 45.45%. Meanwhile the tapered fiber with agarose gel coating produces

a better sensitivity of 0.0228mV/% with a higher slope linearity of more than 98.36% and a limit of detection of 0.921%. The limit of detection is calculated by dividing the standard deviation with the sensitivity, which indicates that the system is more efficient when the value is lower. Figures 5.5 and 5.6 show the variation of the transmitted light against the relative humidity for the POF with agarose gel at 1% and 1.5 % weight content deposited onto the tapered region respectively. Again, the intensity of the transmitted light decreases as the relative humidity changes from 50 to 80%. The tapered fiber with agarose gel of 1% weight content shows a sensitivity of 0.0103 mV/% with a slope linearity of more than 94.95% and a limit of detection of 2.635% while the one with agarose gel of 1.5% weight content produces a sensitivity at 0.0079 mV/% with a slope linearity of more than 98.53% and a limit of detection of 6.853%. The limit of detection is calculated by dividing the standard deviation with the sensitivity, indicates that the system is more efficient. In all there pattern, the output voltage is found to be decreasing. This is because, as the RH increases, the polymer swells in the presence of water molecules. According to Lee et al. [2007] the RI value of agarose gel varies from 1.52 to 1.54 when RH changes from 20% to 80%. The humidity sensitive layer of the composite has an RI value which is higher than that of the core which creates a lossy waveguide.

The transfer function for the output voltage versus relative humidity is obtained as follows for agarose gel coating ratios of 0.5, 1 and 1.5% respectively.

$$y = -0.0228x + 3.3468 \quad (5\text{-}2)$$

$$y = -0.0103x + 2.5859 \quad (5\text{-}3)$$

$$y = -0.0079x + 2.1189 \quad (5\text{-}4)$$

and the following transfer function is obtained for the fiber without the agarose gel coating

$$y = 0.0028x + 0.3634 \quad (5.5)$$

In short, bare tapered fiber is immune to humidity change but tapered fiber coated with hydrophilic material such as agarose gel demonstrates a good sensitivity. Agarose has a high porosity which allows the gel to absorb moisture and perform as humidity sensor. The agarose gel used is based on swelling nature of hydrophilic materials which causes refractive index changes in accordance with humidity and modulates the light propagating through the fiber. The fiber with agarose gel of 0.5% weight content shows higher sensitivity in comparison with 1% and 1.5% due to the effect of pore size. As mentioned by Stellan et al. [1981] the porosity of agarose gels decreases as the concentration of agarose increases. In addition to that, the lower limit of detection for the tapered fiber with agarose gel compared to bare fiber shows that the system is more efficient.

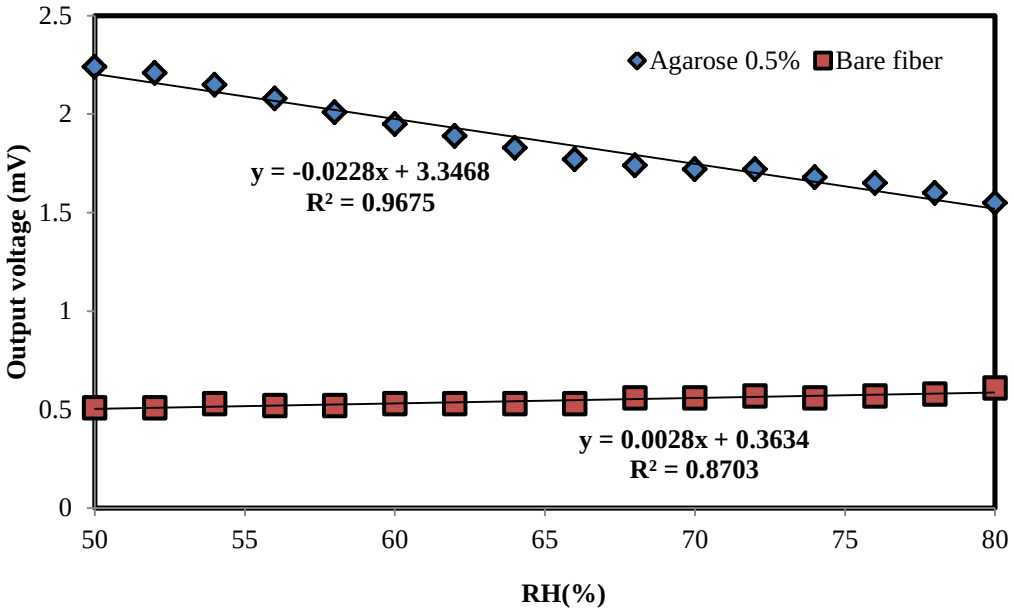

Figure 5.4:Output voltage against RH for the bare fiber and tapered fiber with agarose gel of 0.5% weight content.

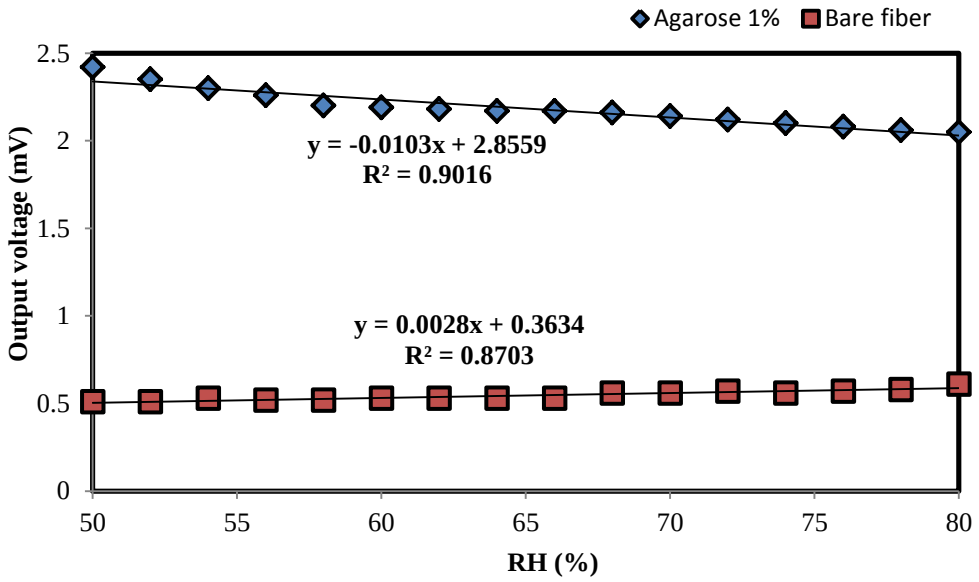

Figure 5.5:Output voltage against RH for the bare fiber and tapered fiber with agarose gel of 1% weight content

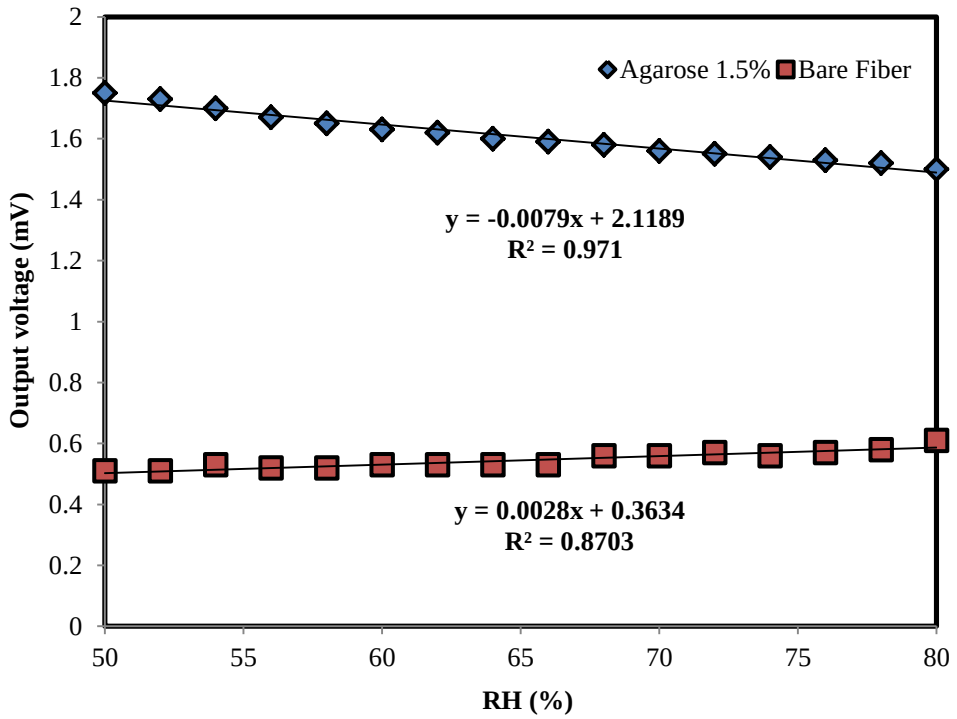

Figure 5.6:Output voltage against RH for the bare fiber and tapered fiber with agarose gel of 1.5% weight content

Reversibility of the results is another important issues that need to be justified for practical application of any sensor system. As for that, this parameter is tested for the reported system. In the experiment, the output measurement as a function of concentration are recorded for two different runs and the results are compared in Figure 5.7. As can be noticed from the figure, the maximum difference between the two runs is about ±0.05mV, which is acceptable for a full-scale output of 2.25 mV.

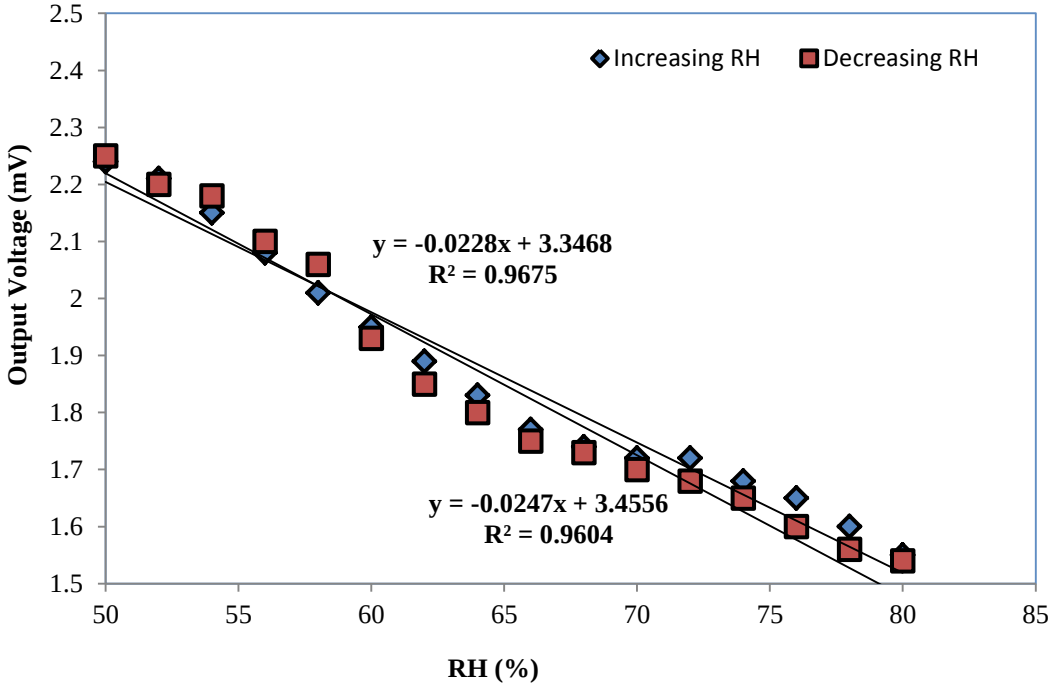

Figure 5.7:The reversibility of the results obtained for two different runs (RH).

The performance characteristic of the proposed sensor is summarized in Table 5.1. Overall, the sensor is observed to be sufficiently stable with standard deviations of 0.021mV for agarose gel of 0.5% weight content, 0.027mV for agarose gel of 1% weight content and 0.054mV for agarose gel of 1.5% weight content as recorded for a time duration of 100 second. These results show that the proposed sensor is able to gauge relative humidity in real time.

Table 5.1:Table performance of the proposed sensor

Performances	Bare fiber	Fiber with agarose 0.5% weight content	Fiber with agarose 1% weight content	Fiber with agarose 1.5% weight content
Sensitivity	0.0028	0.0228	0.0103	0.0079
Linearity	93.28	98.36	94.95	98.53
Std Deviation	0.1509	0.021	0.027	0.054
Limit of detection	53.89	0.921	2.635	6.835

5.5 Tapered fiber with HEC/PVDF coating for RH sensor

Hydroxyethyl cellulose is a gelling and thickening agent resulting from cellulose. It is extensively used in cosmetics, cleaning solutions, and other domestic products. Meanwhile, Hydroxyethylcellulose/ polyvinylidenefluoride (HEC/PVDF) composite is a class of polymeric material known for its excellent water absorption properties [Muto et al., 2003]. Therefore, in this section, tapered POF is coated by a polymer blend of HEC/PVDF composite to sense the change in RH. The coating of the tapered fiber changes its optical properties in response to an external stimulus. The tapered fiber with the composite coating acts as an effective refractive index cladding that allow more lights to be transmitted in hydrates state. The coating with HEC/PVDF composite increases the sensitivity of the proposed sensor due its ability to swell in a humid atmosphere resulting in a drop in its refractive index below that of the core and thus allowing more transmission from the tapered fiber. The measurement is based on

intensity modulation technique where the output voltage of the transmitted light is investigated for changes in RH.

5.5.1 Experimental proceduce

For the preparation of HEC/PVDF, 1 g of PVDF powder (Mw = 275,000) was dissolved in 120 ml dimethyl formamide (DMF) at the 90^{o}C in water bath. Then, the PVDF solution was cooled down to room temperature before 4 g of hydroxyethyl cellulose (HEC) was added to the solution. The mixed solution was continuously stirred at room temperature for about 10 hours in order to get a completely homogenous solution as described by Muto et al. [2003]. Figures 5.8 (a) and (b) show a sample of HEC/PVDF composite solution and its microscopic image respectively.

(a) (b)

Figure 5.8:Image of (a) HEC/PVDF composite, (b) microscopic image of HEC/PVDF composite.

The linear type of tapered POF was then prepared using acetone, de-ionized water and sand paper in accordance with chemical etching technique as described in the previous sections. The tapered fiber used in this study has a stripped region waist diameter of 0.45 mm as recommended by Beres et al. [2011]. Both ends of the POF

were held and straightened on translation stages to deposit the HEC/PVDF onto the tapered fiber. In the process, the prepared HEC/PVDF composite solution was slowly dropped onto the tapered region of the fiber using syringe and left to dry for 48 hours. Figures 5.9 (a) and (b) show the microscope images of the original un-tapered and tapered POF, which have a cladding diameter of 1 mm and 0.45 mm respectively. Figure 5.9(c) shows the tapered fiber coated with HEC/PVDF composite.

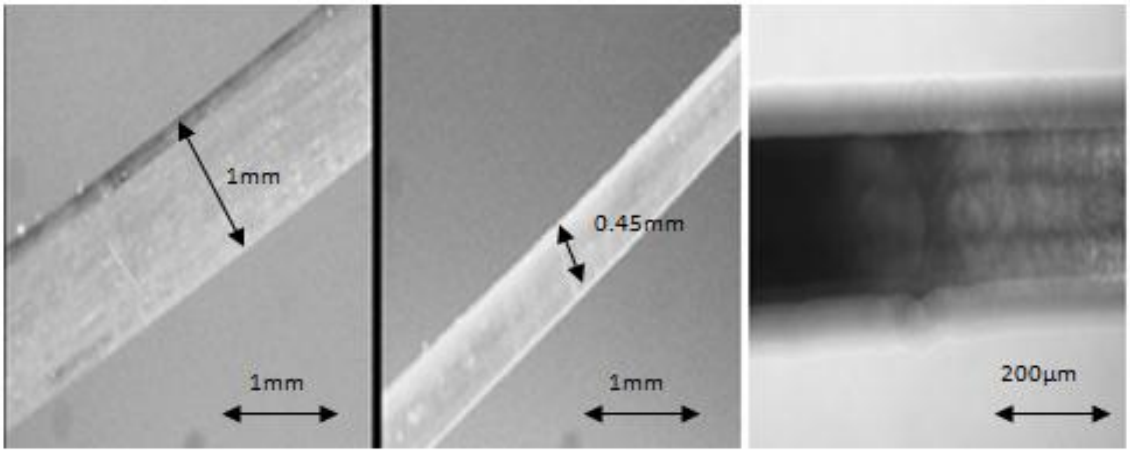

(a) (b) (c)

Figure 5.9: Microscopic images of (a) un-tapered POF (with diameter of 1 mm), (b) Tapered POF (with diameter of 0.45 mm) and (c) Tapered POF with HEC/PVDF composite.

5.5.2 Performance of the sensors

The sensor experiment is carried out using a similar setup of Fig. 5.3. In the experiment, the transmitted output voltage is measured for changes in RH using the fabricated tapered POF coated with HEC/PVDF composite as a probe. Fig. 5.10 shows the variation of the transmitted light from the tapered POF against the RH for fiber with and without HEC/PVDF composite deposited onto the tapered region. The change in the

intensity of the transmitted light of the HEC/PVDF composite on tapered fiber increases with RH in a quadratic manner. The adjusted R-square value or the coefficient of the determination is the measure of the goodness of fit which is 0.9869. The considerably high values of the adjusted R-square allow the prediction of unknown RH by the model. This is opposed to the trend demonstrated by the bare fiber where the output remains constant despite the increase of RH. According to Muto et al. [2003], the refractive index of hydroxyethylcellulose (HEC) film, which was measured using Abbe's refractometer, changed from 1.51 in the dry state to 1.48 in humid air with 80% RH. The humidity sensitive layer of the composite has an RI value which is higher than that of the core in dry state. This situation creates a lossy waveguide and as the cladding layer hydrates, the RI value falls below that of the core and increases the intensity of light propagating through the core.

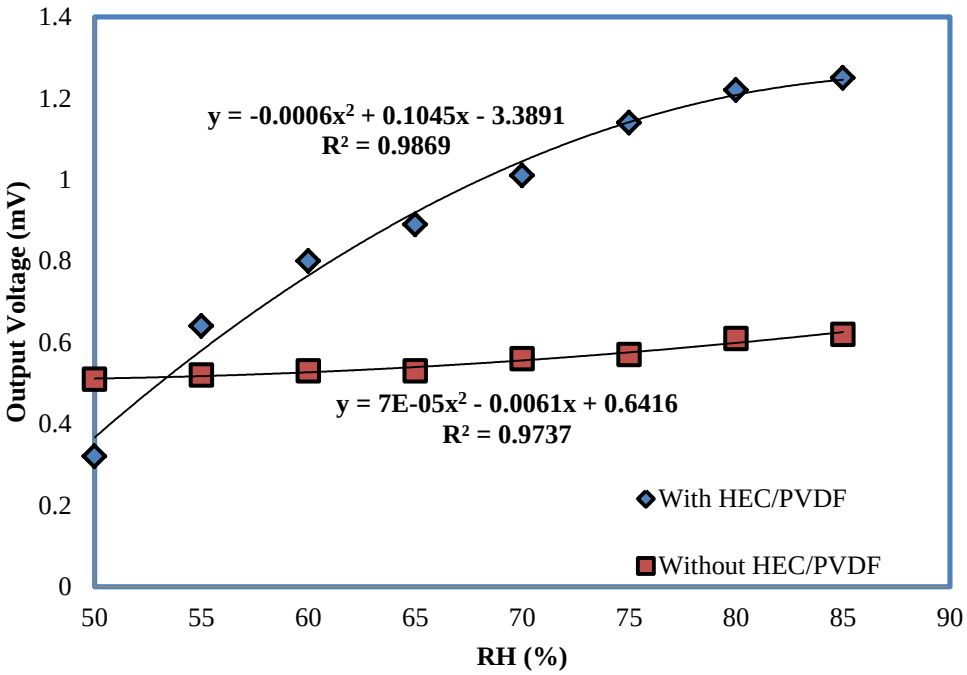

Figure 5.10:Output voltage against RH for the proposed tapered POF based sensor with and without HEC/PVDF composite

Figure 5.11 depicts the output voltage from the photo-detector which shows that the transmitted light intensity linearly increases as the RH rises from 55 to 80%. The bare fiber (without HEC/PVDF) has a sensitivity of 0.0034 mV/% with a slope linearity of more than 94.71% and limit of detection of 45.45%. Meanwhile the probe with the HEC/PVDF composite produces a better sensitivity of 0.0231 mV/% with a better slope linearity of more than 99.65% and a limit of detection of 5.75%. Again, the lower limit of detection for the probe with HEC/PVDF shows that the system is more efficient. The lower limit of detection, calculated by dividing the standard deviation with the sensitivity, indicates that the system is more efficient.

The transfer function for the output voltage versus relative humidity is obtained as follows for the sensor with HEC/PVDF coating.

$$y = 0.0231x + 0.6083 \quad (5\text{-}6)$$

and the following transfer function is obtained for the fiber without the HEC/PVDF coating

$$y = 0.0034x + 0.3219 \quad (5\text{-}7)$$

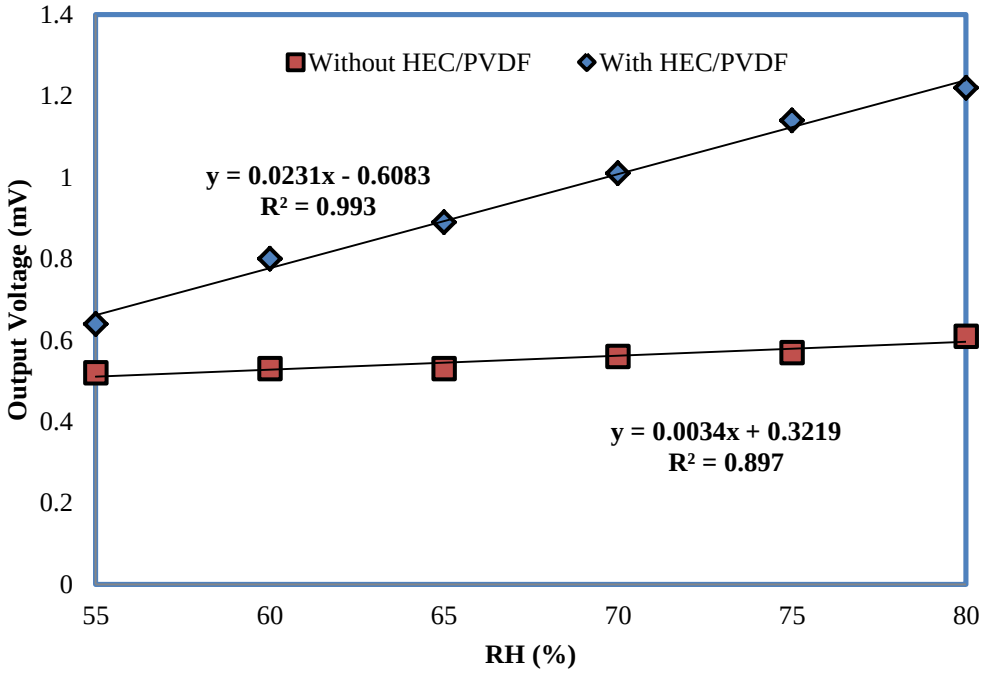

Figure 5.11: Performance of Humidity Sensor with and without HEC/PVDF composite

Reversibility capability of the sensor is also investiagted. The experiment on investigating the relation between output voltage and RH is carried out for two different approaches; increasing and decreasing manners. The results are compared in Figure 5.12, where the maximum difference between the two runs is about ±0.05mV. This difference is acceptable since the full-scale output is 1.26 mV.

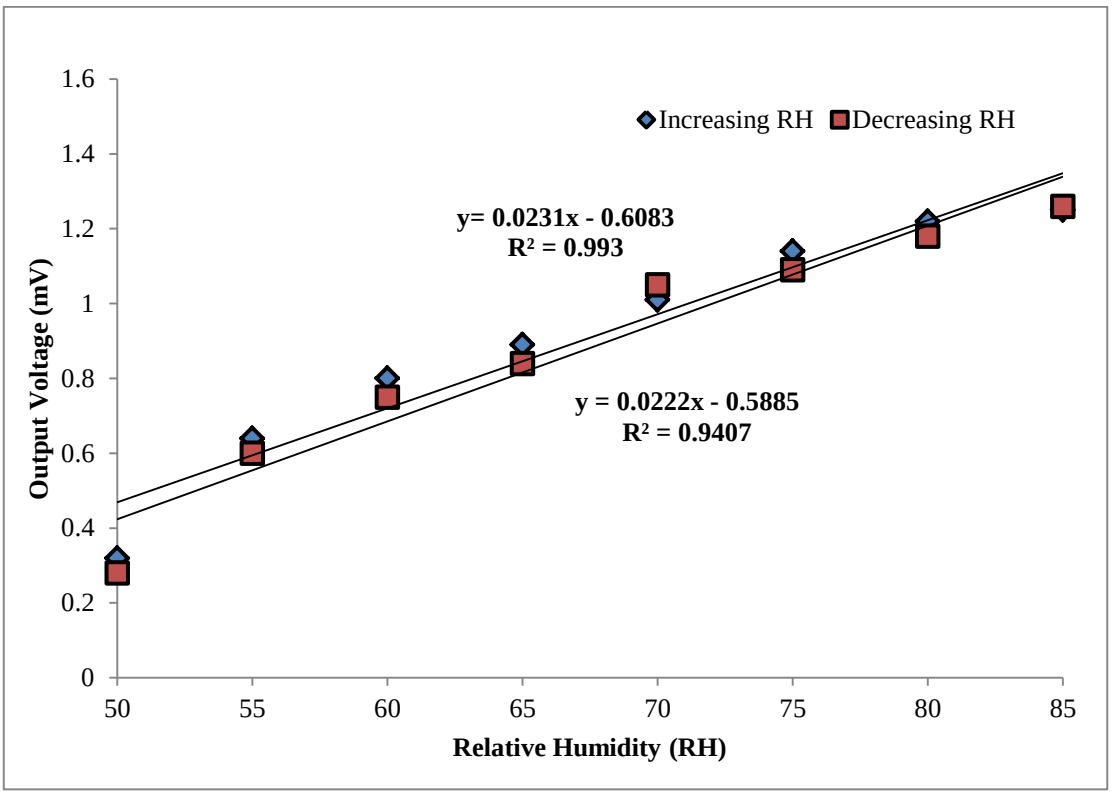

Figure 5.12:The reversibility of the results obtained for two different runs (RH).

The performance characteristic of the proposed sensor is summarized in Table 5.2. Overall, the sensor is observed to be sufficiently stable with a standard deviation of 0.133mV for POF probe with HEC/PVDF composite as recorded in time duration of 100 second. Throughout the experiment, the corresponding output voltage was measured by a lock-in amplifier which provided accurate measurements even though the signal was relatively very small compared to noise. Furthermore, a well-regulated power supply was used for the red He-Ne laser and this minimizes the fluctuation of source intensity. These results show that the proposed sensor is suitable for measuring RH.

Table 5.2:Performance of the proposed sensor

Performances	With HEC/PVDF	Without HEC/PVDF
Sensitivity	0.0231mV/%	0.0033mV/%
Linearity	96.72%	96.54%
Std deviation	0.133mV	0.1509mV
Limit of detection	5.75%	45.45%

5.6 Tapered fiber with Zinc Oxide Coating for RH sensor

Zinc Oxide (ZnO) is a semiconductor with a bandgap of 3.3 eV and has been a subject of intense interest in recent years for various applications such as communication, biosensor etc [Zhang et al., 2005; Coleman & Jagadish, 2006; Yakimova et al., 2012]. It has a wide range of properties including a range of conductivity from metallic to insulating (including n-type and p-type conductivity), high transparency, piezoelectricity, wide-bandgap semiconductivity, room-temperature ferromagnetism, and huge magneto-optic and chemical-sensing effects [Schmidt-Mende & MacManus-Driscoll, 2007]. The advantages of ZnO are that it can be easily processed by wet chemical etching and has shown an excellent stability under high-energy radiation. In addition, it can be grown in a variety of nanostructured morphologies by various low cost and low temperature methods [Djurisic, Ng, & Chen, 2010]. These nanostructures have many unique advantages such as high surface area and high sensitivity even at room temperature [Schmidt-Mende & MacManus-Driscoll, 2007]. For instance, light coupled to nanostructures enhances the optical interaction

between the device and the ambient environment [Liu et al., 2012]. Besides, in combination with immobilized enzymes, it can also enhance the direct electron transfer between the enzyme's active sites and the electrons [Ali et al., 2012]. Therefore, many new sensors have been developed based on the ZnO nanostructure. For instance, ZnO nanowires grown on the surface of gold coated on flexible plastic substrate has been demonstrated as a good uric acid biosensor [Usman Ali et al., 2011]. In our earlier work, a low cost and simple uric acid biosensor was also demonstrated using a ZnO nanostructure on tapered POF.

The deposition of ZnO nanostructures have been demonstrated on various polymer and silica substrates [Zubia & Arrue, 2001; Kim et al; 2012]. Looking at the compatibility of ZnO crystal structure, there is no apparent difference between polymer and silica, as both do not have defined crystal structures. In this section, a new sensor for detecting changes in RH is proposed and demonstrated using a tapered POF coated with ZnO nanostructures, which is grown using both seeded and non-seeded techniques. The ZnO nanostructures on the tapered fiber induce changes of the optical properties in response to an external stimulus. The measurement is based on intensity modulation technique to detect the changes in RH.

5.6.1 Experimental procedure for ZnO based RH sensor.

The tapered POFs were prepared based on chemical etching technique using acetone, de-ionized water and sand paper. They have a stripped region waist diameter of 0.45 mm and the total length 10 mm, which is similar to the previous sensors. The preparation for ZnO nanostructures on the tapered fiber consists of two primary steps: First, the seed layer to grow the ZnO nanostructures on the fiber was developed using a simple manual dip coating technique. The seeded solution was prepared using zinc acetate dehydrate ($Zn(CH_3COO)_2 \cdot 2H_2O$) as a precursor dissolved in isopropanol with

molarity of 0.025 M. The solution was stirred at 60° C for 2 hours in ambient to yield a clear and homogenous solution. Then, the solution was cooled down to room temperature for the coating process. The fiber was manually dipped into the seeding solution and was dried at 50° C to evaporate the solvent and to remove the organic residuals. This coating and drying method was repeated for 5 times to increase the thickness of the tapered fibers.

Following this, another solution was prepared to grow ZnO nanostructures on the bare tapered fiber and ZnO seeded tapered fiber. This is done by dissolving 0.01M zinc nitrate hexahydrate ($Zn(NO3)_2.6H_2O$ and 0.01M hexamethylenetetramine (HMTA) in 100ml deionized water. The deposition process of ZnO nanorods on the fibers was performed using sol-gel immersion method by suspending the bare and seeded-ZnO fibers in the growth solution at 60°C for 15 hours. Figures 5.13(a) and (b) show the field emission scanning electron microscopy (FESEM) images of ZnO nanostructures grown on seeded and non-seeded tapered fiber, respectively. A similar RH sensor experiment was carried out for both sensor probes using a similar experimental setup of Figure 5.3.

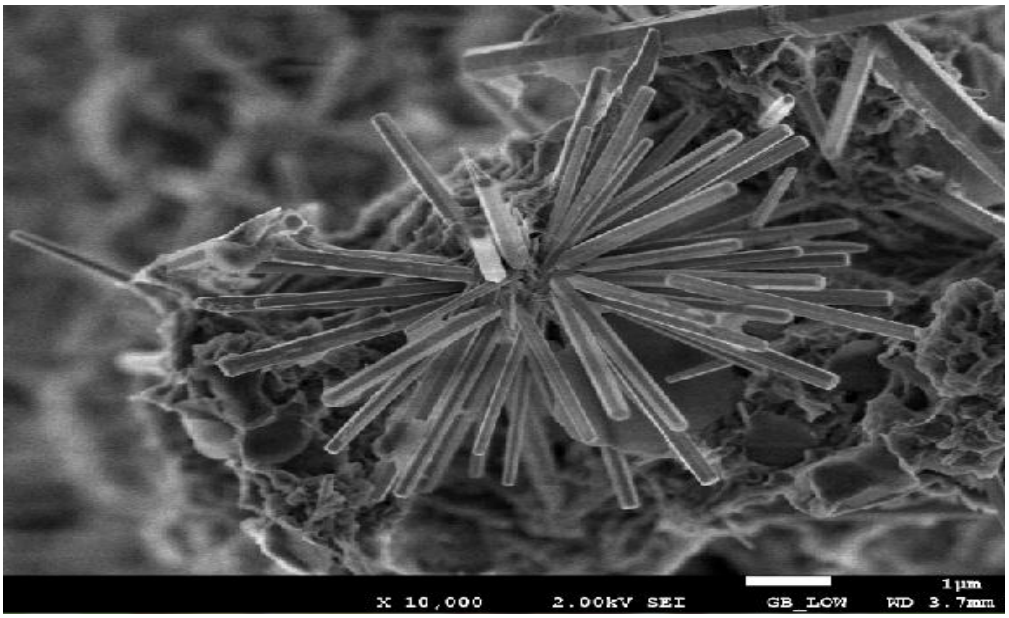

(a)

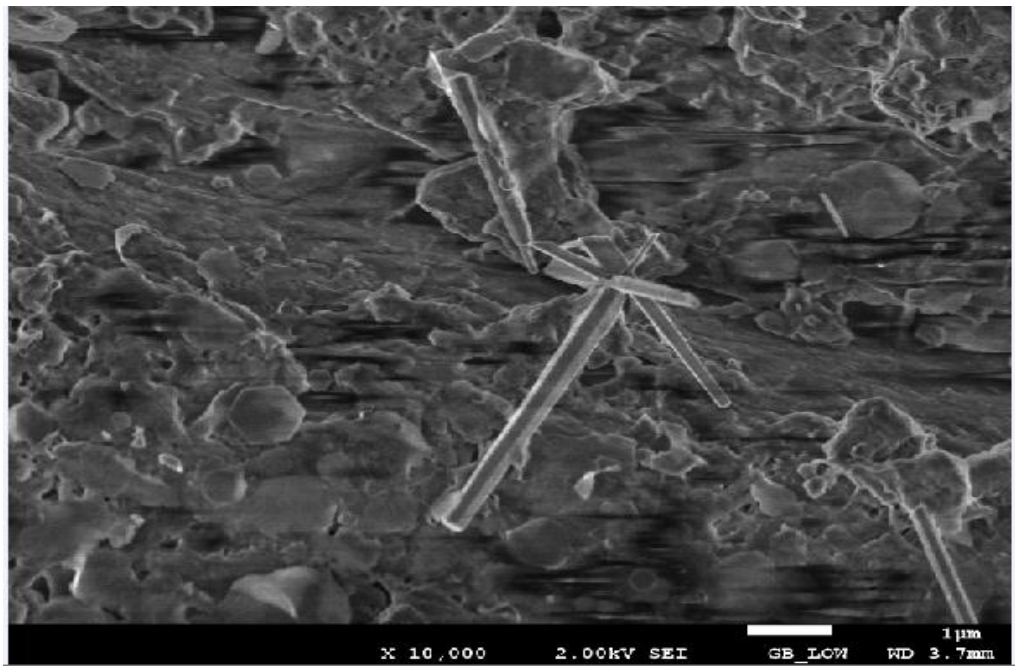

(b)

Figure 5.13:FESEM images with ZnO nanostructures grown on seeded tapered fiber (Fig.5.13(a)) and on non-seeded tapered fiber (Fig.5.13(b)).

5.6.2 Performance of the sensors

Figure 5.14 shows the sensing result of the transmitted light from the tapered POF coated with ZnO nanostructures grown using the seeded and non seeded technique against the RH. The change in the intensity of the transmitted light decreases linearly with RH for both cases. According to Liu et al. [2012], the effective refrective index (RI) of ZnO composite varies from 1.698 to 1.718 with RH change from 10-95%. The ZnO composite are exposed to an environment of humidity causes rapid surface adsorption of water molecules. The optical properties of ZnO composite surfaces are modulated by the surface adsorption of water molecules. The increase of water molecules being absorped on ZnO composite results in an increase of relative humidity [Liu et al., 2012]. The increasing water molecules cause an increase in both effective RI of surrounding medium and absorption coefficient of the ZnO composite surfaces and

leads to larger leakage of light. Therefore, the transmission light reduces with the RH increment as shown in Figure 5.14.

As shown in Figure 5.14, the sensor configured with non-seeded ZnO nanostructures has a sensitively of 0.0057mV/% with a slope linearity of more than 91.67% and limit of detection of 13.84%. On the other hand, the sensitivity of the improved sensor with seeded ZnO nanostructures is 0.0258mV/% with a slope linearity of more than 95.48% and limit of detection of 0.143%. It is found that the sensitivity of the sensor is significanly improved by the seeding technique. Evidently seeding the tapered fiber with ZnO nanoparticles as seeds has enhanced the growth of nanorods. In the non-seeded sample, the morphorlogy of the ZnO layer were unstructured suggesting the growth of layers comprising of nanoparticles. This is attributed to the ZnO nanostructures grown by this techniques, shown in Figure 5.13(a). These rods absorb more water and increases the sensitivity of the sensor. In addition, the seeding technique reduces the limit of detection, which indicates that the sensor system is more efficient. The reversibility capability of the sensor is also investigated and the result is shown in Figure 5.15. As shown in the figure, the maximum difference between the two runs is only about ±0.05mV, which indicates that the sensor has a very good reversibility.

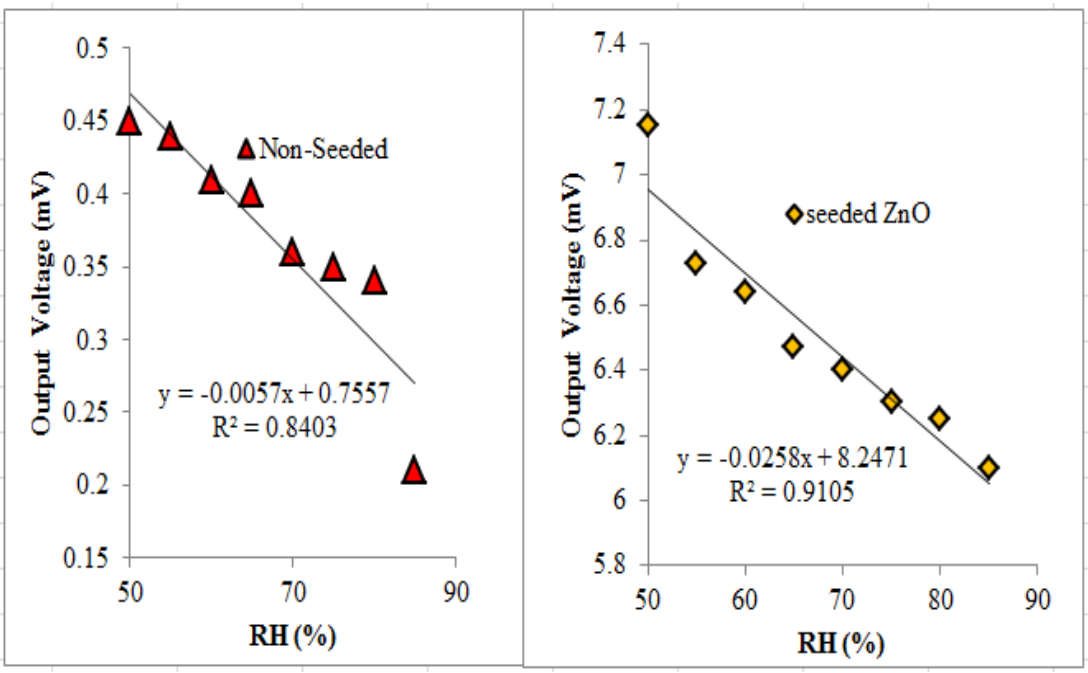

Figure 5.14:Sensing results for the proposed relative humidity sensor using a tapered POF coated with ZnO nanostructure.

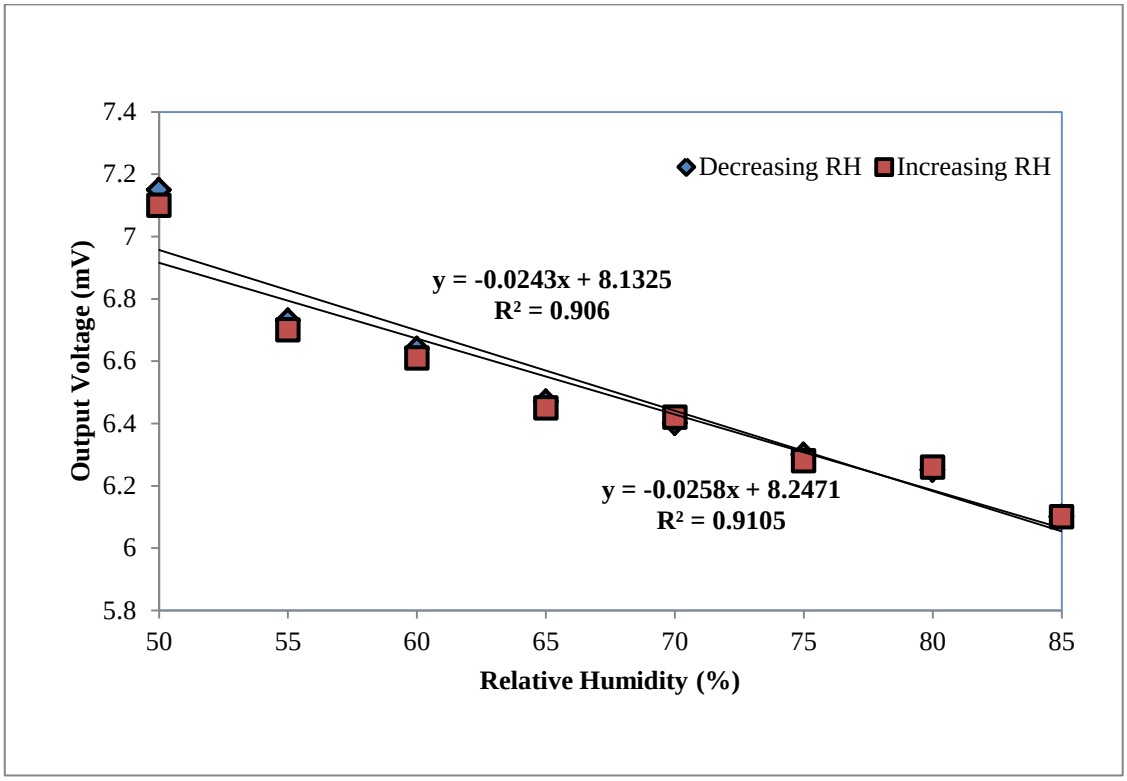

Figure 5.15:The reversibility of the results obtained for two different runs (RH)

The performance characteristic of the proposed sensor is summarized in Table 5.3. The sensor is observed to be sufficiently stable for RH changes with standard deviations of 0.0037mV and 0.0789mV as the measurement is taken for 100 seconds for the probe obtained by seeded and non-seeded processes, respectively. These results show that the tapered POF with ZnO nanostructures is capable for RH detection. It is also found that the seeding approach improves the sensitivity and limit of detection of the sensor.

Table 5.3:The performance of the proposed RH sensor

Performances	**ZnO Coating**	**ZnO Grown**
Sensitivity	0.0057 mV/%	0.0258 mV/%
Linearity	91.67 %	95.42 %
Standard deviation	0.0789mV	0.0037mV
Limit of detection	13.84%	0.143%

5.7 Summary

Three RH sensors have been proposed and demonstrated using tapered POF in conjunction with various sensitive coating materials. These materials are agarose gel, Hydroxyethylcellulose/ polyvinylidenefluoride (HEC/PVDF) and zinc oxide (ZnO). Their refractive indices vary with the amount of surrounding water vapor with a good repeatability and sensitivity. The sensors are based on an intensity modulation and uses PMMA plastic tapered fibers coated with the sensitive materials as a probe. Hence, these humidity sensors might be preferred by some application requiring less cost and sensitivity. Variations of refractive index are achieved through the changes in relative

humidity. Subsequent performance analysis allows the identification of the experimental dependence of the surrounding refractive index sensitivity on the three different sensitive coating materials.

It is observed that the probe sensitivity improves with the coating. Since the cladding area of the tapered POF has been removed, the sensitive material works as passive cladding and its refractive index can influence the amount of power loss as the signal propagates through the tapered region. This is attributed to the difference in refractive index between the cores and cladding that influences the amount of light confinement inside the core. In case of agarose gel and HEC/PVDF, variations of refractive index are achieved when the polymers swell as the water molecules attached to the surface. The RH sensor with agarose gel coating (0.5 wt.%) produces a sensitivity of 0.0228 mV/% with a higher slope linearity of more than 98.36% and a limit of detection of 0.921%. With HEC/PVDF coating, the sensor sensitivity is slightly improved to 0.0231 mV/% with a better slope linearity of more than 99.65%. On the other hand, the effective refrective index of ZnO composite changes with RH. When the composite are exposed to an environment of humidity, it causes rapid surface adsorption of water molecules and changes its optical property. The increase of RH causes an increase in both effective refractive index of surrounding medium and absorption coefficient of the ZnO composite surfaces, which leads to larger leakage of light. It is found that the sensitivity of RH sensor with ZnO nanostructures grown on seed tapered fiber is 0.0258mV/%. The sensor has a slope linearity of more than 95.48% and limit of detection of 0.143%.

Once again, the lower standard of deviation and limit of detection of the POF probe with sensitive materials indicates that the proposed sensors are stable and efficient. The lock-in amplifier provides accurate measurements and the well-regulated power supply used for the red He-Ne laser and minimizes the fluctuation of source

intensity. These results show that the proposed sensor is applicable and useful for the relative humidity measurement and shows that the sensitive coating materials have successfully enhanced the performance of the fiber sensor.

Chapter 6

Conclusions and Future Works

6.1 Conclusions

The plastic optical fiber (POF) is replacing silica fibers especially for sensor applications due to its admirable uniformity and other physical properties in term of strength and flexibility. Compared to the silica fibers, it can be stretched further without breaking, simpler and less expensive components and lighter weight. The efforts to develop smaller but more sensitive and accurate sensors to cater to a large range of physical, chemical and biomedical measurements constitute a substantial drive for optoelectronics research today. Recently, tapered optical fibers have attracted many interests especially for sensing applications due to a higher portion of evanescent field interacting with the physical ambience of its surrounding. The measuring or sensing of refractive index is one of importance scientific technique for sensors. Refractive index is a fundamental material property for which its accurate measuring is crucial in many applications. Any change in the optical or structural characteristic of the chemical, provokes a change in the effective index of the optical fiber, changing its transmission properties. To enhance the sensitivity of surrounding refractive index variation around the optical fibers, the tapered fiber is coated with sensitive materials. The coated tapered fiber changes optical properties in response to an external stimulus.

In our work presented here, the fabrication of tapered PMMA fibers are firstly demonstrated based on the heat-and-pull technique and chemical etching technique. The sensors are demonstrated to measure the refactive index of the external liquid using a probe, which is obtained by these two techniques. It is found that chemical-etched taper provides better performance in term of repeatability. The repeatability of the etching

process in terms of taper ratio and shape and its superior sensitivity has led to its further use in realizing several practical evanescent field sensors. In this work, various evanescent field absorption sensors are developed for electrolyte and nonelectrolyte solutions using the PMMA tapered fiber probe. The effect of chemical etching, size of fiber for better sensitivity, bending effect and refractive index of the solvent on the sensitivity of the sensor have been reported successfully.

In Chapter 4, the tapered fiber are coated with sensitive coating materials such as graphene, single walled carbon nanotube and zinc oxide and demonstrated as a sensor to detect uric acid concentration. Variations of refractive index are achieved through the use of different concentration of uric acid solution. Subsequent performance analysis allows the identification of the experimental dependence of the surrounding refractive index sensitivity on the three different sensitive coating materials. It is observed that the transmitted light intensity improves with the sensitive material coating. Simple fiber optic chemical sensors have been succesfully demonstrated to measure uric acid change between the range from 100ppm to 500ppm. Table 6.1 below summarizes the performance of the proposed chemical sensors.

Table 6.1:Performance of chemical sensors

	Bare fiber	Fiber with graphene	Fiber With SWCNT-PEO	Fiber with ZnO nanostructure
Sensitivity (mV/ppm)	0.0003	0.0021	0.0023	0.0025
Linearity (%)	97.65	98.88	98.6	98.28
Std Deviation (mV)	0.029	0.016	0.016	0.014
Limit of detection (ppm)	96.67	7.61	6.95	5.6

It is observed that the fiber without the coating has the lowest sensitivity of 0.0003mV/ ppm with a slope linearity of more than 97.65. By coating the tapered fiber probe with graphene, the sensitivity of the sensor increases to 0.0021mV/ppm with a better slope linearity of more than 98.88%. The performance of the sensor can be further improved by using SWCNT-PEO composite as a sensitive material. The sensor produces a sensitivity of 0.0023 mV/% with a slope linearity of more than 98.6 % and a limit of detection of 6.95 ppm. The performance of the tapered fiber based sensor is also investigated using nanostructures instead of normal coating as a sensive material. It is found that by growing a seeded Zinc oxide nanostructures on the tapered fiber, the sensor produces a sensitivity of 0.0025mV/ppm, which is slightly higher than the other sensors. The sensitive material works as passive cladding and its refractive index influences the amount of power loss as the signal propagates through the tapered region. This is attributed to the difference in refractive index between the core and cladding that influences the amount of light confinement inside the core. The tapered fiber with sensitive coating materials such as graphene, single walled carbon nanotube and zinc oxide are successfully demonstrated as a sensor to detect uric acid concentration.

In Chapter 5, the tapered fiber are coated with sensitive coating materials such as agarose gel, Hydroxyethylcellulose/ polyvinylidenefluoride (HEC/PVDF) and zinc oxide (ZnO) for sensing relative humidity (RH) changes. It is observed that the transmitted light intensity improves with the sensitive material coating. The performance characteristic of the RH sensors is summarized in Table 6.2.

Table 6.2:Performance of the RH sensors

	Bare fiber	**Fiber with agarose 0.5% weight content**	**Fiber with HEC/PVDF composite**	**Fiber with ZnO nanostructure**
Sensitivity (mV/%)	0.0028	0.0228	0.0231	0.0258
Linearity (%)	93.29	98.36	99.65	95.48
Std Deviation (mV)	0.1509	0.021	0.133	0.0037
Limit of detection (%)	45.45	0.921	5.75	0.143

Simple fiber optic RH sensors have been succesfully demonstrated to measure RH within a range from 50 to 80%. It is observed that the transmitted light intensity increases linearly the increase of RH at surrounding the probe. The sensor with agarose gel of 0.5% weight content produces a sensitivity of 0.0228 mV/% with a slope linearity of more than 98.36% and a limit of detection of 0.927%. We believe that other hydrophilic materials can also be used to coat the tapered POF as long as its refractive index can change in accordance with relative humidity to modulate the light propagating through the fiber. For instance, the use of tapered POF coated with HEC/PVDF composite as the humidity sensor probe produces a sensitivity of 0.0231 mV/% and a linearity of more than 99.65%. The limit of detection is calculated to be 5.75%. The humidity sensitive layer of the composite has an RI value which is higher than that of

the core in dry state. This situation creates a lossy waveguide and as the cladding layer hydrates, the RI value falls below that of the core and increases the intensity of light propagating through the core. The rise in humidity level thus reduces the effective refractive index of the composite cladding thus allowing more light to be transmitted. However, the better sensivity is achieved with the growth of ZnO nanostructure on the tapered POF. This sensor provides the highest sensitivity of 0.0258mV/% with a slope linearity of more than 95.48% and limit of detection of 0.143%.

In conclusion, the sensive material plays an important roles in both chemical and RH sensors. Since the cladding area of the tapered POF has been removed, the sensitive material works as passive cladding and its refractive index can influence the amount of power loss as the signal propagates through the tapered region. This is attributed to the difference in refractive index between the core and cladding that influences the amount of light confinement inside the core. This shows that the sensitive coating materials have successfully enhanced the performance of these POF sensors.

6.2 Recommendations for future works

Summarizing, the applicability of manufactured sensors depends on the deposition technique utilized while the sensitivity of manufactured sensors strongly depends on the coating materials used. Therefore, the important area of research includes coating sensitive material on the tapered fibers. In order to further improve on fabricating biosensors, a suitable sensitive coatings is needed to interact and perform with complex medium. Recently zinc oxide has attracted much attention within scientific community as a ‘future material’. However, further studies are needed on the optical, structure properties and the dopping effect of this material. In the future, work should include comprehensive and more detailed study on high efficiency sensors using this nanostructures. As a final remark, there are vast research opportunities to be explored in the applications that take advantage of sensors based system.

References

Ahmad, A.B.H. (1994). Development of a Portable Optical Fiber Chemical Sensor Measuring Instrument, in Department of Instrumentation and Analytical Science. University of Manchester: United Kingdom, 187.

Ali, S. M. U., Ibupoto, Z. H., Kashif, M., Hashim, U., & Willander, M. (2012). A potentiometric indirect uric acid sensor based on ZnO nanoflakes and immobilized uricase. *Sensors*, *12*(3), 2787-2797.

Ang, P. K., Chen, W., Wee, A. T. S., & Loh, K. P. (2008). Solution-gated epitaxial graphene as pH sensor. *Journal of the American Chemical Society*,130(44), 14392-14393.

Ao, Z. M., Yang, J., Li, S., & Jiang, Q. (2008). Enhancement of CO detection in Al doped graphene. *Chemical Physics Letters*, 461(4), 276-279.

Arregui, F. J., Ciaurriz, Z., Oneca, M., & Matıas, I. R. (2003). An experimental study about hydrogels for the fabrication of optical fiber humidity sensors.*Sensors and Actuators B: Chemical*, *96*(1), 165-172.

Arregui, F. J., Cooper, K. L., Yanjing, L. I. U., MATIAS, I. R., & CLAUS, R. O. (2000). Optical fiber humidity sensor with a fast response time using the ionic self-assembly method. *IEICE Transactions on electronics*, 83(3), 360-365.

Arregui, F. J., Fernandez-Valdivielso, C., Ilundain, I., & Matias, I. R. (2000). A pH sensor made using cellulosic coating on a biconically tapered singlemode optical fiber. In Proceedings of SPIE, the International Society for Optical Engineering (Vol. 4185, pp. 464-467). Society of Photo-Optical Instrumentation Engineers.

Arrue, J., Jiménez, F., Aldabaldetreku, G., Durana, G., Zubia, J., Lomer, M., & Mateo, J. (2008). Analysis of the use of tapered graded-index polymer optical fibers for refractive-index sensors. *Optics express*, *16*(21), 16616-16631.

Azamian, B. R., Davis, J. J., Coleman, K. S., Bagshaw, C. B., & Green, M. L. (2002). Bioelectrochemical single-walled carbon nanotubes. *Journal of the American Chemical Society*, 124(43), 12664-12665.

Banerjee, D., Lao, J. Y., Wang, D. Z., Huang, J. Y., Ren, Z. F., Steeves, D., ... & Sennett, M. (2003). Large-quantity free-standing ZnO nanowires. *Applied Physics Letters*, 83(10), 2061-2063.

Bariain, C., Matías, I. R., Arregui, F. J., & Lopez-Amo, M. (2000). Optical fiber humidity sensor based on a tapered fiber coated with agarose gel. *Sensors and Actuators B: Chemical*, 69(1), 127-131.

Bariain, C., Romeo, I., Garrido, J., & Laguna, M. (2000). Detection of volatile organic compound vapors by using a vapochromic material on a tapered optical fiber. *Applied Physics Letters*, *77*(15), 2274-2276.

Bartlett, R. J., Philip-Chandy, R., Eldridge, P., Merchant, D. F., Morgan, R., & Scully, P. J. (2000). Plastic optical fibre sensors and devices. *Transactions of the Institute of Measurement and Control*, *22*(5), 431-457.

Batumalay, M., Ahmad, F., Lokman, A., Jasim, A. A., Harun, S. W., & Ahmad, H. (2014). Tapered plastic optical fiber coated with single wall carbon nanotubes polyethylene oxide composite for measurement of uric acid concentration. *Sensor Review*, *34*(1), 75-79.

Beres, C., de Nazaré, F. V. B., de Souza, N. C. C., Miguel, M. A. L., & Werneck, M. M. (2011). Tapered plastic optical fiber-based biosensor–Tests and application. *Biosensors and Bioelectronics*, *30*(1), 328-332.

Berger, C., Poncharal, P., Yi, Y., & de Heer, W. (2003). Ballistic conduction in multiwalled carbon nanotubes. *Journal of nanoscience and nanotechnology*,3(1-2), 1-2.

Bethune, D. S., Klang, C. H., De Vries, M. S., Gorman, G., Savoy, R., Vazquez, J., & Beyers, R. (1993). Cobalt-catalysed growth of carbon nanotubes with single-atomic-layer walls. *Nature* 363, 605-607.

Bilro, L., Alberto, N., Pinto, J. L., & Nogueira, R. (2012). Optical sensors based on plastic fibers. *Sensors*, *12*(9), 12184-12207.

Bradley, K., Cumings, J., Star, A., Gabriel, J. C. P., & Grüner, G. (2003). Influence of mobile ions on nanotube based FET devices. *Nano Letters*, 3(5), 639-641.

Brambilla, G., Finazzi, V., & Richardson, D. (2004). Ultra-low-loss optical fiber nanotapers. *Optics Express*, *12*(10), 2258-2263.

Carucci, A., & Casini, S. (2012). *U.S. Patent No. 20,120,308,490*. Washington, DC: U.S. Patent and Trademark Office.

Chen, Q., Claus, R. O., Mecham, J. B., Vercellino, M., Arregui, F. J., & Matias, I. R. (2002, March). Optical fiber sensors for breathing diagnostics. In*International Symposium on Biomedical Optics* (pp. 14-20). International Society for Optics and Photonics.

Cheng, R., Yang, H., Shao, M. Y., Hu, T., & Zhou, X. D. (2009). Dental erosion and severe tooth decay related to soft drinks: a case report and literature review. *Journal of Zhejiang University Science B*, *10*(5), 395-399.

Chopra, S., McGuire, K., Gothard, N., Rao, A. M., & Pham, A. (2003). Selective gas detection using a carbon nanotube sensor. *Applied Physics Letters*, 83(11), 2280-2282.

Chow, K. K., Tsuji, M., & Yamashita, S. (2010). Single-walled carbon-nanotube-deposited tapered fiber for four-wave mixing based wavelength conversion. *Applied Physics Letters*, *96*(6), 061104-061104.

Cole, B. E., & Zook, D. J. (2006). *U.S. Patent No. 7,057,402*. Washington, DC: U.S. Patent and Trademark Office.

Coleman, V. A., & Jagadish, C. (2006). Basic properties and applications of ZnO. *Zinc Oxide Bulk, Thin Films and Nanostructures: Processing, Properties, and Applications*, 1-20.

Cong, J., Zhang, X., Chen, K., & Xu, J. (2002). Fiber optic Bragg grating sensor based on hydrogels for measuring salinity. *Sensors and Actuators B: Chemical*,*87*(3), 487-490.

Cooper, K. R., Ma, Y., Wikswo, J. P., & Kelly, R. G. (2004, July). Simultaneous monitoring of the corrosion activity and moisture inside aircraft lap joints. In *Smart Structures and Materials* (pp. 656-666). International Society for Optics and Photonics.

Corres, J. M., Arregui, F. J., & Matias, I. R. (2006). Design of Humidity Sensors Based on Tapered Optical Fibers. *Journal of Lightwave Technology* , 24 (11), 4329–4336.

Corres, J. M., Arregui, F. J., & Matías, I. R. (2007). Sensitivity optimization of tapered optical fiber humidity sensors by means of tuning the thickness of nanostructured sensitive coatings. *Sensors and Actuators B*: Chemical, 122(2), 442-449.

Corres, J. M., Bravo, J., Matias, I. R., & Arregui, F. J. (2006). Nonadiabatic tapered single-mode fiber coated with humidity sensitive nanofilms. *Photonics Technology Letters, IEEE*, *18*(8), 935-937.

Corres, J. M., Matias, I. R., Bravo, J., & Arregui, F. J. (2008). Tapered optical fiber biosensor for the detection of anti-gliadin antibodies. *Sensors and Actuators B*: Chemical, 135(1), 166-171.

D.D. Ebbing, S.D. Gammon. (1999). General Chemistry 6th Edition, Boston New York.

Deng, C., Chen, J., Chen, X., Xiao, C., Nie, L., & Yao, S. (2008). Direct electrochemistry of glucose oxidase and biosensing for glucose based on boron-doped carbon nanotubes modified electrode. *Biosensors and Bioelectronics*, *23*(8), 1272-1277.

Djurisic, A. B., Ng, A. M. C., & Chen, X. Y. (2010). ZnO nanostructures for optoelectronics: material properties and device applications. *Progress in Quantum Electronics*, *34*(4), 191-259.

Dong, X., Long, Q., Wei, A., Zhang, W., Li, L. J., Chen, P., & Huang, W. (2012). The electrical properties of graphene modified by bromophenyl groups derived from a diazonium compound. *Carbon*, *50*(4), 1517-1522.

Ebbing, D.D. and Gammon, S.D. (1999). General chemistry 6th Edition, Boston New York.

Eggleton, B., Kerbage, C., Westbrook, P., Windeler, R., & Hale, A. (2001). Microstructured optical fiber devices. *Optics Express*, *9*(13), 698-713.

Elosua, C., Matias, I. R., Bariain, C., & Arregui, F. J. (2006). Volatile organic compound optical fiber sensors: A review. *Sensors*, 6(11), 1440-1465.

Filippov, V., Chamorovskii, Y., Kerttula, J., Kholodkov, A., & Okhotnikov, O. G. (2008). Single-mode 212 W tapered fiber laser pumped by a low-brightness source. *Optics letters*, 33(13), 1416-1418.

French, W. G., MacChesney, J. B., O'Connor, P. B., & Tasker, G. W. (1974). *Optical waveguides with very low losses. Bell System Technical Journal*, 53(5), 951-954.

Gaston, A., Lozano, I., Perez, F., Auza, F., & Sevilla, J. (2003). Evanescent wave optical-fiber sensing (temperature, relative humidity, and pH sensors). *Sensors Journal*, IEEE, 3(6), 806-811.

Gaston, A., Perez, F., & Sevilla, J. (2004). Optical fiber relative humidity sensor with polyvinyl alcohol film. Appl. Opt. , 43 (21), 4127–4132.

Geim, A. K., & Novoselov, K. S. (2007). The rise of graphene. *Nature materials*,*6*(3), 183-191.

Gentleman, D. J., & Booksh, K. S. (2006). Determining salinity using a multimode fiber optic surface plasmon resonance dip-probe. *Talanta*, *68*(3), 504-515.

Gerdt, D. W., & Gilligan, L. H. (1988, March). Variable coupler fiber optic sensor. In OE/Fibers' 87 (pp. 25-31). International Society for Optics and Photonics.

Golden, J. P., Anderson, G. P., Rabbany, S. Y., & Ligler, F. S. (1994). An evanescent wave biosensor. II. Fluorescent signal acquisition from tapered fiber optic probes. Biomedical Engineering, IEEE Transactions on, 41(6), 585-591.

Golnabi, H., Bahar, M., Razani, M., Abrishami, M., & Asadpour, A. (2007). Design and operation of an evanescent optical fiber sensor. *Optics and lasers in engineering*, 45(1), 12-18.

Grattan, K. T. V., & Sun, T. (2000). Fiber optic sensor technology: an overview. *Sensors and Actuators A*: Physical, 82(1), 40-61.

Gravina, R., & Bernini, R. (2009). Polymer optical fiber tapers for biosensing applications. In SPIE BiOS: Biomedical Optics (pp. 717305-717305). *International Society for Optics and Photonics.*

Gravina, R., Testa, G., & Bernini, R. (2009). Perfluorinated plastic optical fiber tapers for evanescent wave sensing. *Sensors*, 9(12), 10423-10433.

Grossman, B. G., Yongphiphatwong, T., & Sokol, M. (2005). In situ device for salinity measurements (chloride detection) of ocean surface. *Optics & Laser Technology*, *37*(3), 217-223.

Guiseppi-Elie, A., Lei, C., & Baughman, R. H. (2002). Direct electron transfer of glucose oxidase on carbon nanotubes. *Nanotechnology*, 13(5), 559.

Guo, S., & Albin, S. (2003). Transmission property and evanescent wave absorption of cladded multimode fiber tapers. *Optics express*, 11(3), 215-223.

Guo, S., & Albin, S. (2003). Transmission property and evanescent wave absorption of cladded multimode fiber tapers. *Optics express*, *11*(3), 215-223.

Guo, T., Tam, H. Y., Krug, P. A., & Albert, J. (2009). Reflective tilted fiber Bragg grating refractometer based on strong cladding to core recoupling. *Optics express*, *17*(7), 5736-5742.

Gupta, B. D., Dodeja, H., & Tomar, A. K. (1996). Fibre-optic evanescent field absorption sensor based on a U-shaped probe. *Optical and quantum electronics*, 28(11), 1629-1639.

Guzmán-Sepúlveda, J. R., Guzmán-Cabrera, R., Torres-Cisneros, M., Sánchez-Mondragón, J. J., & May-Arrioja, D. A. (2013). A Highly Sensitive Fiber Optic Sensor Based on Two-Core Fiber for Refractive Index Measurement. *Sensors,13*(10), 14200-14213.

Hanyes, J. (2005). Fiber Optics Technician's Manual, 3rd Edition. New York: Delmar Publisher.

Harun, S. W., Batumalay, M., Ahmad, F., Lokman, A., Jasim, A. A., & Ahmad, H. (2014). Tapered plastic optical fiber coated with single wall carbon nanotubes polyethylene oxide composite for measurement of uric acid concentration. *Sensor Review*, *34*(1), 9-9.

Harun, S., Batumalay, M., Lokman, A., Arof, H., Ahmad, H., & Ahmad, F. (2013). Tapered Plastic Optical Fiber Coated with HEC/PVDF for Measurement of Relative Humidity. *Sensors Journal*, IEEE, Volume:13, Issue: 12, 4702-4705.

Ho, C. H., Lin, S. H., Hu, H. C., & Tsay, Y. F. (2009). CHL1 functions as a nitrate sensor in plants. *Cell*, *138*(6), 1184-1194.

Hopkins, H. H., & Kapany, N. S. (1954). A flexible fiberscope, using static scanning. *Nature*, Vol 173, No 4983, 39-41.

Hoshi, T., Saiki, H., & Anzai, J. I. (2003). Amperometric uric acid sensors based on polyelectrolyte multilayer films. *Talanta*, 61(3), 363-368.

Hsu, K. C., Chen, N. K., Chou, S. Y., Liaw, S. K., Lai, Y., & Chi, S. (2009). Bandpass filter with variable bandwidth based on a tapered fiber with external polymer cladding. *Photonics Technology Letters*, IEEE, 21(13), 935-937.

Huang, M. H., Wu, Y., Feick, H., Tran, N., Weber, E., & Yang, P. (2001). Catalytic growth of zinc oxide nanowires by vapor transport. *Advanced Materials*, 13(2), 113-116.

Huang, Y., Dong, X., Shi, Y., Li, C. M., Li, L. J., & Chen, P. (2010). Nanoelectronic biosensors based on CVD grown graphene. *Nanoscale*, *2*(8), 1485-1488.

Iadicicco, A., Cusano, A., Cutolo, A., Bernini, R., & Giordano, M. (2004). Thinned fiber Bragg gratings as high sensitivity refractive index sensor. *Photonics Technology Letters, IEEE*, *16*(4), 1149-1151.

Iijima, S. (1991). Helical microtubules of graphitic carbon. *Nature*, 354(6348), 56-58.

Iijima, S., & Ichihashi, T. (1993). Single-shell carbon nanotubes of 1-nm diameter. *Nature* 363, 603-605.

Iveković, D., Japec, M., Solar, M., & Živković, N. (2012). Amperometric Uric Acid Biosensor with Improved Analytical Performances Based on Alkaline-Stable H2O2 Transducer. Int. *J. Electrochem*. Sci, 7, 3252-3264.

Jain, A., Yang, A. H., & Erickson, D. (2012). Gel-based optical waveguides with live cell encapsulation and integrated microfluidics. *Optics Letters*, *37*(9), 1472-1474.

Jeff, H. (1999). City of Light: The story of fiber Optics. New York: Oxford University Press.

Jha, R., Villatoro, J., & Badenes, G. (2008). Ultrastable in reflection photonic crystal fiber modal interferometer for accurate refractive index sensing. *Applied Physics Letters*, 93(19), 191106-191106.

Kang, X., Wang, J., Wu, H., Aksay, I. A., Liu, J., & Lin, Y. (2009). Glucose oxidase–graphene–chitosan modified electrode for direct electrochemistry and glucose sensing. *Biosensors and Bioelectronics*, 25(4), 901-905.

Kao, K. C., & Hockham, G.A. (1966). Dielectric-fibre surface waveguides for optical frequencies. Electrical Engineers, Proceedings of the Institution of,113(7), 1151-1158.

Kashiwagi, K., & Yamashita, S. (2009). Deposition of carbon nanotubes around microfiber via evanascent light. *Opt. Express*, *17*(20), 18364-18370.

Keck, D. B., Maurer, R. D., & Schultz, P. C. (2003). On the ultimate lower limit of attenuation in glass optical waveguides. *Applied Physics Letters*, 22(7), 307-309.

Khairnar, V. P. K. R. (2008). Fabrication and numerical evaluation of the tapered single mode optical fiber: Detection of change in refractive index. *Indian Journal of Pure & Applied Physics*, 46, 23-29.

Khalil, S., Bansal, L., & El-Sherif, M. (2004). Intrinsic fiber optic chemical sensor for the detection of dimethyl methylphosphonate. *Optical Engineering*, 43(11), 2683-2688.

Khijwania, S. K., & Gupta, B. D. (1999). Fiber optic evanescent field absorption sensor: effect of fiber parameters and geometry of the probe. *Optical and Quantum Electronics*, 31(8), 625-636.

Khranovskyy, V., Tsiaoussis, I., Yazdi, G. R., Hultman, L., & Yakimova, R. (2010). Heteroepitaxial ZnO nano hexagons on p-type SiC. *Journal of Crystal Growth*, 312(2), 327-332.

Kieu, K., & Mansuripur, M. (2007). Femtosecond laser pulse generation with a fiber taper embedded in carbon nanotube/polymer composite. *Optics letters*,*32*(15), 2242-2244.

Kim, J. Y., Chang, H., Kim, M. S., Leem, J. Y., Ballato, J., & Kim, S. O. (2012). Low-temperature growth of multiple-stack high-density ZnO nanoflowers/nanorods on plastic substrates. *Nanotechnology*, *23*(48), 485606.

Koehne, J., Chen, H., Li, J., Cassell, A. M., Ye, Q., Ng, H. T., ... & Meyyappan, M. (2003). Ultrasensitive label-free DNA analysis using an electronic chip based on carbon nanotube nanoelectrode arrays. *Nanotechnology*, 14(12), 1239.

Koehne, J., Li, J., Cassell, A. M., Chen, H., Ye, Q., Ng, H. T., ... & Meyyappan, M. (2004). The fabrication and electrochemical characterization of carbon nanotube nanoelectrode arrays. *Journal of Materials Chemistry*, 14(4), 676-684.

Kong, J., Franklin, N. R., Zhou, C., Chapline, M. G., Peng, S., Cho, K., & Dai, H. (2000). Nanotube molecular wires as chemical sensors. *Science*, 287(5453), 622-625.

Kude, V., & Khairnar, R. (2008). Fabrication and numerical evaluation of the tapered single mode optical fiber: Detection of change in refractive index. *Indian Journal of pure and applied physics* , 46, 23-29.

Kuila, T., Bose, S., Khanra, P., Mishra, A. K., Kim, N. H., & Lee, J. H. (2011). Recent advances in graphene-based biosensors. *Biosensors and bioelectronics*, 26(12), 4637-4648.

Kurihara, H., Torigoe, S., Omura, M., Saito, K., Kurihara, M., & Matsubara, S. (1998). DNA fragmentation induced by a cytoplasmic extract from irradiated cells. Radiation research, 150(3), 269-274.

Lee, K. J., Wawro, D., Priambodo, P. S., & Magnusson, R. (2007). Agarose-gel based guided-mode resonance humidity sensor. *Sensors Journal, IEEE*, 7(3), 409-414.

Leenaerts, O., Partoens, B., & Peeters, F. M. (2008). Adsorption of H_2O, NH_3, CO, NO_2, and NO on graphene: A first-principles study. *Physical Review B*, 77(12), 125416.

Li, D., Mueller, M. B., Gilje, S., Kaner, R. B., & Wallace, G. G. (2008). Processable aqueous dispersions of graphene nanosheets. *Nature nanotechnology*, 3(2), 101-105.

Li, F., Chai, J., Yang, H., Han, D., & Niu, L. (2010). Synthesis of Pt/ionic liquid/graphene nanocomposite and its simultaneous determination of ascorbic acid and dopamine. *Talanta*, 81(3), 1063-1068.

Li, J., & Ng, H.T. (2003). Carbon Nanotubes Sensors. H.S. Nalwa, Ed., Santa Barbara, California, American Scientific.

Li, J., Lu, Y., Ye, Q., Cinke, M., Han, J., & Meyappan, M. (2003). Carbon Nanotube sensors for gas and organic vapor detection. *Nano Letters*, 3(7), 929-933.

Li, Y., Harris, E., Chen, L., & Bao, X. (2010). Application of spectrum differential integration method in an in-line fiber Mach-Zehnder refractive index sensor. *Optics Express*, *18*(8), 8135-8143.

Li, Y., Meng, G. W., Zhang, L. D., & Phillipp, F. (2000). Ordered semiconductor ZnO nanowire arrays and their photoluminescence properties. *Applied Physics Letters*, 76(15), 2011-2013.

Lian, H., Sun, Z., Sun, X., & Liu, B. (2012). Graphene doped molecularly imprinted electrochemical sensor for uric acid. *Analytical Letters*, *45*(18), 2717-2727.

Liang, W., Bockrath, M., Bozovic, D., Hafner, J. H., Tinkham, M., & Park, H. (2001). Fabry-Perot interference in a nanotube electron waveguide. *Nature*, 411(6838), 665-669.

Liao, C. R., Wang, D. N., He, X., & Yang, M. W. (2011). Twisted optical microfibers for refractive index sensing. *Photonics Technology Letters, IEEE*,*23*(13), 848-850.

Liao, C. W., Chou, J. C., Sun, T. P., Hsiung, S. K., & Hsieh, J. H. (2006). Preliminary investigations on a new disposable potentiometric biosensor for uric acid. *Biomedical Engineering, IEEE Transactions* on, 53(7), 1401-1408.

Liao, M., Chaudhari, C., Yan, X., Qin, G., Kito, C., Suzuki, T., & Ohishi, Y. (2010). A suspended core nanofiber with unprecedented large diameter ratio of holey region to core. *Optics Express*, *18*(9), 9088-9097.

Lim, K. S., Harun, S. W., Damanhuri, S. S. A., Jasim, A. A., Tio, C. K., & Ahmad, H. (2011). Current sensor based on microfiber knot resonator. *Sensors and Actuators A:* Physical, 167(1), 60-62.

Liu, N., Luo, F., Wu, H., Liu, Y., Zhang, C., & Chen, J. (2008). One-Step Ionic-Liquid-Assisted Electrochemical Synthesis of Ionic-Liquid-Functionalized Graphene Sheets Directly from Graphite. *Advanced Functional Materials,18*(10), 1518-1525.

Liu, Y., Zhang, Y., Lei, H., Song, J., Chen, H., & Li, B. (2012). Growth of well-arrayed ZnO nanorods on thinned silica fiber and application for humidity sensing. *Optics Express*, *20*(17), 19404-19411.

Loh, K. P., Bao, Q., Ang, P. K., & Yang, J. (2010). The chemistry of graphene.Journal of Materials Chemistry, 20(12), 2277-2289.

Lovely, M. R., Radhakrishnan, P., Nampoori, V. P. N., & Vallabhan, C. P. G. (1996). Evanescent wave sensor to monitor the etching rate of an optical fibre.

Luo, S., Liu, Y., Sucheta, A., Evans, M. K., & Van Tassell, R. (2002). Applications of LPG fiber optical sensors for relative humidity and chemical-warfare-agents monitoring. In *Photonics Asia 2002* (pp. 193-204). International Society for Optics and Photonics.

Lye, P. G., Boerkamp, M., Ernest, A., & Lamb, D. W. (2005). Investigating the sensitivity of PMMA optical fibres for use as an evanescent field absorption sensor in aqueous solutions. In *Journal of Physics: Conference Series* (Vol. 15, No. 1, p. 262). IOP Publishing.

Mathew, J., Thomas, K. J., Nampoori, V. P. N., & Radhakrishnan, P. (2007). A comparative study of fiber optic humidity sensors based on chitosan and agarose. *Sens. Transducers J*, 84(10), 1633-1640.

Matias, I. R., Arregui, F. J., & Lo, M. (2000). Tapered optical-fiber-based pressure sensor. *Optical Engineering*, 39(8), 2241-2247.

Meng, H., Shen, W., Zhang, G., Tan, C., & Huang, X. (2010). Fiber Bragg grating-based fiber sensor for simultaneous measurement of refractive index and temperature. *Sensors and Actuators B: Chemical*, *150*(1), 226-229.

Merchant, D. F., Scully, P. J., & Schmitt, N. F. (1999). Chemical tapering of polymer optical fibre. *Sensors and Actuators A: Physical*, *76*(1), 365-371.

Messica, A., Greenstein, A., & Katzir, A. (1996). Theory of fiber-optic, evanescent-wave spectroscopy and sensors. *Applied Optics*, 35(13), 2274-2284.

Minas, G., Martins, J. S., Ribeiro, J. C., Wolffenbuttel, R. F., & Correia, J. H. (2004). Biological microsystem for measuring uric acid in biological fluids. *Sensors and Actuators A: Physical*, 110(1), 33-38.

Musameh, M., Wang, J., Merkoci, A., & Lin, Y. (2002). Low-potential stable NADH detection at carbon-nanotube-modified glassy carbon electrodes. *Electrochemistry Communications*, 4(10), 743-746.

Muto, S., Suzuki, O., Amano, T., & Morisawa, M. (2003). A plastic optical fiber sensor for real-time humidity monitoring. *Measurement Science and Technology*, 14(6), 746.

Nagaraja, P., Krishna, H., Shivakumar, A., & Shrestha, A. K. (2012). Development of quantitative enzymatic method and its validation for the assay of glucose in human serum. *Clinical biochemistry*, *45*(1), 139-143.

Nagata, J., Honma, S., Morisawa, M., & Muto, S. (2007). Development of polymer optical waveguide-type alcohol sensor. In *Photonics Asia 2007* (pp. 682920-682920). International Society for Optics and Photonics.

Newbrun, E., & Frostell, G. (1978). Sugar restriction and substitution for caries prevention. *Caries Research*, *12*(Suppl. 1), 65-73.

Novoselov, K. S., Geim, A. K., Morozov, S. V., Jiang, D., Zhang, Y., Dubonos, S. V., ... & Firsov, A. A. (2004). Electric field effect in atomically thin carbon films. *Science*, 306(5696), 666-669.

Oakley, K. P., O'Sullivan, N. M., Kenny, R. P., & Hussey, C. D. (1994). Loss and spectral control in fused tapered couplers. *Optical Engineering*, 33(12), 4006-4019.

Palais, J.C. (2005). Fiber Optic Communications. 5th ed, Prentice Hall.

Pan, Z. W., & Wang, Z. L. (2001). Nanobelts of semiconducting oxides. *Science*, 291(5510), 1947-1949.

Park, K. S., Choi, H. Y., Park, S. J., Paek, U. C., & Lee, B. H. (2010). Temperature robust refractive index sensor based on a photonic crystal fiber interferometer. *Sensors Journal, IEEE*, *10*(6), 1147-1148.

Peres, N. M. R., Guinea, F., & Neto, A. C. (2006). Electronic properties of disordered two-dimensional carbon. *Physical Review B*, 73(12), 125411-125423.

Polynkin, P., Polynkin, A., Peyghambarian, N., & Mansuripur, M. (2005). Evanescent field-based optical fiber sensing device for measuring the refractive index of liquids in microfluidic channels. *Optics letters*, *30*(11), 1273-1275.

Pumera, M. (2010). Graphene-based nanomaterials and their electrochemistry. *Chemical Society Reviews*, 39(11), 4146-4157.

Rahman, H. A., Harun, S. W., Yasin, M., & Ahmad, H. (2012). Fiber-Optic Salinity Sensor Using Fiber-Optic Displacement Measurement With Flat and Concave Mirror. Selected Topics in Quantum Electronics, *IEEE Journal*, 18(5), 1529-1533.

Rahman, H. A., Harun, S. W., Yasin, M., Phang, S. W., Damanhuri, S. S. A., Arof, H., & Ahmad, H. (2011). Tapered plastic multimode fiber sensor for salinity detection. *Sensors and Actuators A: Physical*, 171(2), 219-222.

Rahman, H., Harun, S., Yasin, M., & Ahmad, H. (2012). Fiber-Optic salinity sensor using Fiber-optic displacement measurement with flat and concave mirror. IEEE *Journal of selected topics in quantum electronics*, 18 (5).

Schedin, F., Geim, A. K., Morozov, S. V., Hill, E. W., Blake, P., Katsnelson, M. I., & Novoselov, K. S. (2007). Detection of individual gas molecules adsorbed on graphene. *Nature materials*, 6(9), 652-655.

Schmidt-Mende, L., & MacManus-Driscoll, J. L. (2007). ZnO–nanostructures, defects, and devices. *Materials today*, *10*(5), 40-48.

Shadaram, M., Martinez, J., Garcia, F., & Tavares, D. (1997). Sensing ammonia with ferrocene-based polymer coated tapered optical fibers. *Fiber & Integrated Optics*, 16(1), 115-122.

Shan, C., Yang, H., Song, J., Han, D., Ivaska, A., & Niu, L. (2009). Direct electrochemistry of glucose oxidase and biosensing for glucose based on graphene. *Analytical Chemistry*, 81(6), 2378-2382.

Shang, N. G., Papakonstantinou, P., McMullan, M., Chu, M., Stamboulis, A., Potenza, A., ... & Marchetto, H. (2008). Catalyst-Free Efficient Growth, Orientation and Biosensing Properties of Multilayer Graphene Nanoflake Films with Sharp Edge Planes. *Advanced functional materials*, 18(21), 3506-3514.

Shen, J., Shi, M., Li, N., Yan, B., Ma, H., Hu, Y., & Ye, M. (2010). Facile synthesis and application of Ag-chemically converted graphene nanocomposite. *Nano Research*, 3(5), 339-349.

Shi, L., Chen, X., Liu, H., Chen, Y., Ye, Z., Liao, W., & Xia, Y. (2006). Fabrication of submicron-diameter silica fibers using electric strip heater. *Opt. Express*, *14*(12), 5055-5060.

Sinha, N., Ma, J., & Yeow, J. T. (2006). Carbon nanotube-based sensors. *Journal of nanoscience and nanotechnology*, 6(3), 573-590.

Skinner, A. J., & Lambert, M. F. (2011). An automatic soil pore-water salinity sensor based on a wetting-front detector. *Sensors Journal, IEEE*, *11*(1), 245-254.

Song, Y. W., Morimune, K., Set, S. Y., & Yamashita, S. (2007). Polarization insensitive all-fiber mode-lockers functioned by carbon nanotubes deposited onto tapered fibers. *Applied physics letters*, *90*(2), 021101-021101.

Stankovich, S., Dikin, D. A., Dommett, G. H., Kohlhaas, K. M., Zimney, E. J., Stach, E. A., ... & Ruoff, R. S. (2006). Graphene-based composite materials. *Nature*, 442(7100), 282-286..

Star, A. Gabriel, J.C.P., Bradley, K., & Gruner, G. (2003). Electronic detection of specific protein binding using nanotubes FET devices. *Nano Letters*, 3(4), 459-463.

Stellan, H. and Yao, K. (1981), High performance liquid chromatography of macromolecules on agarose and its derivates, *Journal of Chromatography A*, Volume 215, 317-322.

Stetter, J. R., & Maclay, G. J. (2004). Carbon nanotubes and sensors: A review. *Enabling Technology for MEMS and Nanodevices*, 357-382.

Stiebeiner, A., Garcia-Fernandez, R., & Rauschenbeutel, A. (2010). Design and optimization of broadband tapered optical fibers with a nanofiber waist. *Optics Express*, *18*(22), 22677-22685.

Sumetsky, M., Dulashko, Y., & Hale, A. (2004). Fabrication and study of bent and coiled free silica nanowires: Self-coupling microloop optical interferometer. *Optics Express*, 12(15), 3521-3531.

Suzuki, O., Miura, M., Morisawa, M., & Muto, S. (2002). POF-type optic humidity sensor and its application [as breathing-condition monitor]. In Optical Fiber Sensors Conference Technical Digest, 2002. Ofs 2002, 15th (pp. 447-450).

Tai, Y. H., & Wei, P. K. (2010). Sensitive liquid refractive index sensors using tapered optical fiber tips. *Optics letters*, *35*(7), 944-946.

Tao, S., Winstead, C. B., Jindal, R., & Singh, J. P. (2004). Optical-fiber sensor using tailored porous sol-gel fiber core. *Sensors Journal, IEEE*, *4*(3), 322-328.

Thyagarajan, K. and A. Ghatak. (2007). Fiber Optic Essentials, ed. E. Desurvire. New Jersey, John Wiley & Sons Inc.

Tian, Y., Wang, W., Wu, N., Zou, X., & Wang, X. (2011). Tapered optical fiber sensor for label-free detection of biomolecules. *Sensors*, *11*(4), 3780-3790.

Tompa, G. S., Sun, S., Provost, L. G., Mentel, D., Sugrim, D., Chan, P., ... & Lee, A. (2007). Large Area Multi-Wafer MOCVD of Transparent and Conducting ZnO Films. In Materials Research Society Symposium Procreedings (Vol. 957, p. 161). Warrendale, Pa.; Materials Research Society; 1999.

Tracey, P. M. (1991). Intrinsic fiber-optic sensors. Industry Applications, *IEEE Transactions*, 27(1), 96-98.

Udd, E. (1991). Fiber Optic Sensors: An Introduction for Scientists and Engineers. New York.

Udd, E., & Spillman, W. B. (1991). Fiber optic sensors. John Wiley & Sons.

Upcroft, P., & Upcroft, J. A. (1993). Comparison of properties of agarose for electrophoresis of DNA. *Journal of Chromatography B: Biomedical Sciences and Applications,* 618(1), 79-93.

Usman Ali, S. M., Alvi, N. H., Ibupoto, Z., Nur, O., Willander, M., & Danielsson, B. (2011). Selective potentiometric determination of uric acid with uricase immobilized on ZnO nanowires. *Sensors and Actuators B: Chemical*, *152*(2), 241-247.

Van Heel, A. C. (1954). A new method of transporting optical images without aberrations. *Nature*, Vol 173, No.4392, 39.

Velankar, Y. P., & Shadaram, M. (2003). Tapered optical fiber for WDM applications. In Applications of Photonic Technology (pp. 298-302). International Society for Optics and Photonics.

Villatoro, J., Monzón-Hernández, D., & Talavera, D. (2004). High resolution refractive index sensing with cladded multimode tapered optical fibre. *Electronics letters*, *40*(2), 106-107.

Visconti, F., de Paz, J. M., & Rubio, J. L. (2010). What information does the electrical conductivity of soil water extracts of 1 to 5 ratio (w/v) provide for soil salinity assessment of agricultural irrigated lands? *Geoderma*, *154*(3), 387-397.

Vivekchand, S. R. C., Rout, C. S., Subrahmanyam, K. S., Govindaraj, A., & Rao, C. N. R. (2008). Graphene-based electrochemical supercapacitors. *Journal of Chemical Sciences*, 120(1), 9-13.

Vo-Dinh, T., Alarie, J. P., Cullum, B. M., & Griffin, G. D. (2000). Antibody-based nanoprobe for measurement of a fluorescent analyte in a single cell. *Nature biotechnology*, *18*(7), 764-767.

Voss, T., Svacha, G. T., Mazur, E., Müller, S., Ronning, C., Konjhodzic, D., & Marlow, F. (2007). High-order waveguide modes in ZnO nanowires. *Nano letters*,*7*(12), 3675-3680.

Wang, P., Brambilla, G., Ding, M., Semenova, Y., Wu, Q., & Farrell, G. (2011). High-sensitivity, evanescent field refractometric sensor based on a tapered, multimode fiber interference. *Optics letters*, *36*(12), 2233-2235.

Wang, X., Zhi, L., & Müllen, K. (2008). Transparent, conductive graphene electrodes for dye-sensitized solar cells. *Nano letters*, 8(1), 323-327.

Wolchover, N. A., Domachuk, P., Cronin-Golomb, M., Luan, F., George, A. K., Knight, J., & Omenetto, F. G. (2007). High nonlinearity glass photonic crystal nanowires. In *Conference on Lasers and Electro-Optics*. *Optical Society of America*.

Wolfbeis, O. (2004). Fiber-Optic Chemical Sensors and Biosensors. Anal. Chem. , 76, 3269-3284.

Wolfbeis, O. S. (2004). Fiber-optic chemical sensors and biosensors. *Analytical Chemistry*, 76(12), 3269-3284.

Wong, A. C., Chung, W., Tam, H. Y., & Lu, C. (2011). Single tilted Bragg reflector fiber laser for simultaneous sensing of refractive index and temperature. *Optics express*, *19*(2), 409-414.

Woolley, A. T., Guillemette, C., Cheung, C. L., Housman, D. E., & Lieber, C. M. (2000). Direct haplotyping of kilobase-size DNA using carbon nanotube probes. *Nature biotechnology*, 18(7), 760-763.

Xia, T. H., Zhang, A. P., Gu, B., & Zhu, J. J. (2010). Fiber-optic refractive-index sensors based on transmissive and reflective thin-core fiber modal interferometers. *Optics Communications*, *283*(10), 2136-2139.

Xu, F., Horak, P., & Brambilla, G. (2007). Optical microfiber coil resonator refractometric sensor. *Optics Express*, *15*(12), 7888-7893.

Xu, J., & Saeys, M. (2008). First principles study of the stability and the formation kinetics of subsurface and bulk carbon on a Ni catalyst. *The Journal of Physical Chemistry C*, 112(26), 9679-9685.

Xu, J., & Saeys, M. (2008). First principles study of the stability and the formation kinetics of subsurface and bulk carbon on a Ni catalyst. *The Journal of Physical Chemistry C*, 112(26), 9679-9685.

Xue, S., van Eijkelenborg, M. A., Barton, G. W., & Hambley, P. (2007). Theoretical, numerical, and experimental analysis of optical fiber tapering. Lightwave Technology, *Journal of Physical Chemistry C*, 25(5), 1169-1176.

Yakimova, R., Selegård, L., Khranovskyy, V., Pearce, R., Lloyd Spetz, A., & Uvdal, K. (2012). ZnO materials and surface tailoring for biosensing. *Frontiers in bioscience* (Elite edition), 4, 254-278.

Yang, S., Hsu, H. C., Liu, W. R., Cheng, H. M., & Hsieh, W. F. (2007). Correlation between photoluminescence and varied growth pressure of well-aligned ZnO nanorods on fused silica substrate. *Optical Materials*, *30*(3), 502-507.

Yao, B. D., Chan, Y. F., & Wang, N. (2002). Formation of ZnO nanostructures by a simple way of thermal evaporation. *Applied Physics Letters*, 81(4), 757-759.

Yeo, T. L., Eckstein, D., McKinley, B., Boswell, L. F., Sun, T., & Grattan, K. T. V. (2006). Demonstration of a fibre-optic sensing technique for the measurement of moisture absorption in concrete. *Smart materials and structures*, *15*(2), N40.

Yeo,T.L., Sun,T., & Grattan,K.T.V., (2008). Fibre Optic Sensor Technologies for Humidity and Moisture Measurement. *Sensors and Actuators A*: 144 (2008), 280-295.

Yuan, J., & El-Sherif, M. A. (2003). Fiber-optic chemical sensor using polyaniline as modified cladding material. *Sensors Journal, IEEE*, 3(1), 5-12.

Zen, J. M., & Lo, C. W. (1996). A glucose sensor made of an enzymatic clay-modified electrode and methyl viologen mediator. *Analytical chemistry*, *68*(15), 2635-2640.

Zhang, S., Kopp, V. I., Churikov, V., & Zhang, G. (2009). PANDA-based in-fiber linear polarizers. In SPIE OPTO: Integrated Optoelectronic Devices (pp. 72120D-72120D). International Society for Optics and Photonics.

Zhang, T., Mubeen, S., Myung, N. V., & Deshusses, M. A. (2008). Recent progress in carbon nanotube-based gas sensors. Nanotechnology, 19(33), 332001.

Zhang, Y., Yu, K., Jiang, D., Zhu, Z., Geng, H., & Luo, L. (2005). Zinc oxide nanorod and nanowire for humidity sensor. *Applied surface science*, 242(1), 212-217.

Zhao, C., Wan, L., Wang, Q., Liu, S., & Jiao, K. (2009). Highly sensitive and selective uric acid biosensor based on direct electron transfer of hemoglobin-encapsulated chitosan-modified glassy carbon electrode. *Analytical Sciences*, 25(8), 1013-1017.

Zhao, Y., Pang, F., Dong, Y., Wen, J., Chen, Z., & Wang, T. (2013). Refractive index sensitivity enhancement of optical fiber cladding mode by depositing nanofilm via ALD technology. *Optics express*, 21(22), 26136-26143.

Zhou, Q., Shahriari, M. R., Kritz, D., & Sigel Jr, G. H. (1988). Porous fiber-optic sensor for high-sensitivity humidity measurements. *Analytical Chemistry*,*60*(20), 2317-2320.

Zibaii, M. I., Kazemi, A., Latifi, H., Azar, M. K., Hosseini, S. M., & Ghezelaiagh, M. H. (2010). Measuring bacterial growth by refractive index tapered fiber optic biosensor. *Journal of Photochemistry and Photobiology B: Biology*, *101*(3), 313-320.

Zubia, J., & Arrue, J. (2001). Plastic optical fibers: An introduction to their technological processes and applications. *Optical Fiber Technology*, *7*(2), 101-140.

Appendix

Selections of published works are attached in this appendix.